CHALMERS

# A Parametric Study of Shoulder Belt Interactions with the PIPER Scalable Child Human Body Model in Frontal and Frontal Offset Impacts

Master's thesis in Biomedical Engineering Master's Program

JOSEFINE BERNTSSON

Mechanics and Maritime Sciences
CHALMERS UNIVERSITY OF TECHNOLOGY
Göteborg, Sweden 2018

MASTER'S THESIS IN BIOMEDICAL ENGINEERING MASTER'S PROGRAM

# A Parametric Study of Shoulder Belt Interactions with the PIPER Scalable Child Human Body Model in Frontal and Frontal Offset Impacts

JOSEFINE BERNTSSON

Mechanics and Maritime Sciences
Division of Vehicle Safety
CHALMERS UNIVERSITY OF TECHNOLOGY
Göteborg, Sweden 2018

A Parametric Study of Shoulder Belt Interactions with the PIPER Scalable Child Human Body Model in Frontal and Frontal Offset Impacts
JOSEFINE BERNTSSON

© JOSEFINE BERNTSSON, 2018

Master's thesis 2018:81
Mechanics and Maritime Sciences
Division of Vehicle Safety
Chalmers University of Technology
SE-412 96 Göteborg
Sweden
Telephone: +46 (0)31-772 1000

Cover:
The cover image depicts a 6 year old PIPER scalable child HBM using a seat belt in the LS-DYNA environment.

Chalmers Reproservice
Göteborg, Sweden 2018

A Parametric Study of Shoulder Belt Interactions with the PIPER Scalable Child Human Body Model in Frontal and Frontal Offset Impacts
Master's thesis in Biomedical Engineering Master's Program
JOSEFINE BERNTSSON
Mechanics and Maritime Sciences
Division of Vehicle Safety
Chalmers University of Technology

# ABSTRACT

Motor Vehicle Crashes (MVC) are among the leading causes of deaths for children globally. Complementary to the fatality risk, traffic road accidents are responsible for an even larger number of severe pediatric injuries which can lead to permanent impairment. Actions towards reducing or preferably eliminating this problem are to improve the design, accessibility and regulations of child restraint systems as well as implementation of these in actual passenger vehicles. Computer Aided Engineering (CAE) has become an integrated part of the contemporary automotive industry, providing the opportunity to perform crash tests using a simulation platform as a complement to physical crash tests. Finite Element Human Body Models have the potential to become a powerful tool in the virtual assessment of injury tolerances, kinematic behavior and interaction with vehicle interior design. Although substantial efforts have been contributed to the development of male HBM:s, in particular in the $50^{th}$ percentile size interval, child size models are receiving less attention. Hence, the Position and Personalize Advanced Human Body Models for Injury Prediction (PIPER) project aimed to provide an open source child HBM, scalable within the range of 1.5-6 years old as well as different percentiles within each age group. In addition a scaling and positioning tool, PIPER Framework, has been released to facilitate personizalisation of FE HBM:s.

This Master's Thesis project has evaluated the sensitivity of the PIPER scalable child model by exposing the PIPER baseline model (6 year old, $50^{th}$ percentile) to three different shoulder belt angles, achieved by altering the D-ring position in an LS-DYNA environment. These belt routing setups have been applied to three different cases which included a belt-positioning booster, a high-back booster and a rear seat only during frontal and frontal offset impact. Kinematic behaviour of the child HBM and the occurrence of undesirable belt performance such as sliding off the shoulder resulting in increased roll-out risk or neck-loading, has been the main evaluating feature. Head accelerations, deflection of sternum and global head injury criteria (HIC) have been estimated and additionally used for comparison between the different parameters. Conclusions were made that the PIPER scalable child model was able to capture different undesired belt interaction behaviours such as roll-out and submarining, although further evaluations are necessary. A visual comparison with data retrieved during the literature review supported the flexible kinematic trajectories of the PIPER scalable child HBM when exposed to the high-severity crash pulses of the parametric study. In terms of injury criteria, the PIPER scalable child HBM appeared to overestimate $HIC_{15}$ values, hence additional research concerning biofidelic injury thresholds for children is necessary.

Keywords: PIPER Scalable Child HBM, Frontal Crash, Frontal Offset Crash, Parametric Shoulder Belt Study

# ACKNOWLEDGEMENTS

I wish to express a great thank you to **Volvo Cars** for supporting this thesis project and **Lotta Jakobsson** for initiating this project and sharing her knowledge and guidance. Thank you to **Tommy Spitza** for LS-Dyna support and to **Isabelle Stockman** for sharing your knowledge within pediatric safety and giving us an exciting tour of the sled crash facilities.

A wonderful thank you to **Robert Thomson** for being our examiner and SAFER for accommodating us and making us feel at home. A very special thank you goes to:

**Putra I Putu Alit** for being our supervisor from the start, taking us under your wings, providing support and guidance throughout our time here.
**Karl-Johan Larsson** via **Autoliv**, for becoming our supervisor, taking a great interest in our project and helping us tremendously with all of our LS-Dyna and HBM related questions as well as the art of performing belt routing.
**Johan Iraeus** for helping us with our model setup and answering all of our never ending questions.
**Carolyn Roberts** for sharing your medical knowledge and providing an important biofidelity perspective.
I would also like to thank my dear colleague **Sarah El-Mobader** for our collaboration when exploring the world of PIPER and LS-Dyna.

Last but not least, I wish to express a very special and lovefilled gratitude to my boyfriend **Andrei Soloviev**, my family **Inger**, **Matilda** and **Veronica** and my friends whom have shown great love, support and understanding during this project. I am also lovingly grateful for my father **Mats** whom taught me about fundamental FEM principles at an early age, a parallel I had not drawn prior to working with this project.

# Abbreviations

| | |
|---|---|
| *ATD* | Anthropometric Test Device |
| *CG* | Center of Gravity |
| *CRS* | Child Restraint Systems |
| *CT* | Computed Tomography |
| *EM* | Energy Management |
| *FIB* | Test Configuration Abbreviation: Frontal Impact Booster |
| *FIBB* | Test Configuration Abbreviation: Frontal Impact Booster with Back |
| *FINB* | Test Configuration Abbreviation: Frontal Impact No Booster |
| *FWRB* | Full Width Rigid Barrier |
| *HBM* | Human Body Model |
| *HIC* | (Global) Head Injury Criterion |
| *MRI* | Magnetic Resonance Imaging |
| *NHTSA* | National Highway Traffic Safety Administration |
| *ODB* | Offset Deformable Barrier |
| *OIB* | Test Configuration Abbreviation: Offset Impact Booster |
| *OIBB* | Test Configuration Abbreviation: Offset Impact Booster with Back |
| *OINB* | Test Configuration Abbreviation: Offset Impact No Booster |
| *PMHS* | Post Mortem Human Surrogates |
| *UMTRI* | University of Michigan Transportation Research Institute |

# GLOSSARIES

| | |
|---|---|
| ***Impact Biomechanics*** | Science of injury control prior, pending and following an automotive crash event. This research field integrates mechanical principles and medical knowledge of humans such as anatomy, physiology and pathophysiology. |
| ***Biofidelity*** | To what extent a model replicates the biological response of a living organism such as a human. |
| ***Posture*** | In what manner a person carries their body. May be applied to both erect and seated positions. |
| ***Sitting/seating height*** | Measured distance from the seated surface to the vertex of the head. |
| ***Booster Cushion*** | Device which elevates a child to improve interaction with seat belt. Consists of a stiff cushion accompanied with belt guides. Also referred to as backless booster. |
| ***Booster Seat*** | Similar purpose as the Booster Cushion with the addition of a back which may include an integrated D-ring. Also referred to as highback booster. |
| ***Shoulder Belt*** | Upper portion of the three-point seat belt, commonly defined from the buckle to the upper anchorage point such as the D-ring. |
| ***Lap Belt*** | Lower portion of the three-point seat belt, usually defined from the lower anchorage point to the buckle. |
| ***Loading Condition*** | Refers to the direction of impact during an automotive crash. Includes for instance frontal, lateral and rear collisions. |

# Contents

**Abstract** **i**

**Acknowledgements** **iii**

**Abbreviations** **v**

**Glossaries** **vii**

**Contents** **ix**

**1 Introduction** **1**
1.1 Thesis outline . . . 1

**2 Medical Background** **3**
2.1 Child Anatomy and Growth . . . 3
2.1.1 Head . . . 3
2.1.2 Neck . . . 5
2.1.3 Thorax . . . 6
2.1.4 Pelvis . . . 8
2.2 AIS . . . 8
2.3 Injury Criteria . . . 8
2.3.1 Head Injury Criterion . . . 8
2.3.2 Head Angular Acceleration Y axis . . . 9
2.3.3 Neck Injury Criterion . . . 9
2.3.4 Viscous Criterion . . . 10
2.4 Crashworthiness . . . 11

**3 Children in Cars** **13**
3.1 Belt Positioning Boosters . . . 14
3.1.1 Booster Cushions . . . 14
3.1.2 Booster Seats . . . 14
3.1.3 Integrated Boosters . . . 15
3.2 Seat Belts . . . 15
3.2.1 Shoulder Belt . . . 15
3.2.2 Lap Belt . . . 16
3.2.3 Parametric Studies of Shoulder Belt Interaction . . . 17
3.3 Energy Mangement - Pretensioner . . . 17
3.4 Missuse of Restraint Systems . . . 18
3.5 Pediatric Regulations and Recommendations . . . 18

**4 Anthropometric Assessment Devices** **21**
4.1 Human Body models . . . 21
4.1.1 Multi-Body Models . . . 22
4.1.2 Finite Element Models . . . 22
4.2 PIPER Scalable Child HBM . . . 22
4.2.1 Validation . . . 23
4.2.2 Neck . . . 24
4.2.3 Thoraco-abdominal and Pelvic regions . . . 24
4.2.4 Upper and Lower Extremities . . . 25
4.2.5 Virtual Sensors . . . 25
4.2.6 Future of the Model . . . 25
4.3 PIPER Framework . . . 26
4.3.1 Check . . . 26
4.3.2 Scaling . . . 26
4.3.3 Pre-Positioning . . . 26

4.3.4 Smoothing . . . 27
4.4 Finite Element Method . . . 27

**5 Objective** **31**
5.1 Purpose . . . 31

**6 Methods** **33**
6.1 Feasibility Study . . . 33
6.1.1 Background: Case 2017 . . . 33
6.1.2 Process . . . 33
6.2 Parameter Study . . . 37
6.2.1 Parameter Angles . . . 37
6.2.2 Restraint Configuration . . . 38
6.2.3 Loading Conditions . . . 39

**7 Results - Feasibility Study** **43**

**8 Results - Parameter Study** **49**
8.1 Kinematic Analysis . . . 49
8.2 Trajectory Comparison . . . 64
8.2.1 Linear and Angular Accelerations . . . 67
8.2.2 Global Head Injury Criteria . . . 69
8.2.3 Upper Neck Tension Forces . . . 70
8.2.4 Chest Deflection . . . 71
8.2.5 Simulation Metrics . . . 73

**9 Discussion** **77**
9.1 Sensitivity of the PIPER Child Scalable HBM . . . 77
9.1.1 Sensitivity Towards D-ring Position . . . 77
9.1.2 Sensitivity Towards Belt Assisting Devices . . . 79
9.2 Injury Biofidelity of the PIPER Scalable Child HBM . . . 81
9.2.1 Comparison of Accelerations . . . 81
9.2.2 Global Head Injury Criteria . . . 82
9.2.3 Neck $F_z$ . . . 83
9.2.4 Chest Deflection . . . 83
9.3 Robustness of the PIPER Child Scalable HBM and the PIPER Personalization Framework . . . 83

**10 Conclusions** **85**
10.1 Evaluation of the PIPER Scalable Child HBM . . . 85
10.2 Future Work and Recommendations . . . 85

**Appendix A** **87**

**Appendix B** **89**

**Appendix C** **91**

**References** **93**

# 1 Introduction

Every fourth minute, a child dies due to road traffic crashes. In 2012, a total of 186 300 children under the age of 18 were killed in vehicle accidents and even more were severely injured [1]. In the age group of 5-17 years old, road traffic injury is among the top four fatality causes and for the age group of 15-17 years old, it is ranked as the primary threat to life. A comparison performed by the World Health Organization (WHO) concluded that traffic induced fatalities were almost three time as likely to occur in low- to middle income countries than high income countries [1]. Although being a complex problem which needs to be addressed from multiple perspectives, research targeting child safety both inside and outside the vehicle is an urgent matter.

Crashworthiness is essential in order to gain knowledge regarding overall safety of vehicles where Anthropometric Test Devices (ATD:s) such as dummies are considered the golden standard for regulatory testing of vehicles and restraint systems. Dummies are able to provide significant amount of data in a physiological environment but their biofidelity, especially for pediatric dummies, has been questioned by a growing body of research [2, 3]. In general, biomechanical data and injury tolerances related to the pediatric community is insufficient. This can be derived from that less research has been devoted to this field as well as ethical dilemmas concerning data and testing related to child injuries. Crash tests and ATD:s are expensive and additional disadvantages are that the model is fixed in size with respect to age and anthropometric variations within each age group. Computer Aided Engineering (CAE) has become an integrated part of automotive design due to rapid improvements in hardware and computational time. Within this field, biofidelic numerical Human Body Models (HBM) have demonstrated great potential to provide complementary information from virtual impact simulations to the physical crash test data. Adult HBM have been a subject of intense research whereas the development of a pediatric HBM has been given less attention. Child HBM could facilitate optimization of safety system and contribute the body of knowledge concerning pediatric injury mechanisms. Barriers for implementation of these advanced HBM are difficulties to position them in a vehicle environment as well as robustness of the model. Thus, the aim of the European project PIPER [4] was to adhere to these barriers and issues by developing a positioning and personalization software which facilitates handling of the Finite Element (FE) HBM:s and to collaborate on the development of a continuously scalable child HBM, referred to as the PIPER scalable child model. Both the PIPER framework software and the PIPER model which is scalable between and within the ages of 1.5-6 year old have now been publicly released. Advantages of a functional scalable model is the ability to conduct testing of a larger population with a wider spread of anthropometric measurements. Enabled positioning may also allow for detailed investigations of missuse behaviour which significantly reduces the protective properties of restraint systems and is particularly interesting for pediatric safety aspects [5]. Although further research efforts need to address the gap of pediatric biomechanical data, the PIPER model is an important step towards incorporating the pediatric perspective into automotive design and engineering.

Primary aim of this Master's Thesis project is to evaluate whether the PIPER scalable child model has reached a maturity level sufficient to be used in assessment of safety applications for industrial and extensive scientific purposes. This aim places demands on three main areas; robustness, kinematic validity and injury biofidelity. Model robustness concerns stability of simulations as well as the ability to use the model in varying configurations and loading conditions. Kinematic validity entails whether the model can accurately capture childrens behaviour in impact scenarios, where this study will specifically target interaction with the shoulder belt. Final main area assesses the model's ability to portray reasonable injury thresholds, a capability which is challenged by the lack of biomechanical pediatric data.

## 1.1 Thesis outline

Initially, an observational literature review was conducted in order to provide a body of knowledge of important areas related to the assessment. The first chapter comprises age-dependent characteristics of anatomical structures with emphasis on body parts interacting with the shoulder belt as well as research on relevant injury criteria and thresholds. Second chapter will evaluate the interaction between children and vehicles as well as restraint systems from a pediatric perspective. In this chapter, design of standardized tests and implications of such structures will be addressed. Final theory chapter will cover the basics of ATD:s dummies and provide a brief descriptions of Finite Element Method. Further description of HBM:s and PIPER in particular is additionally included in this section. Outline of the project is presented in Figure 1.1.

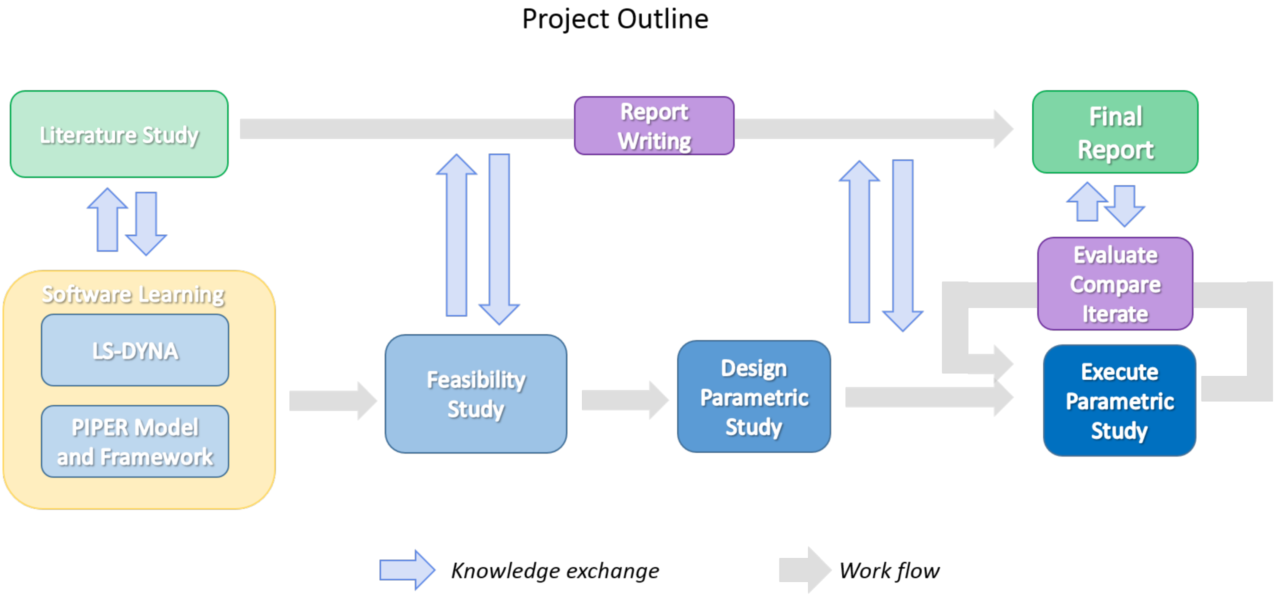
Project Outline
Literature Study
Report Writing
Final Report
Evaluate Compare Iterate
Software Learning
LS-DYNA
PIPER Model and Framework
Feasibility Study
Design Parametric Study
Execute Parametric Study
Knowledge exchange
Work flow

Figure 1.1: *Schematic overview including the main project activities.*

Subsequent phase involved a feasibility study which aimed to reproduce results from the accident reconstruction methodology by Giordano et al. [6] using the PIPER scalable child HBM. Purpose of the feasibility study was partly to become familiarized with the tools and methods associated with the PIPER scalable child HBM, as a well as testing the robustness of the model and the personalization software.

Based on knowledge gathered during the literature review, the parametric study was designed. Potential varying factors were for instance different positions of the shoulder belts, loading conditions, child supportive restraint systems, ages and sizes of the occupant. Following the simulations, results from both the feasibility and the parametric studies were assembled and reviewed during their corresponding result chapters. Visual comparison of kinematic behaviour and suitable injury thresholds were for instance estimated. In the discussion chapter, the reported findings were discussed and condensed to a couple of final conclusions and recommendations for future work.

# 2 Medical Background

## 2.1 Child Anatomy and Growth

Children are not miniature adults since their anthropometric proportions and anatomical material structure significantly differ from that of adults. Thus, simple scaling of adult tools and models will not suffice to protect the children in an optimal way [7]. In addition, physical and biological discrepancies are of greater magnitude between different pediatric age groups than respective age gaps for adults [2]. A significant number of investigations have been performed concerning injury tolerance curves for adults comprising body parts such as head, face, spine, thoracoabdominal area as well as extremities. For children on the other hand, literature identifies an urgent need for more research concerning pediatric biomechanical data [8].

The growth process proceeds throughout a lifetime in local interval spurts which are relatively similar across humans. For instance, an average infant height is about 50 [cm] and throughout the first year, it increases with approximately 50 %. In general, the height from birth has been doubled by the fourth year and the adult height is about twice that of the height at 2 years old [7].

Design of safety systems in vehicles needs to evaluate and consider age-related proportions between body parts. As an example, seated height of an infant is approximately 70 % of the child's height meanwhile a 3 year old has an estimated sitting height of 57 %. During adolescents, the average sitting height converges to a little bit above 50 % of the total height [7]. For infants, the head occupies a quarter of the total body length whereas for an adult the head is approximately $1/7^{th}$ of the full height [7]. By tracing the geometrical midpoint of a person, it originates from slightly above the umbilicus, moving below the umbilicus at the age or 2 and by late puberty, the geometrical mid-point can be found in proximity to the pubic symphysis [7]. The center of gravity, similar to the geometrical midpoint, varies with age as well as the positioning of the body. For instance, one investigation concluded that it was difficult to estimate a child's seated center of gravity which required assessment using a cross-section formed as an asymmetrical ellipsoid [9]. In addition it was concluded that the test subjects had a center of gravity above the lap belt which in turn generates different kinematics with a more forward throw of the head. Subsequent sections exemplifies some structural and material anatomical differences between adults and children as well as among different pediatric age groups which influences the biomechanical responses during impact scenarios. Hence, aiming to provide a base of arguments for why research needs to be specifically dedicated towards pediatric biomechanics.

### 2.1.1 Head

#### Skull Anatomy

The human skull entails the neurocranium and viscerocranium bones. Neurocranium, also known as the brain case, refers to the eight cranial bones which forms the back and the upper part of the skull where the major bones are the frontal, parietal and occipital bones. Viscerocranium denotes the 14 facial bones such as the mandible, maxillas and the zygomatics. For an adult skull, the flat bones in the neurocranium are fused together whereas a fetal skull is characterized by having fibrous sutures joining the skull bones [10].

An analogy of the sutures could be expansion joints, facilitating birth as well as the growth of the brain in an evenly manner. In case any of these sutures close prematurely, this part cannot continue to grow. Due to these sutures, the skull of a child is significantly more deformable. Full obliteration of sutures due to ossification appears around the age of 20 years as the skull has reached its final size. The area of durable fibrous tissues between the bone plates are referred to as fontanelles and a fetal skull have six of them which are depicted in Figure 2.1. The largest one is referred to the anterior fontanelle with an area of 25 mm followed by the posterior fontanelle. Each fontanelle closes at different time intervals where for instance the mastoid fontanelle closes around 6-8 weeks, the posterior ones ossifies by approximately 2-3 months of age and the anterior fontanelle, placed at the top of the head, closes between 18-24 months [7, 10]. Research indicates that the skull employs structural and thickness properties to compensate for the less durable and stiffer sutures. However, additional research on pediatric sutures is required to provide further information.

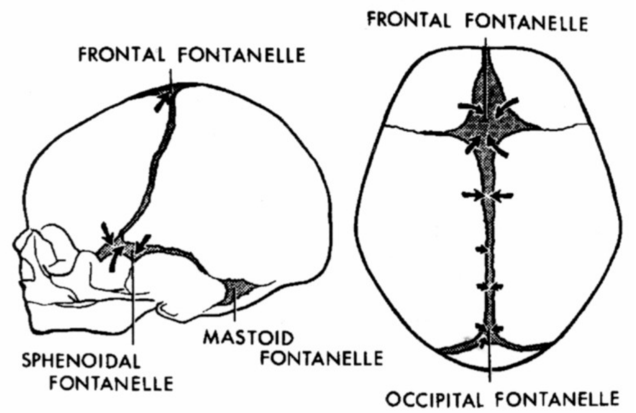

Figure 2.1: *Approximate positions and sizes of the fontanelles, as presented by Burdi et al. [7]*

In terms of material properties, the adult skull comprises three layers: one soft cancellous bone referred to as the diploe layer surrounded by two rigid cortical bones. Cortical bone structure is relatively dense and hard, and it can be found in the exterior layers of most bones in the body. Cancellous bone tissue, also referred to as trabecular or spongy, scores lower on density and stiffness. This tissue can often be found at the endpoints of bones such as close to joints or inside the vertebrae. For the adult skull, the outer cortical bone is thick and durable whereas the inner cortical bone is thin and brittle. The diploe layer additionally contains the red bone marrow. For a newborn, the skull mainly comprises one cortical bone and not until the ages of 3-6 months old the skull tissue begins to transform into the previously described sandwich structure. [10]

### Brain Anatomy

Volume of the brain increases relatively rapidly. At infancy, the brain is approximately a quarter of adult size, despite the fact that the total weight of a new born baby is only 5% of an adult's weight [7]. Already at the age of 2 years old, the brain has grown to approximately 80% of the adult brain size and at 5 years old the brain volume has reached adult size. During the period from 4-20 years the white brain matter, which consists of myelinated axons where myeline provides the white colour, linearly increases in volume in the dorsal prefrontal cortex. Gray matter of the brain, receiving its gray colour from the cell bodies of the neurons, grows non-linearly to maximum size at 12 years of age and from that point decreases until reaching the age of 20 [10, 11].

### Injuries to Head and Brain

Leading cause of fatalities and severe disabilities among children and adolescents within the United States is Traumatic Brain Injury (TBI), an umbrella term for injuries related to for instance blunt force trauma or shock to the head [12–16]. For children in motor vehicle accidents, head trauma are deemed as both the most serious as well as the most frequent type of injury [7]. One study from 1959 comprising more than 14,500 accidents in U.S., children up to the age of 11 years had an incidence of head injuries of 77% in comparison to 69 % for adolescents and 70 % for adults. Another study from 1967 by Kihlberg and Gensler which investigated close to 34 000 vehicle crashes supported these results. Biomechanically this could be explained by that the pediatric head is proportionally larger than that of an adult, which affects the interaction with both restraint systems and the vehicle interior for children since the center of gravity is elevated. In combination with underdeveloped spinal muscles with respect to the head inertia, this generates implications with the seat belt which may enable extensive flexion and comparatively larger kinematic trajectories during loading conditions such as frontal impact. Less stiff pediatric skull structure reduces the child's ability to withstand head impact [7].

### 2.1.2 Neck

#### Skeletal structure

An average human vertebral column consists of 33 vertebrae divided into 5 regions, see Figure 2.2. Individual variations may occur in the Coccyx, commonly referred to as the tailbone, which usually comprises 4 fused vertebrae but can vary between 3 and 5. One important function of the spine is the accommodation of the spinal cord which derives from the foramen magnum [8].

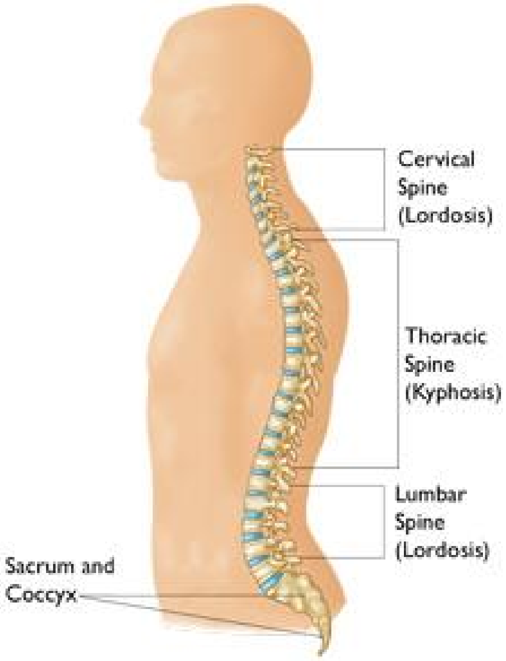

Figure 2.2: *Schematic view over the classification of the vertebral column [17].*

Neck refers to the cervical spine including surrounding soft tissue. The first vertebra C1 positioned just beneath the skull is referred to as the Atlas, and the second vertebra, C2, goes by the name of Axis. Without these two vertebrae, it would be impossible to move the head or the neck. In addition, they support the skull as well as shielding the spinal cord. Due to the increased volume of cartilaginous tissue present in the sutures between the ossification centers of the vertebrae, the pediatric vertebral anatomy is a weaker structure than that of the adult [8].

A broad categorization has been conducted on the age related effects on the development of the cervical spine [18] as can be observed in Table 2.1 which captures the average time it takes for the vertebrae to fuse. Fully developed vertebral anatomy appears in the late teens. Naturally, the mass and relative volume of the head will affect the cervical spine in terms of induced stress. As both the relative proportions as well as the mass of the head will endure different phases, this will influence the biomechanical load on the cervical vertebrae [8]. Uncinate processes are saddle like extrusions on the body of the vertebra and appears on the third cervical vertebra until the first thoracic vertebra. These extrusions combine with the superior vertebra to become a fibrous uncovertebral joint. Function of the fibrous uncovertebral joint is to fixate the disk posterolaterally, reduce lateral bending and generate coupled motions [8].

| Group ID | Age Category | Vertebral Activity |
|---|---|---|
| *I* | Infant - 1 Year old | Observation of three primary centers |
| *II* | 1-3 Years old | Fusion of Posterior Synchondrosis |
| *III* | 3-6 Years old | Fusion of the Bilateral Anterior Neurocentral Synchondroses |
| *IV* | 11-14 Years old | Secondary Ossification with development of the Uncinate and Uncovertebral anatomy |

Table 2.1: Main developmental stages of the cervical vertebrae [8]

Another important age dependent feature is the synovial facet joint. Facet joints are planar joints between each neighbouring pair of vertebrae and for every movement in the vertebral column, at least two facet joints on each side of the moved vertebra are activated. Joints in upper region of the spine are more horizontal whereas the lower vertebrae are increasingly oblique. The degree of obliqueness increases with respect to age [8]. Pediatric facet joints are thus relatively horizontal which reduces structural resistance towards transverse loading in terms of shear [2]. For instance, a relatively common phenomena among children up to 7 years old is pseudosubluxation. Pseudosubluxation is a misalignment of cervical vertebrae, usually observed between C2 and C3, and can be derived from a combination of less stiff vertebral material properties as well as the more horizontal facet joints [8].

Cross sectional area as well as the lateral breadth of the neck muscles responsible for flexion and extension is a function of age, implying a positive correlation between neck muscle strength and increased age [8]. In combination with the relatively larger mass of the head, dampening effect of the neck muscles among children is less resistant to violent motions of the head [7].

#### Neck Related Injuries

One identified issue for children in automotive impact scenarios is the risk of tearing the cervical spine when applying a large force on the head while keeping the thorax and shoulders relatively fixed [7, 19]. Adult vertebral anatomy are more likely to endure intense tensile forces and can handle decelerations up to 100 g [20]. Resulting injuries are commonly fractures to the vertebrae. In contrast, the growth induced flexible tissues of the child's neck structure increases the likelihood of separation and deformation of the verterbrae. If this occurs, the sensitive spinal cord is exposed and the probability of severe injuries to the nerves increases [20]. In addition, reduced neck protection during abrupt decelerations may lead to rapid rotational or lateral head movements which can impair arteries supplying blood to brain and nerves. During impact, a child's head is more likely to snap forward in a whip-like trajectory due to heavier head on a weaker neck structure. In comparison, an adult head would be more inclined to hyperflex forward with the chin impacting the upper torso [7].

### 2.1.3 Thorax

Thorax is an important structure in terms of vehicle restraint systems. It plays a central role in the interaction with both seat belt and airbags during for instance frontal and lateral loading conditions. In order to optimize the restraint systems, further knowledge about the pediatric biomechanics of the thorax is required [8]. The skeletal structure of the thorax comprises 12 pairs of ribs, 12 thoracic vertebrae and the sternum as can be seen in Figure 2.3.

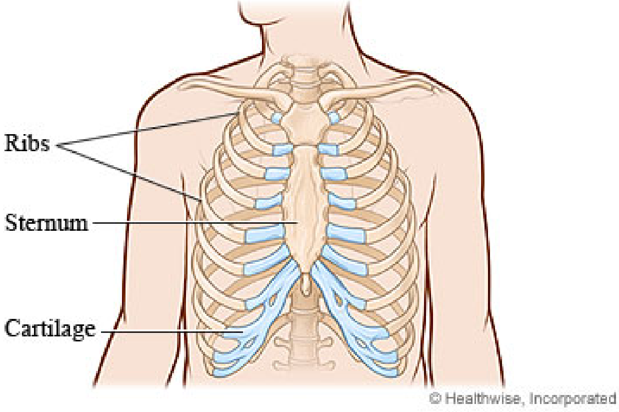

Figure 2.3: *Anatomical overview of ribs, sternum and cartilage [21].*

A number of ribs are coupled to the sternum using costal cartilage. Function of the thorax is for instance to protect the heart including the cardiovascular center, the lungs and the thymus gland. Sternum is constructed out of 6 primary bones which includes the manubrium, 4 sternebrae and the xiphoid process. Following the anatomical growth process, the final sternebrae is developed at about 1 year of age and the xiphoid process occurs during the interval from 3 to 6 years old. Sternebrae starts to fuse at the age of 4 years old and is continuous process which is finalized around the age of 20 years old. From a lateral view, the sternum is lowered in comparison to the vertebral column from infancy until the age of 2-3 years old. This event results in a downward angle of the ribs. As the child grows up, the costal cartilage will calcify, affecting the stiffness of the rib cage structure [2, 8]. Although limited, efforts have been made concerning the pediatric biomechanical properties of the thorax. Cadaver studies have demonstrated that the average breaking load under quasi-statically loading conditions for three ribs from child cadavers were 240 [N] [10]. In a study where a large inhomogenous group was investigated, results showed that the mean dynamic breaking loads for ribs in the age interval below 14 years old were 234 [N], peaking in the subsequent test group between 15-64 years old at 372 [N]. For elderly above the age of 65 years old the lowest value was measured to 173 [N] [22]. Another study [23] concluded that for the cancellous bones of the lumbar spine, ultimate compressive strength amplified throughout childhood reaching a peak at 20 years old followed by a decrease as a function of age. Additional research has concluded that the ultimate tensile strength of the costal cartilage at 0.46 [MPa] remains the same until the age of 19 years old, although the ultimate relative elongation declined until same age limit [10].

Performance corridors scaled from blunt sternal impact tests were estimated for a 3 year old and a 6 year old using a high-speed video camera complemented with an impactor accelerometer [24]. In a sternal impact test, the deflection is measured between the impactor and the spine. However, the number of pediatric PHMS test subjects for impact testing are relatively few, therefor additional methodologies needs to be developed in order to correctly assess the thoracic response of children [10].

### Thoracic Injuries

Commonly, children are less likely to receive rib fractures in comparison to grownups. Tests conducted on thoracic impact resulted in no pediatric rib fractures [25] meanwhile for adults tested under similar conditions a significant number received fractures to the ribs [26]. Theories for these results concerns a more flexible rib cage for children due to higher proportions of cartilaginous tissues and structural differences [2]. Instead of rib fractures, children are more likely to be subjected to pneumothoraces, i.e. collapsed lungs, which is less common among adults. Other implications may be damages to the heart [7]. This poses a concern when estimating a thoracic injury criteria for children or scaling thoracic injury criteria from adults since the primary injury mechanism comprises soft tissue damages, not rib fractures [10].

### 2.1.4 Pelvis

The skeletal structure of pelvis may be described as a ring consisting of two hemi-pelves joint posteriorly by the sacrum and anteriorly by the pubic symphysis. Each hemi-pelvis is constructed from three bones referred to as ischium, ilium and pubis which originates from three main ossification centers [27]. Following birth, the pelvis is primarily cartilaginous [2]. Ossification of the bone structures continues up to the age of 8 years old [2]. Full fusion appears at puberty, generating an increasingly stable pelvic ring [2]. Ossification of the iliac crest, a part considered important for the interaction with lap belt [2], will not be finalized until the age of 25 years old [27]. In belt fit studies of the lap belt, the projection Anterior Superior Iliacic Spine (ASIS) is considered an important landmark [27, 28]. Due to material properties in terms of a higher level of cartilage, the pediatric pelvis is able to absorb more energy prior to fractures than that of an adult pelvis. One study reviewing clinical data [29] of adults over the age of 16 years old were twice as likely to receive pelvic fractures in comparison to their pediatric counterpart.

## 2.2 AIS

The Abbreviated Injury Scale (AIS) categorizes injuries according to a severity based 6 level rating for each anatomical region where 1 is the lowest severity level and 6 is the most severe [30]. Estimated severity is rated based on the relative importance with respect to the entire body. Intended purpose of this scale is to standardize the classification of injuries received from vehicle crashes, creating a universal platform for injury comparison. In the revision from 2005, reasons for injury have been widened to include in principle all potential injury mechanisms using a 4-digit code [30]. Core principles associated with AIS comprise for instance that the scale should be simple to use, the terminology should be standardized, applicable for a wide range of injury causations and attuned for various sizes of data assortments. The ranking is categorized anatomically, i.e. geographically, instead of physiologically. Physiologically implies process oriented. AIS is time independent and assumes a baseline of a healthy average adult. Severity measurements are based on different dimensions such as threat to life, mortality, hospitalization, cost and duration for treatment, quantity of energy dissipated or absorbed, permanent impairment, disability and quality of life [30].

## 2.3 Injury Criteria

Injury criteria refers in this project to metrics commonly applied in the field of automotive impact scenarios which estimates the probability that an occupant sustain a particular injury. Criteria such as the global head injury criterion, angular head acceleration, neck injury criterion and chest deflection will be described.

### 2.3.1 Head Injury Criterion

Head Injury Criterion (HIC) is employed to estimate the probability of head injury when exposed to impact. Initially it was developed in the 1970s for motor vehicle accidents, but has later been adopted by other disciplines such as sports and protective equipment. HIC is originally founded on a tolerance curve derived by evaluating human cadaver heads exposed to free falls on rigid, flat surfaces where the forehead acted as initial surface of impact. Subsequently, additional tests comprising animals, human volunteers, clinical data as well as an increased spread of impact conditions has generated the modern HIC where skull fractures or concussion were considered as failure conditions [10].

According to SAE J1727 [31], HIC is calculated as presented in Equation 2.1 where $a(t)$ [g] refers to the resulting acceleration in X, Y and Z directions and $(t_1, t_2)$ [s] refers to the start versus end times of the averaging time interval. Interval limits are usually set to 15 [ms] or 36 [ms], but lower intervals can be used in order to maximize the HIC function [31].

$$HIC = (t_2 - t_1) * \Big(\frac{1}{(t_2 - t_1)} \int_{t_1}^{t_2} a(t)dt\Big)^{2.5} \tag{2.1}$$

The HIC criterion was developed for adults, yet efforts have been conducted to derive a pediatric HIC curve by employing the adult HIC combined with angular thresholds [32]. Elastic modulus of skull bone tissue has been used to derive material scaling[33]. In a NHTSA report concerning improved injury criteria, following scaling for HIC values have been proposed in Equation 2.2.

$$\lambda_{HIC} = \frac{(\lambda_E)^2}{(\lambda_L)^{1.5}} \tag{2.2}$$

In Equation 2.2, $\lambda_E$ represents the material scale factor whereas $\lambda_L$ depicts the scaling factor associated with length of the head [33]. Furthermore, NHTSA used a FE approach for scaling HIC values which compared a deformable head model with a rigid model of a dummy head. Breaking strain was implemented as failure condition where the 6 year old skull was estimated to an adult strain failure of 0.5% meanwhile 2% and 1% thresholds were utilized for the 3 and 1 year olds respectively. Limitations on both availability and existence of pediatric and adult tissue data must be considered when evaluating the results calculated for dummies seen in Table 2.2 [33].

| **Age Group** | **Breaking Strain** | **FEA $HIC_{15}$ Dummy** | **Scaled AAMA** $HIC_{15}$ |
|---|---|---|---|
| *1 YO* | 2% | 200-300 | 390 |
| *3 YO* | 1% | 300-400 | 570 |
| *6 YO* | 0.5% | 500-600 | 723 |
| *Adult* | 0.5% | 700 | 700 |
| *Small Female* | 0.5% | 700 | 779 |
| *Mid-Sized Male* | 0.5% | 700 | 700 |

Table 2.2: Scaling factors for $HIC_{15}$ based on Finite Element Analysis (FEA) methodology and AAMA proposal [33].

Due to insufficient biomechanical data and uncertainties in the scaling technique, NHTSA employed the values presented in Table 2.3 where the value of male and adult data was set to the maximum limit and engaged as a threshold for 6 year old as well as a small female. Although ATD thresholds cannot be seen as equivalent to HBM thresholds, due to limited availability of comparative data such values could be employed for comparison, potential indicators and discussion.

| | **Large Male** | **Mid-Sized Male** | **Small Female** | **6 YO** | **3 YO** | **1 YO** |
|---|---|---|---|---|---|---|
| *Proposed HIC15 Limit* | 700 | 700 | 700 | 700 | 570 | 390 |

Table 2.3: Suggested $HIC_{15}$ limits for dummy age groups [33]

### 2.3.2 Head Angular Acceleration Y axis

Angular head acceleration assessed around the Y-axis is calculated by comparing the Z-acceleration of the head's center of gravity ($a_{CG_Z}$) with the Z-acceleration of the skullcap ($a_{sc_Z}$). Measurements of the acceleration of the skullcap should be extracted at the same altitude (Z-coordinate) and lateral position (X-coordinate) as the **CG**, where **D** represents the distance between the two measurement points. Angular acceleration $a_{ang_Y}$ may be retrieved according to Equation 2.3.

$$a_{ang_Y} = \frac{a_{sc_Z} - a_{cg_Z}}{D} \tag{2.3}$$

### 2.3.3 Neck Injury Criterion

The neck injury criterion $N_{ij}$ consists of four metrics which includes forces via axial loading and moments in the sagittal plane. Indices are then substituted by TE, TF, CE and CF where T corresponds to tension, C for compression, E for Extension and F for flexion [33]. These parameters can either be calculated using data retrieved from the upper neck at the occipital condyle or at the base of the neck [31]. Prior to conducting the calculations according to Equation 2.4, the accelerometer data must filtered as recommended by SAE J211-1.

$$N_{ij} = \frac{F_Z}{F_{ZC}} + \frac{M_Y}{M_{YC}} \tag{2.4}$$

In Equation 2.4, $F_Z$ corresponds to the tension/compression force in the Z-direction and $M_Y$ represent the moment about the Y-axis, either at the occipital condyle or the base of the neck. $F_{ZC}$ and $M_{YC}$ are their critical intercept counterparts. For this project, only tensile forces will be evaluated based on thresholds used in the EuroNCAP protocol [34].

### 2.3.4 Viscous Criterion

Viscous criterion V*C is a predictive index which addresses injuries to soft tissue by take into account the deformation velocity combined with compression of the thoracoadbominal region [35] as demonstrated in Equation 2.5.

$$V * C = V(t)C(t) \tag{2.5}$$

Here, V(t) corresponds to the deformation velocity described as $V(t) = dD(t)/dt$ where D(t) is the deformation of the rib or abdomen. C(t) denotes the instant compression and is calculated according to $C(t) = D(t)/D_0$ where $D_0$ depicts the initial depth of the torso [35].

For ATD:s, the SAE J1727 recommends calculations according to Equation 2.6. Prior to the calculation of the V*C, the data should be filtered as endorsed by SAE J211-1 or CFC180 [31].

$$V * C = SF * dD_x/dt * dxD_0 \tag{2.6}$$

In Equation 2.6, $D_x$ represented the longitudinal chest compression, $dD_x/dt$ its velocity, $SF$ equals a scaling factor and $D_0$ corresponds to a normalization factor of the chest depth [31].

In 2008, Ouyang et al. conducted thoracic impact testing on pediatric Post Mortem Human Surrogates (PMHS) [25]. Results from the testing is depicted in Table 2.4.

| **Subject** | Impact Velocity $[m/s]$ | Chestband Deformation $[mm]$ | Sternal V*C $[m/s]$ | T4 acceleration $[g]$ | Force $[N]$ |
|---|---|---|---|---|---|
| 2 YO F [1] | 5.9 | 57.7 | 1.9 | 73.2 | 740 |
| 2.5 YO M [2] | 5.9 | 45.0 | 2.7 | 63.9 | 790 |
| 3 YO M [3] | 6.0 | 44.8 | 2.1 | 63.9 | 825 |
| 3 YO F [4] | 6.0 | 44.9 | 1.5 | 124.8 | 750 |
| 5 YO M [5] | 6.4 | 55.7* | 2.1 | 62.4 | 900 |
| 6 YO M [6] | 5.9 | 44.5* | 0.7 | 71.2 | 1200 |
| 6 YO M [7] | 6.5 | 31.5 | 1 | 91.7 | 1560 |
| 7.5 YO F [8] | 6.0 | 48.7* | 1.6 | 64 | 900 |
| 12 YO F [9] | 6.2 | 72.3 | 4.5 | 35.6 | 1130 |

Table 2.4: Results from thoracic impact tests on PHMS [25]

Average values from the test are enclosed in Table 2.5. Conclusions were drawn that the injuries sustained to the PHMS did not demonstrate any correlation between the parameters sternal V*C, peak T4 acceleration

| Age Group | Sternal V*C [m/s] | T4 accelerations [g] | Maximum Force [N] |
|---|---|---|---|
| *2-4 YO* | 1.35 +- 0.62 | 81.5 +- 29.2 | 776.3 +- 39 N |
| *5-12 YO* | 2.05 +- 0.5 | 65 +- 20.1 | 1138 +- 271.7 |

Table 2.5: Average results of thoracic impact testing [25]

or maximum chest deformation. One potential correlation could be drawn on energy dissipation and PHMS thoracic injury [25].

Out of the 9 test subjects, 7 retrieved post-mortal injuries out of which 6 was assessed as pneumothorax. Child thresholds concerning thoracoabdominal injuries are limited [25]. ECE-R44 implies injury tolerance of 55 g pending a duration of 3 [ms] [36] meanwhile in U.S., similar criterion for adult ATD:s is 60 g for 3 [ms]. Limitations associated with low precision of the chest band measurements of the study by Ouyang et al. have been addressed in a master thesis by Parent [24].

## 2.4 Crashworthiness

A single automotive crash event can be classified as a sequence of multiple collisions. Primary collision occurs between the car and another object such as other vehicles, road traffic users and stationary objects. Pending initial collision, the occupants will continue with the previous velocity of the vehicle. Usage of restraint systems will determine whether the occupants are going to continue with this speed head on until stopped by the interior environment of the vehicle including other occupants or being decelerated by the restraint system such as belt geometry and airbags. Concluding impact occurs between the occupant's internal organs and the skeletal structure or surrounding supporting tissues [20]. Loading conditions are commonly categorized as frontal, lateral, rear impact or roll-over. One variation of frontal impacts is overlap crashes where the front structure of the car collides with another vehicle at a lateral displacement of the car's full width. In addition to generating a different load distribution than full frontal crash, it also adds an angular motion to the vehicle. EuroNCAP conducts frontal impact tests using a 40 % overlap with a deformable barrier [34]. Another variation of frontal impact, also applicable to side impact, is the oblique loading direction which places the vehicle under an angle.

Frontal car crashes are the most common type of impact direction, occurring at a roughly estimated factor 2 when comparing to lateral impacts. However, due to a pediatric fatality rate close to twice as high for side impact and roll-over scenarios, the amount of child fatalities are about the same [20]. Fatality risk is in addition dependent on selected seat position within the vehicle [37]. Increased risk for severe injuries was observed for seat positions in proximity to the point of impact and intrusions.

Common denominator for all loading conditions is that the head is the most injured body part, regardless of age interval or restraint configuration as can be seen in Table 2.6. For children restrained forward facing in the rear seat, injury mechanism for head trauma comprises interaction with interior environment such as the door panel, windows and front seat [38]. Emergency maneuvers are actions such as steering and braking which occurs prior to impact of crash. Such maneuvers have been observed to influence the kinematic response of pediatric occupants as well as interfering with performance of restraint systems [38], suggesting that pre-crash scenarios should be included when evaluating head injuries. Among the loading conditions, less attention have been directed towards the variation for frontal/side oblique and frontal offset loading. For instance, a parametric study of belt interaction using sled tests of PMHS demonstrated that an amplified axial rotation of the torso during lateral oblique angle of 30° resulted in an increased sideways head excursion in comparison to full lateral impact [39].

| **Body Part** | **Frontal Crashes** | | **Near-Side Crashes** | | **Far-side Crashes** | |
|---|---|---|---|---|---|---|
| | **0–7 YO CRS** | **8–15 YO Seat Belt** | **0–7 YO CRS** | **8–15 YO Seat Belt** | **0–7 YO CRS** | **8–15 YO Seat Belt** |
| *General AIS2+ injury risk per 1000 children in crashes* | 3.0 | 12.7 | 6.7 | 29.3 | 3.6 | 14.6 |
| *Head [%]* | 55.7 | 49.3 | 60.5 | 69.6 | 46.8 | 59.3 |
| *Face [%]* | 8.2 | 10.4 | 1.2 | 4.6 | 3.2 | 6.7 |
| *Chest [%]* | 4.4 | 9.0 | 4.9 | 4.6 | 4.8 | 5.9 |
| *Abdomen [%]* | 4.4 | 8.3 | 1.2 | 6.3 | 3.2 | 6.7 |
| *Neck/spine [%]* | 2.2 | 1.5 | 2.5 | 1.5 | 1.6 | 2.2 |
| *Upper extremity [%]* | 7.1 | 14.4 | 8.6 | 8.9 | 27.4 | 14.4 |
| *Lower extremity [%]* | 18.0 | 7.0 | 21.0 | 4.6 | 12.9 | 4.8 |

Table 2.6: Probability of AIS2+ injuries stratified by loading direction as presented by Arbogast et al. [10]. Vehicle models from 1998 and more recent.

# 3 Children in Cars

A variety of child restraint systems (CRS) are available on the market where weight and age are primary distinguishing factors [20]. For younger children, devices such as Rearward Facing Child Restraints, Rearward Facing Convertible Restraints and Car-Bed Restraints developed for infants are available which commonly includes integrated belt restraint systems [20]. However, this study will investigate the effect of restraint systems for forward facing children utilizing the three-point seat belts, hence elaboration will proceed on belt positioning boosters. An overview of different CRS is provided in Figure 3.1.

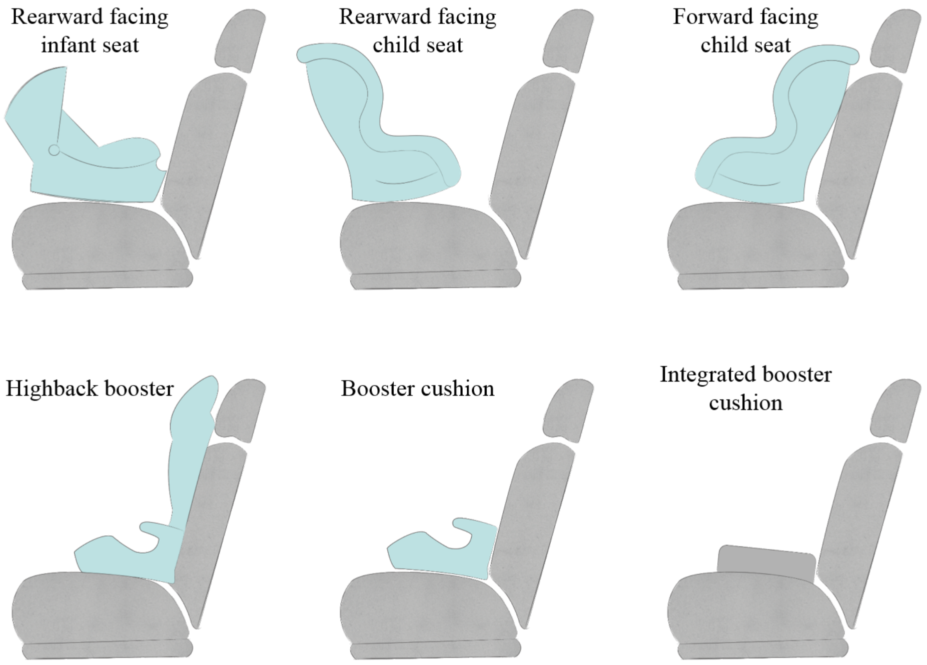
Rearward facing infant seat
Rearward facing child seat
Forward facing child seat
Highback booster
Booster cushion
Integrated booster cushion

Figure 3.1: *Schematic overview of typical CRS where the upper row contains restraint systems targeting smaller children which provides integrated belt systems. The lower row includes CRS for older children and utilizes the three-point seat belt provided by the car itself. For this study, the highback booster and the booster cushion will be evaluated. Image is provided by courtesy of Volvo Cars Corporation.*

Recommendations for usage of rearward facing CRS varies between different countries. For instance, in US the guidelines are set up to 2 years old whereas in Sweden the recommendation is up to 4 years old [40]. Since the rearward position distributes the load over a larger area, it is considered to be more efficient in reducing severe injuries and fatalities [7]. In for instance a frontal collision, by positioning the child rearwards the loads are transferred from the underdeveloped, weaker pelvis up to the back which is a stronger and wider structure. It also reduces loading of the neck induced by a proportionally larger head inertia. Since the pelvis will not be fully developed until mid puberty, belt positioning boosters are recommended between the ages of 4-12 in Sweden. Klinich et al. have provided guidelines in order to help parents assess their children's size with respect to appropriate restraint systems [41]. These included parameters such as standing height and clothed weight whereas age was not deemed a proper metric due to the anthropometric spread within each age group. They also concluded that children who were taller had an improved static belt fit in comparison to shorter children of the same weight. These findings support the need for individual assessments of suitable restraint setup which provides optimal protective affect for the specific child. Additionally, the report concludes that metrics such as age and weight are not sufficient for this type of classification.

## 3.1 Belt Positioning Boosters

Booster cushions, highback booster seats and integrated booster cushions are the three main types of belt positioning boosters (BPB) employing the regular vehicle seat belt [2]. Apart from the belt routing features of BPB, the elevation of the young occupants as well as the achieved seat cushion geometry play important roles for the belt fit [28].

CRS have an estimated fatality or severely injured risk probability reduction of 70 % [42] meanwhile seat-belt restraint system for adults was approximated to a risk reduction of 50 % during similar time period [20, 43–45]. In a static belt study conducted at UMTRI comprising 44 children in the ages of 5-12 years old, the booster setup of highest performance was able to provide optimal lap-belt scores with respect to the ASIS for at least 75 % of the test subjects. As a comparison, less than 25 % of the test subjects in the age interval of 6-12 achieved similar levels of belt score in the top performing vehicles without the assistance of a booster [3]. A further study of the data concluded that even children of the largest dimensions were subjected to worse lap belt fit when seated on a regular car seat than a child of the smallest anthropometric dimensions positioned in a low performance belt-positioning booster [3]. Another study observed children's seating postures with and without a belt positioning booster using naturalistic video analysis methodology [46]. During this investigation it was noted that approximately half of the test subjects slouched when positioned without a booster meanwhile when seated on a booster, slouching was seldom witnessed. If slouching occurred on the booster, the lap belt fit was significantly improved by the belt positioning guides of the booster. Risks associated with a slouching seating posture is loading of the relatively soft abdomen, instead of the pelvis, which can lead to severe internal damages and trauma to the lumbar spine. This phenomena is referred to as submarining. Slouched behaviour could be derived from the fact that the child's thighs were too short in comparison to the depth of the rear seat, causing discomfort. This conclusion is supported by findings of Reed et al. [28] which states that a straightened posture will positively influence the activation of the pelvis during crash loadings. Data analysis of the UMTRI static belt study concluded that the anthropometric variations had smaller effect on the belt fit than variations between boosters [28]. Effects of the lap belt anchorage were attenuated when using a booster cushion [28]. Another important aspect when evaluating booster cushions is the design of the restraint system which may enable improper usage if poorly developed. This is considered an important parameter since erroneous belt routing will significantly increase the safety inefficiencies of BPB.

Seat belts were originally designed and optimized for adult passengers [20], thus the booster provides elevation of the child and belt routing which are designed to improve the belt loading of the child. Improved lap belt fit reduces the risk of loading the abdomen instead of the pelvis [47, 48]. One study concluded that different vehicles provided different risk of abdominal injuries for children where the lap belt angle was potentially an important variable [49]. When a child outgrows the CRS with integrated belt systems, the boosters offers a transitional phase prior to using the stand-alone seat belts as the vehicle environment is usually still too large for the anthropometric dimensions of a child [3, 20].

### 3.1.1 Booster Cushions

Booster cushions are here defined as a backless BPB where the main purpose is to elevate the child to improve belt interaction and reduce slouchiness by providing a more comfortable leg position [41]. By improving the seated position, prevalence of seat belt injuries such as abdominal and spinal injuries associated with lap belt loading is reduced. Routing of the seat belt under the provided belt guides couples the booster cushion to the vehicle.

### 3.1.2 Booster Seats

Booster seats, or highback boosters, are publicly perceived as being more safe than their backless counterpart although no statistical difference in performance between the two has been demonstrated [50]. In addition, this study confirmed that BPB did reduce injury risk for children in the age interval of 4-8 years old.

If side structures are included for the booster seat, additional benefits are provided support for the head and torso of sleeping occupants or potential side protection for the head. In addition, the investigation concluded that side supports of highback boosters may confine the lateral motions during sleep [51]. One disadvantage is that the booster cushion places the occupant further away from the seat due to added back volume which may negatively impact the head kinematics with respect to the front seat. It has also been indicated that this position may be less comfortable for a subset of children. Research has demonstrated that when children are awake, the side structures makes the occupants lean forward in order to for instance see through the window or interact with the driver. Such induced behavior added even further displacement in the forward direction where the head and shoulders were not in contact with the backrest [46, 52]. A study performed on children in the interval of 7-9 years old concluded that the child occupants were less likely to maintain contact with the booster seats' back in comparison to occupants positioned on integrated booster cushions [46]. It was established that the children displayed a larger variation of seating postures in the booster seat than in the integrated booster cushion. Additionally, it was noted that a portion of the test subjects found it uncomfortable to be positioned with their back against the backrest and arms within the side structures.

### 3.1.3 Integrated Boosters

Integrated booster refers to built-in booster cushions in the vehicle [53]. The purpose of the integrated boosters is to facilitate utilization as well as reducing missusage of the child restraint systems [54]. Manufactured into the vehicle, the responsibility of proper installation is removed from the users. Additionally, it reinforces the coupling link between the cushion and the compartment of the vehicle [20]. Drawbacks are that it is not possible to move the booster to another vehicle or simply remove it once it has served its purpose [20]. According to literature, the reception of the integrated booster has been low although National Transportation Safety Board (NTSB) has provided recommendations that all car manufacturers should provide the option of integrated child restraints [20].

## 3.2 Seat Belts

Seat belt is an important restraint system which aims at coupling the occupant to the compartment's movements. In a crash, the vehicle's velocity will abruptly decelerate. An unrestrained occupant would in this scenario not be able to decelerate at the same pace and instead continue with the previous speed of the vehicle until colliding with the car's interior, most likely resulting in difficult traumas. For a restrained occupant, the belt will act with a restrictive force on the passenger in opposing direction of the travel which forces the passenger to comply with the kinematics of the compartment. This reduces injuries related to collision with the interior environment and distributes the impact during a prolonged time period [20].

A study conducted in Ontario on fatal crash data estimated an odds ratio of fatalities or severe injuries to be 0.6 between the belted and unbelted pediatric occupants in the age interval of 4-14 years old [55]. Another study executed in Wisconsin proposed that if all children in the age group of 8-15 years old would use seat belt, an estimated 72 % of the fatalities and hospital admissions would decrease with 45% respectively 32% [56]. Biomechanic optimization of seat belts today concerns the trade off between reducing the risk of belt-induced damages and impact on the thoraco-abdominal region while at the same time reducing head excursions and head interaction with the interior environment of the vehicle [39]. Proper seat belt fit is based on the principle that the belt should be placed onto body part which facilitates loading of skeleton instead of soft tissues such as subcutaneous, muscular and connective tissues [3].

### 3.2.1 Shoulder Belt

Optimal load path for shoulder belts is centered over the clavicle and continues along the thorax across the mid sternum [3]. Importance is emphasized on maintaining a flat belt web across the chest to accomplish an ideal load distribution. Inboard shoulder belt positions in proximity to the neck are concomitant with discomfort which may induce belt missuse behavior such as non-optimal rerouting of the belt. Shoulder belt located too far outboard may glide off the shoulder, reducing the belt's ability to restrain the chest during impact which could cause the occupant to roll-out of the belt and/or extreme head excursions combined with an amplified risk of injury [20, 28, 57]. A study comprising 155 children in the age interval of 6 to 12 has demonstrated that in order to attain a comfortable and proper utilization of the belt loading, the pediatric occupant must have a seated height of at least 74 cm [41].

#### Pediatric Injuries Shoulder Belt

Poor shoulder belt fit for children has been associated with amplified risk of skull, brain, neck and face damages [7, 58], in particular when the seat belt is subjected to improper routing such as behind the back [59]. Previously, research concluded that the probability of receiving injuries due to shoulder belt placement in proximity to the neck is relatively low [20], although some reports have been made about vertebral and spinal damages. However, it was not possible to exclude other factors due to deficient information concerning restraint and loading conditions [20]. Recent case studies have reported prevalence of shoulder belt-induced flexion-distraction fractures of the cervical spine [60]. These fractures occur between two cervical vertebrae where the inferior one is held back by the shoulder belt causing flexion of the neck to appear above the belt meanwhile the head continues forward, generating a momentum centered at the upper contact point of the belt and neck. This new rotational centre is shifted anteriorly of the neck and reduces the number of vertebrae included in the rotation. For children, the vertebrae may be dislocated which in turn can damage the spinal cord, leading to permanent impairments such as paralysis.

### 3.2.2 Lap Belt

The lap belt is intended to interact with the pelvis to achieve an optimal loading during crash. In order to acquire this interaction, optimal lap belt positioning is considered to be placed below the anterior superior iliac spines (ASIS) [3]. It has also been concluded that the lap belt should be placed fully below the ASIS on the thighs due to the paediatric pelvis geometry and postures [3, 61]. However, these spines begin to develop later where the earliest is at 10 years old. This poses a problem for optimal lap belt engagement for young children. In combination with the smaller pelvic area when seated, the risk for abdominal injuries increases [7].

Straight seating posture where the pelvis is placed as vertical as possible and properly positioned close to the back rest, with feet preferably on the floor, is important to acquire good lap belt fit. Apart from correct positioning below the ASIS, this posture reduces the likelihood of the belt gliding up to the abdomen. According to Burdi et al., straightened seating posture is less likely among children due to curvature of the spine as well as the pelvic angle [7]. The probability of slouching the pelvis increases if the length of the child's thighs is too short with respect to the rear seat cushion as they cannot bend the knees over the edge [41]. This argument was supported by an analysis of UMTRI data where shortening the cushion length have displayed improved lap belt fit [3]. A study conducted on predictors for abdominal injury probability among child occupants indicated that lap belt angle (lower anchorage) affected the risk of unwanted loading of the abdomen [49].

#### Pediatric Injuries Lap Belt

Seat belt syndrome comprises injuries inflicted on the abdominal region due to lap belt loading [28] where it has been demonstrated that the most frequent mechanism of injury is belt loading directly onto damaged organs. Examples of associated injuries are intestinal injuries, rupture of the mesenterey as well as spinal flexion-distraction injuries referred to as Chance fractures [47]. Children in the age interval of 4-8 years old are more likely to attain an abdominal injury graded to AIS2 than their younger (0-3 years old) and older (9-15 years old) counterparts. Children in the ages of 9-15 years old were less likely to attain abdominal injuries than the age group of 4-8 years old [49] and reasons for these discrepancies were generally assumed to be a correlation between body size and belt fit. Recent observations have however noted that pediatric test subjects in similar sizes of small grown-ups achieve achieved worse lap belt fit than the smallest test subject positioned in a booster. The study concluded based on laboratory findings and field observations that potentially the reason for a lower abdominal injuries in the older age group is not necessarily due to increased body size but rather derived from behavior and postural differences [28]. Another study reported that children below the age of 8 years old were four times as likely to receive a hollow visceral injury compared to a solid one when not employing appropriate CRS [62]. Another witnessed risk is the incidence of damages to the abdominal aorta in conjunction with bowel and/or lumbosacral injuries [63].

### 3.2.3 Parametric Studies of Shoulder Belt Interaction

A parametric study on pediatric shoulder and lap belt fit based on a distribution of vehicles was conducted at UMTRI on 44 children aged 5-12 years old, both with and without child restraints such as booster cushions and high-back boosters [64]. A regression analysis was performed on shoulder belt fit based on the following parameters; occupant stature, length of the seat cushion, angle of back cushion as well as locations of D-ring anchorage [3]. Location of the D-ring is defined by angles with respect to an estimated H-point. H-point refers to the Hip-point of physical ATD:s which is used to position the dummy correctly in a seat. Humans do not have a H-point, thus must this be approximated. Angles of the D-ring can according to the FMVSS 210 either be defined in the longitudinal plane [XZ-plane] or in the frontal plane [YZ-plane]. Upper and lower thresholds on the parameters have been depicted in Table 3.1.

| **Parameter** | **Range** | **Units** |
|---|---|---|
| *Seat Cushion Length* | 400-500 | [mm] |
| *Seat Back Angle [XZ]* | 18-33 | [°] |
| *D-Ring 1 [YZ]* | 18 -40 | [°] |

Table 3.1: Upper and lower interval limits of parameters associated with the interior environment of the vehicle.

Following the regression analysis, it was concluded that lap belt angle as well as the D-ring angle were the strongest predictors for lap and shoulder belt fit respectively [3]. The regression equations were applied on data from 46 vehicles for children in the range of 6-12 years old without the usage of booster-cushions [3]. It was observed that D-ring angles of 18° produced a shoulder belt position in too close proximity to the neck for 90 % of the 6 year olds. In contrast, the outboard angle of 40 degrees was assessed to be too far out on the shoulder for approximately 95 % of 6 year olds and basically all of the test subjects aged 12 years old [3].

Based on the UMTRI study, it was observed that both D-ring and lower anchorage locations had a greater impact on the shoulder and lap belt fit without a booster. It was also concluded that the usage of boosters were able to attenuate the influence of lap belt angle on lap belt fit. When secluding the shoulder belt routing associated with some high-back boosters, the position of the D-ring significantly influenced the shoulder belt fit [28].

Interaction between the shoulder belt and the rear back cushion was observed to confound the regression analysis of shoulder belt fit. For this study setup, the effect was abridged by removing the back seat bolster but it was not applicable for all vehicles. Further research was recommended to evaluate the impact of this interaction [28]. It was also concluded that simulations or dummies were potential methods for evaluating belt fit, assuming that the ATD:s are based on pediatric anthropometric data [28]. Only minor interactions between the D-ring locations and angles of the lap belt had been demonstrated during pre-tests, thus the study did not investigate the effect of these variables independently [3].

They concluded that for vehicles with most appropriate geometric conditions, 25 % of the children within the targeted age group received suitable lap belt fit. For the shoulder belt, it was observed that for 20% of the tested vehicles, the shoulder belt was too far inboard meanwhile another 20% of the vehicles facilitated a belt fit that was too far outboard. Thus, the study established that an estimated 75 % of the targeted paediatric group were improbable to achieve proper belt fit.

## 3.3 Energy Mangement - Pretensioner

Energy management in vehicle safety design comprise systems such as belt pretensioners, load limiters and airbags [2]. Until recently, energy management systems of the rear seat have received less attention than for the front seat occupants [65]. At the moment, an increasing trend has been observed in terms of confirmed benefits of including belt derived energy management systems in the rear seat, based on impact tests using ATD:s, adult PMHS and PMHS with child anthropometry [39, 66–69]. Advantages comprise risk reduction for injuries to neck and chest in frontal and lateral loading conditions as well as enhanced kinematic performances. Purpose of the pretensioner is to decrease slack in the seat belt which can lead to a more rapid coupling between the occupant and the vehicle [69]. Front seat typically employs pretensioners of higher forces such as 3 [kN], although the force experienced by the occupant is usually reduced due to a routing path over the D-ring. Typical force levels for rear-seat pretensioners approximate 1.5 [kN] [69]. A simplified curve representing the force loaded onto the shoulder belt by the pretensioner with a force of 1.5 [kN] will be implemented in the parametric study.

## 3.4 Missuse of Restraint Systems

Issues observed with child restraint system are missuse behaviors, which reduces the protective performance of the restraint system [20]. For high impact speed scenarios, this reduction in protection can have severe consequences. Naturalistic driving recordings have depicted a variety of seating positions associated with young occupants [46, 70]. Seated behavior of a child is influenced by both the design of the system as well as the time period and environment inside and outside of the car. For instance, side supports are advantageous if travelling by night or if the child is tired since the occupant may use these for support. On the other hand, if the child is awake in an active state or wishes to engage with the fellow passengers in the car, the side support could be in the way. Comfortability of the occupant is another important aspect which may induce missuse behavior [20]. In the scenario when a booster cushion is implemented, missuse behavior may be improper routing of the belt where for instance the shoulder belt may be drawn behind the child's back or beneath the arm. Positioning the shoulder belt underneath the arm is associated with heavy loading of thorax leading to internal injuries whereas routing around the back is concomitant with a higher positioning of the lap belt close to the buckle. Another scenario is that the lap belt may be positioned above the belt guides of the booster, which leads to direct loading of the abdomen. Belt slack is a different type of missuse which delays the coupling of the child and the vehicle compartment. Another observational study comprising 564 children in belt-positioning boosters identified at minimum one belt positioning error for 64.8 % of the cases. In this study, the most common missuses were that the shoulder belt was either placed above the armrest or not correctly positioned on the center of the shoulder [57]. Child occupants do not usually sit as a dummy ATD:s and pediatric seated posture can be either involuntary postures following the car's behavior or self-selected which is related to comfort or occupant activities [71]. Recommendations are to implement methods for evaluating missuse related to child restraints. Further research and developments should address evaluation tools for child occupants such as for instance pediatric ATD:s and HBM:s. This, in order to include a greater spread of sizes and ages as well as increasing the biofidelity of such tools which is an important factor in order to counter problems associated with missuse behaviour.

## 3.5 Pediatric Regulations and Recommendations

In the European Union, children with a height less than 135 [cm] must be restrained by appropriate child restraints approved by UNECE Regulation No 44/03 or No 129. Member nations of the UN are allowed to select between a height limit of 135 and 150 cm, where for instance Germany has determined a height limit of 150 up to the age of 12 years old. In U.S., the age limit for using child restraint varies between states where age interval for the laws may range from less than 1 year and include up to 7 year olds [40]. Additionally, the level of severity for breaking these laws varies among different states. Generically, children in U.S. aged 4-8 years old are recommended to use booster cushions. NHTSA recommends however to stay in a booster between 8-12 years old until the child has outgrown the booster [72].

Federal Motor Vehicle Safety Standards (FMVSS) is the U.S. counterpart of ECE R44 which are used for testing child restraints. Both utilize a specific test bench, where discrepancies between the bench and actual vehicle seats have been identified [73, 74]. Observations have been made concerning suboptimal development of independent child restraint systems dimensioned for passing the regulatory sled test but are not evaluated as a part of the entire car [52]. It is also argued that since booster cushions are utilizing the belt systems of the car, these seats should be developed and evaluated in the dynamic setting of the vehicle [75]. On the U.S. market, boosters are tested according to FMVSS 213 requirements which include a dynamic sled test on a standardized test seat in a frontal impact loading condition using crash dummies. There are no requirements placed on the static belt fit performance of the booster. Reed et al. highlights the inabilities of the dynamic testing to properly evaluate the static belt fit where one of the reasons addresses the limitations of the ATD:s to correctly capture the pelvic geometry of children [64]. Another concern of the setup is that the ideal conditions achieved with the test bench using positionable configurations for the D-ring and lower belt anchorage is not a realistic representation of the varying interior geometry of passenger vehicles. Additionally, since the boosters are not tested in a real car environment, the focus of the manufacturers concern the suboptimisation of the boosters in order to pass the tests which may reduce the overall performance of the booster in a car environment.

# 4 Anthropometric Assessment Devices

Conventionally, Anthropometric Test Devices (ATD:s) are utilized for crashworthiness tests. ATD:s are equipped with a set of sensors such as accelerometers, gyroscopes, load cells and deflection sensors which allow measurements of relevant forces and loads an occupant is exposed to during a crash scenario [34]. Video recordings, supported by sensor information, facilitate evaluation of the passenger's kinematic behavior during crashes. These devices are designed to be as biofidelic as possible in terms of form, distribution of mass, size and posture [76]. One fundamental difference between humans and ATD:s, from which the origin of discrepancies may be derived from, is the fact that in order to generate reproducible and reliable results the ATD, unlike humans, must survive multiple crashes without implicating the recorded data. Crash tests with ATD:s yield a great amount of valuable information in a physical environment, disadvantages are however that these tests are expensive and time consuming, and as they are fixed in size it is in general not possible to test for smaller anthropometric and age related variations. Dummies are typically developed for specific unidirectional loading conditions as for instance side, frontal or rear crashes, providing different optimizing features and measurement devices for each dummy. For pediatric occupants, the main dummy series comprise the Hybrid III (3, 6, 10 years old), CRABI, the P (9 months, 18 months, 3, 6, 10 years old) and the Q (0, 1, 1.5, 3, 6, 10 YO) series [2]. The dummies are created based on pediatric anthropometric databases, where for instance the Q-dummies are based on the CANDAT database which includes data from U.S., Europe and Japan [76].

A study using X-ray data compared the pelvises of children where the test subjects were of ages 3, 6 and 10 years old with P-dummies of corresponding ages [61]. These findings found significant differences between the child and dummy pelvises. Although the height of the iliac crest was relatively in accordance to the children, incorporations of the ASIS landmarks were not addressed. In addition, the front geometry of the pelvises was not aligned with the pediatric volunteers. Conclusions were made that the ATD's pelvis was not representative of a child's pelvical anatomy. Implications have also been observed for the shoulder belt interaction and the chest deflection when using the Q6-model [77]. Here, the chest deflection was not aligned with risk of thoracic damages. For instance, the area of the deflection sensor was considerable stiffer than the ATD's ribcage and when the shoulder belt glided of the sensor area, estimations of the chest deflection was significantly undervalued.

Limitations of pediatric data and availability of test specimens have resulted in that the Injury Assessment Reference Values (IARV) for child ATD:s have been derived mainly through geometrical scaling of adult values. Reasons such as different body proportions and material properties are therefore neglected or insufficient, reducing the biofidelity of the pediatric IARV:s [27].

## 4.1 Human Body models

Rapid development in computer hardware and software has made computer-aided engineering (CAE) an important asset within the automotive industry. A general tendency can be observed of transitioning from physical testing to simulation evaluations. For passive safety such as evaluation of restraint systems or structural impact, FE-modelling today plays a vital role in both the industrial sector as well as the research field [78, 79].

Human Body Model (HBM) is an anthropometric tool utilized in a software simulation environment. In contrast to the dummy ATD:s, the HBM is characterized by a higher level of direct customization to a lesser cost. Potential features such as scalability in terms of age and size distribution within the specific age group facilitates testing of an environment for a larger population containing a wider spread. These features are in particular interesting for pediatric modelling and evaluation of child restraints [76]. Whereas the dummy ATD:s are in general designed for one main direction of impact loading such as lateral, frontal or rear crashes, HBM:s are typically omnidirectional which implies that the same HBM can be utilized for different loading conditions. This also enables the potential to evaluate effects of multiple crashes consisting of different loading directions in the future.

Another important aspect of the HBM is the potential to evaluate supplementary injury criteria, such as for instance stress and strain levels experienced by a specific body part. An ATD has specific sensor locations which supports reproducibility but is also a subject to limitations. For the HBM, the resolution of measurements points may increase as they are not restricted by physical sensors. As previously described, the biofidelity of the ATD has been questioned which is partly related to the fact that the dummy must surpass the crash without damages in order for the data to remain valid. Such restrictions are not applied on the HBM, thus providing an opportunity to incorporate an increased flexibility of joints and tissue, making the model increasingly biofidelic. A common denominator for both the HBM and the dummy ATD is the lack of tissue validation data as well as biomechanical kinematics analyses, requiring more extensive research [76]. FE-models require a considerable amount of high resolution medical data in terms of Computed Tomography (CT) and Magnetic Resonance Imaging (MRI) scans. CT-scans may be used to generate a statistical platform of skeletal parts meanwhile the MRI is mainly used to construct the thoracoabdominal tissues [76].

Human body models are typically categorized as being either Multi-Body (MB) models or FE-models, where this thesis will evaluate the performance of one model from the latter, thus only a brief description of MB-models will be provided. FE-models can be further divided into being either passive or active which refers to the activation of muscle tissue. PIPER scalable child HBM is a passive FE-model.

### 4.1.1 Multi-Body Models

MB models are constructed using ellipsoids with kinematic joints. Advantages of these models are shorter computational times and they are relatively easy to use. Contact definitions are however complex and MB:s are mostly used for kinematic analysis [2].

### 4.1.2 Finite Element Models

Characteristics of FE-models comprise high levels of geometrical details for crash simulations with strong contact definitions. Contact definitions are important when analyzing the interaction between the occupant and the restraint system. In particular, FE-models are suitable for assessing injury risk curves when exposed to impact [6]. For instance, computational head FE-models have been advantageous in establishing injury thresholds for Traumatic Brain Injury (TBI) [12].

FE methodology is able to capture advanced geometrical features associated with human anatomy and age related effects in terms of growth [80]. Research has mainly concerned the generation of adult HBM [81, 82] meanwhile pediatric HBM are less prevalent [6, 82]. Due to limited availability of validation data, the models are to a larger extent based on assumptions [82]. One study implied that a pediatric HBM was more likely to capture the interaction with the seatbelt when implementing CRS than the ATD Q6 dummy [77]. These observations entailed both abdominal interaction with lap belt as well as loading from the shoulder belt.

Another area of interest would be to employ the positioning feature of scalable HBM:s which may provide a platform for investigating potential restraint missuse. Such positioning may be difficult with ATD:s due to physical limitations of the dummies' kinematic pattern. Recently, occurrence of adult HBM:s with implemented active muscle response have emerged [81]. Although the main focus for FE HBM is crash loading, by incorporating active muscle response, it would be possible to add restraint systems evaluations in pre-crash scenarios to the repertoire [71, 83].

## 4.2 PIPER Scalable Child HBM

Position and Personalize Advanced Human Body Models for Injury Prediction (PIPER) is a result of a European collaboration. Prior to initiating the project, one identified issue was difficulties in positioning advanced FE HBMs utilized for predicting injury tolerances, thus reducing their prevalence in automotive industry despite acknowledged potential. Another concern was the limited offering of anthropometric variations as well as models for different age groups, in particular for children. Hence, the purpose of this project was to overcome such barriers for implementation, resulting in an open source scalable child model together with a publicly available software for positioning and scaling of FE models. In addition, the software is intended to be non-specific which implies application for other HBM models in addition to the PIPER models [4].

PIPER scalable child HBM is a pediatric FE-model developed in LS-DYNA explicit FE code. Baseline of the model consists of a 6 year old with a mass of 23 [kg] and is scalable within the range of 1.5 to 6 year old [6]. Aim of the model is to capture the age-related differences in anatomy and material properties which was pursued by using medical imaging techniques. CT scans of children aged 1.5, 3 and 6 year old were acquired [84]. Organ and bone outlines as well as areas undergoing cartilage growth were detected using semi-automatic segmentations. Main portion of the skin was additionally retrieved from CT scans, although postprocessing was required. Since the CT scans were attained in a supine position of the test subjects, manual adjustments of vertebrae were executed based on MRI scans of seated adults [85]. Normalization of anthropometric measurements was conducted by incorporating nonlinear scaling in terms of Kriging interpolation referencing Generator of Body Data (GEBOD) regressions [6, 84, 86]. PIPER baseline model attained a stature of 1146 mm and a seated height of 631 [mm] and the scalability correlated well to the UMTRI model [87] for comparable intervals of anthropometric dimensions [84].

PIPER consists of an estimated 542 0000 element divided into 353 anatomical configurations. Model time step during development was $0.32s$ [$\mu$] attaining a 15 gram additional mass scaling [6, 84]. In its final form, the PIPER model comprises of Geometrical data and Metadata. Geometrical data describes the node components, element components (1D, 2D, 3D element types), local coordinate systems and group components. The Metadata structure refers to the functional constrictions and anatomical structures associated with the FE model [88].

### 4.2.1 Validation

Validation of the model included for instance compression and drop test for the head anatomy. Tensile and bending validations were executed for the cervical spine whereas seat belt interaction evaluation and pendulum assessments were conducted for the trunk. Lower extremities were subjected to bending tests and flexibility testing of the vertebral column which was performed using sled tests. In addition, PIPER's performance during lateral impact was evaluated for the pelvis and shoulder area [6, 89]. Out of available validation data in literature, pediatric PMHS validation experiments have been ranked the highest. Validation sets for both frontal and lateral impact have been included in order to evaluate the omnidirectional property associated with HBM:s [84]. Notion should be made concerning the fact that not all validations test have been iterated for updated versions of the PIPER model. Validation matrix for the PIPER scalable child HBM is provided in Appendix A as presented by Beillas et al. [84].

Initial development of the head model was conducted in 2016 by Giordano et al. [80], followed by additional updates. General anatomy of the head model comprises the skull bone, cerebrum, meninges, cerebellum and the cerebrospinal fluid [84]. Spatial resolution was determined to range between 3-5 [mm] which is a trade-off between inclusion of important anatomical details meanwhile achieving stable computations executed within a realistic time period [84]. Assigned material properties to head tissue can be seen in Table 4.1. Here, $E$ [GPa] represents Young's modulus and $v$ corresponds to Poisson's ratio. $\mu_1$ and $\mu_2$ [Pa] describes the first and second shear modulus. $\alpha_i$ are exponents associated with Ogdens hyperelastic model and express material specific constants. $G_i$ [kPa] are shear relaxation modulus, $\beta_i$ [1/s] are shear decay constants and $K$ [GPa] is the bulk modulus. $\rho$ denotes the density expressed in [kg/m$^3$].

| Tissue | Material Properties | Density |
|---|---|---|
| *Scalp Connective Tissue* | Ogden $1st$ order + viscosity<br>$\mu_1 = 12.98 \times 10^4, \alpha_1 = 24.23, G_1 = 1348$<br>$G_2 = 1572, \beta_1 = 3.03, \beta_2 = 0.404$ | 1133 |
| *Scalp Adipose Tissue* | Ogden $1st$ order + viscosity<br>$\mu_1 = 3992, \alpha_1 = 8.82$ | 1133 |
| *Outer Compact Bone* | $E = 9.32, v = 0.22$ | 2000 |
| *Inner Compact Bone* | $E = 9.32, v = 0.22$ | 2000 |
| *Porous Bone* | E=1.0, v=0.24 | 1300 |
| *Brain Tissue* | Ogden $2nd$ order + viscosity<br>$\mu_1 = 53.8, \alpha_1 = 10.1$<br>$\mu_2 = -120.4, \alpha_2 = -12.9$ | 1040 |
| *Cerebrospinal Fluid* | $K = 2.1$ | 1000 |
| *Dura mater, falx, tentorium* | Ogden $1st$ order + viscosity<br>$\mu_1 = 1.78 \times 10^5, \alpha_1 = 23.07$<br>$G_1 = 1.25 \times 10^4, G_2 = 956, G_3 = 2670$<br>$\beta_1 = 2.37, \beta_2 = 0.23, \beta_3 = 0.02$ | 1133 |
| *Pia Mater* | $\mu_1 = 1.40 \times 10^4, \alpha_1 = 23.55$<br>$\mathrm{G}_1 = 1030, G_2 = 78.9, G_3 = 220$<br>$\beta_1 = 2.37, \beta_2 = 0.23, \beta_3 = 0.02$ | 1133 |

Table 4.1: Assigned material properties of PIPER's head model [6]

### 4.2.2 Neck

Meshing of the cervical vertebrae was derived from neck CT-scans retrieved from a 3 year old child. In addition to the vertebrae, the intervertebral disks, the annulus ground substance and the nucleus pulposus were included [84]. Discrete spring elements were implemented to model the main portion of ligaments apart from the transverse ligaments and the vertical cruciate which were described using shell elements. Reason for this is to enable contact surface between the dens of the atlas and the ligament. Neck muscles were replicated as discrete elements coupled in series with attachments to neighboring vertebrae processes to facilitate bending movement [84]. Height of vertebrae and facet angles have been considered in the age-related scaling [90]. Material properties of the neck was retrieved by scaling adult values [91]. In the validating bending tests of the neck it was concluded that the response was within the interval as specified by PMHS testing, although observations should be made concerning the small group of PMHS data [84].

### 4.2.3 Thoraco-abdominal and Pelvic regions

The thoraco-lumbar vertebral column was constructed of rigid vertebrae and coupled by 6 d.o.f beams whereas the ribs, sternum and costal cartilage consist of deformable elements. Connection between the rib cage and the vertebral column was in addition made using 6 d.o.f beams. Efforts have been made to reduce space between the organs. Heart of the PIPER was reproduced as an incompressible bag whereas the lungs consists of compressible bags. In addition, the pelvic is modelled using deformable elements and includes age-related growth cartilage [84]. Muscular tissues of the abdominal wall and retroperitoneal tissues are detached from the flesh tissues, facilitating definitions of the abdominal cavity.

### 4.2.4 Upper and Lower Extremities

Femur and humerus were modelled using deformable elements, with exception of the distal end of humeral diaphysis which in turn was modelled using rigid elements. In addition, the hands, radius and cubites were modelled as rigid. For the glenohumeral and sternoclavicular joints as well as the scapula, sliding contacts have been employed to enable biofidelic movements [84]. Femur diaphysis and tibia fibula comprise deformable elements, and the hip joint was designed as a deformable joint. Patella, distal femur and feet are composed as rigid bodies where the attachments to knee and ankle joints were modelled using 6 d.o.f beams [84].

### 4.2.5 Virtual Sensors

In order to facilitate comparison with dummy ATD:s, in particular Q-dummies, sensors have been integrated in PIPER at similar locations as can be seen in Figure 4.1. Accelerometers were positioned at the head center of gravity, in the posterior of the chest at an altitude of the T6 vertebra and in the pelvic center of gravity. Load cells positioned at the intervertebral disks enables assessments of momentum and forces alongside the vertebral column. Interpolation nodes positioned at the sternum allow chest deflection measurements whereas interpolated nodes alongside the rib cage enables lateral chest compression. Nodal force group measure loading of the abdomen [6].

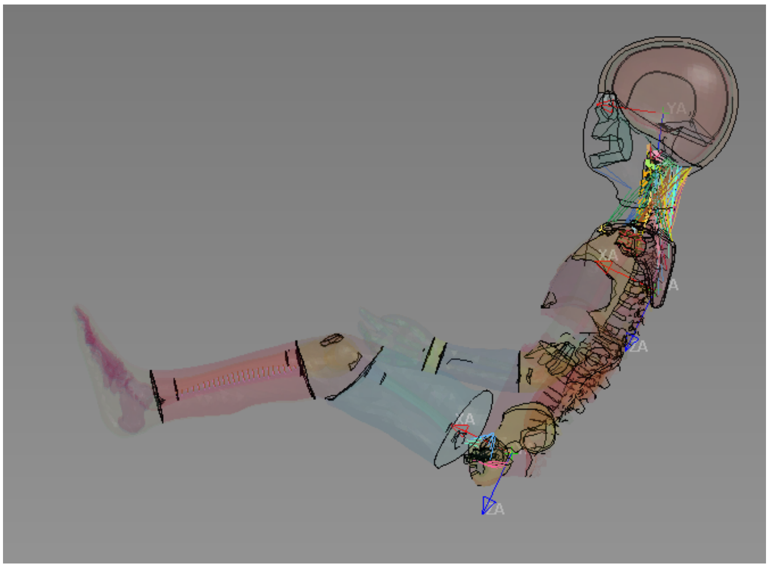

Figure 4.1: *Positions of head, chest and pelvis virtual sensors of the PIPER scalable child HBM.*

### 4.2.6 Future of the Model

Sensitivity analyses will be continued in order to investigate minor discrepancies between the PIPER model and test data [89]. Although it is not anticipated that the response of the model will be coherent with all data samples, the main focus is to understand the level of biofidelity and potential reasons for differences. It should also be noted that the validation material may not be exhausting, where further joint efforts of pediatric material properties research may yield supplementary results. One objective is to implement the ability to scale with additional anthropometric databases than GEBOD, as for instance the Snyder database. PIPER framework already enables dimensioning towards external data sets. Additional databases may also provide the opportunity to test the full boundaries associated with R129 or to generate populations based on other metrics such as BMI. Future work will also target evaluation of injury criteria [84].

## 4.3 PIPER Framework

Initial purpose of the PIPER software framework was to facilitate positioning and scaling of advanced FE HBM models, a task which has been identified as a barrier for industrial implementation [88]. Although the software contains modules specifically designed for the PIPER scalable child HBM, it is intended to function for a variety of HBM models and FE softwares. In Figure 4.2, a schematic overview of available modules in the PIPER framework software is been presented.

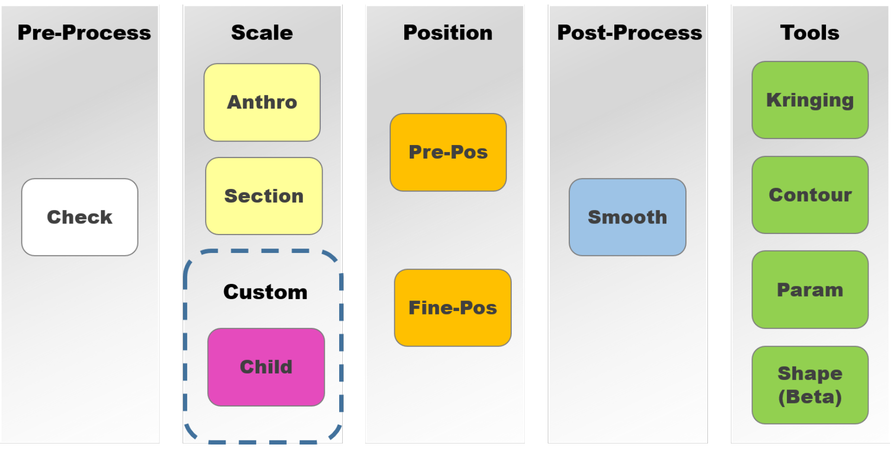

Figure 4.2: *Schematic overview of modules in the PIPER framework software.*

Beneath, some of the modules relevant for the project as well as the applied methodology will be described.

### 4.3.1 Check

First step when importing the HBM model is to examine the model using the Check Module which provides a Diagnostic interface as well as a 3D view. In the Diagnostic interface, information about the model and corresponding metadata is presented.

### 4.3.2 Scaling

Scaling module of the PIPER framework incorporates Kriging nonlinear interpolation [92] with respect to control points generated from Generator of Body Data (GEBOD) regressions [84]. Control points are a set of nodes selected on the baseline of the HBM-model. Interpolation methodologies based on control points refers to the mapping of baseline control points to the target positions by employing a transformation function [92]. Kriging interpolation is a global interpolation method which approximates this transformation function using weighted averages of the target control points' coordinates [92]. Apart from morphing of anatomical landmarks, additional local sets of control points were specifically assigned for age related affects such as proportional differences and facet angle differences in the vertebral column [6]. Anatomical landmarks of the head in combination with dimensions from Snyder et al. 1977 database were used to derive local control points of the head anatomy [84].

### 4.3.3 Pre-Positioning

The pre-positioning module enables interactive placement of body parts where one method is based on angles of anatomical joints with respect to their local coordinate systems. Second option is the controller which translates and rotates skeletal bones which references to the global coordinate system or the local coordinate system of the pelvic. Following importation of the HBM-model to the software, soft tissues are assigned deformable modules and bones are labelled as rigid modules. Movement trajectories of the selected positions are then solved in real-time using equation solvers [6]. Once the final position is achieved, the mesh of the HBM is updated. Observations should be made concerning an error in the software which at the moment excludes positioning of neck, hence this step in the methodology is neglected [88].

### 4.3.4 Smoothing

Upon altering the position of body parts, undesired deformation of the FE mesh such as sharp creases may occur in proximity to the activated joints. The crease detection functionality may be used to identify such deformities in the skin of relevant parts by employing a cluster algorithm which classifies elements according to modifications of their dihedral angle with respect to a baseline model [88]. Dihedral angle refers to the angle between two adjacent elements. Element clusters containing angles which differs above a determined threshold will be identified for further smoothing. In this scenario, the skin of the upper extremities, the trunk and the lower extremities were selected for crease identification.

The next step is to perform a pre-smoothing of the surface using the Taubin Algorithm. This method operates by employing a windowed sinc function interpolation filter to smooth 2D elements which improved minor defects of the surfaces [88]. Smoothing is conducted on potentially identified clusters of the previously selected skin entities. The surface mesh restoration does not affect solid elements where an increased number of deformities may be contained. Thus, mesh evaluation tools are used as pre-cursors before applying Kriging in a box-interpolation which employs similar interpolation technique as previously described, although here in a confined area with the baseline model as reference.

## 4.4 Finite Element Method

Finite element method (FEM) is a numerical technique that approximates partial differential equations and is commonly applied in areas such as structural analysis, fluid dynamics and heat transfer [93]. Analytic solutions may be solvable for simple scenarios, but for more complex cases, numerical methods may be considered necessary. One fundamental principle of FEM is discretization which, in this field, divides a geometry into a network of smaller, finite elements referred to as mesh containing assigned nodal points. These elements can be selected in different forms such as for instance beams, quadrilaterals, triangles or polyhedrons depending on the problem and the dimensions of the structure. Since FEM employs interpolation between the nodes, size of the mesh elements plays a vital role in ensuring convergence of the solution. Reduction of element sizes increases the accuracy of the solution, accompanied by an increase of computational time. Larger elements reduce the computational time, however the accuracy is decreased and too large elements may not be able to converge towards a solution. For each element, a set of nodal equations is assembled, thus FEM is constructed by equation systems of finite partial differential equations. Such approximations are optimized by minimizing the error functions. Estimations of errors can be conducted as a priori, which addresses derivatives and data from the exact solution of the weak formulation. A posteriori error estimations, on the other hand, concern data and derivatives of the approximate FE solution and associated derivatives. Error estimations relates mesh size to convergence of the function. Although a priori errors can estimate convergence, unknown information makes it difficult to estimate where the element size should be smaller. Instead, in adaptive mesh generation, a posteriori error estimates are commonly applied in order to optimize the mesh size for areas which require a higher degree of accuracy [94]. For similar reasons, selection of time step plays a vital role in the convergence of the solution.

Engineering problems may roughly be classified as dynamic or static. In a dynamic analysis, forces at the nodal points are affected by inertia and damping whereas for static or quasi static analyses, these factors may be neglected. In addition for dynamic analysis, the time response is deemed important. Equation 4.1 represents the equation of motion as used in direct integration FEM [95]. Here, **M** represents the mass matrix, **C** the damping matrix and **K** denotes the stiffness matrix. **U** corresponds to the nodal positions and the subnote $n$ represents the time step index. Non-linear material properties forces the stiffness matrix **K** to become a function of time and nodal displacements.

$$[M]\ddot{U}_n + [C]\dot{U}_n + [K]U_n = R_n^{ext} \tag{4.1}$$

Direct integration methodology can be categorized as explicit or implicit. In explicit form, the following time step is calculated based on the previous displacements and its derivatives. In implicit methodology, the subsequent position of the time step is estimated based on the derivatives of the succeding position, thus requiring prediction of the derivatives [95]. Static analyses are typically conducted by employing implicit FEM whereas dynamic simulations can be solved both explicitly or implicitly. Two examples of explicit and implicit methodologies will be presented below.

### Explicit Direct Intergration

This method is based on the central difference theorem where the derivatives of the nodal points **U** may be estimated using Equation 4.2 and 4.3.

$$\dot{U}_n = \frac{1}{2\Delta t}(U_{n+1} - U_{n-1}) \tag{4.2}$$

$$\ddot{U}_n = \frac{1}{2\Delta t^2}(U_{n+1} - 2U_n + U_{n-1}) \tag{4.3}$$

$U_{n+1}$ and $U_{n-1}$ may be estimated using Taylor series expansions to a second order accuracy. Combining Equation 4.2 and 4.3 with the equation of motion 4.1 yields Equation 4.4.

$$\left[\frac{1}{\Delta t^2}M + \frac{1}{2\Delta t}C\right]U_{n+1} = R^{ext} - [K]U_n + \frac{1}{\Delta t^2}[M](2U_n - U_{n-1}) + \frac{1}{2\Delta t}[C]U_{n-1} \tag{4.4}$$

Explicit direct integration is in comparison computationally economical since the internal forces, such as the stiffness matrix multiplied with the current nodal positions $D_n$, can be performed by calculating the summation of the contributions from each element in contrast to reformation and storage of $\mathbf{K}$ for each $\Delta t$. This methodology is in addition capable of handling certain non-linear material properties dependant on strain since the position of $U_n$ is already known, resulting in that the corresponding strain is consequently identified.

Explicit FEM is conditionally stable which implies that the critical time-step must be smaller than the ratio between the minimum element length $l_e$ and the acoustic wave speed $c_e$ as demonstrated in Equation 4.5. This condition is referred to as the CFL after the researchers Courant, Friedrichs and Lewy whom proposed it [95] and could be interpreted as that the time-step should be small enough to restrict the information transmission to not exceed more than one element per time-step. $c_e$ is calculated based on the Young's modulus $E$ and the material density $\rho$. $\omega_{max}$ refers to the highest natural frequency.

$$\Delta t_{crit} \leq \frac{l_e}{c_e}, \quad \left\{ \begin{array}{c} \omega_{max} = 2c/L \\ \text{c}=\sqrt{E/\rho} \\ \Delta t \leq 2/\omega_{max} \end{array} \right. \tag{4.5}$$

In order to achieve larger time-step without violating the CFL condition, one approach is to implement a technique referred to as mass-scaling. Mass-scaling adds a non-physical mass to the structure which allows the time-step to become larger. Adding non-physical mass will affect the results since mass plays a crucial role in force calculations. However, in certain scenarios it may be possible to add non-physical mass without compromising the results such as a small, non-critical area where the effect of mass-scaling may not be significant for the results, thus reducing the computational time.

### Implicit Direct Integration

In contrast to the explicit integration, implicit integration methods are unconditionally stable which does not put a restraint on the time-step other than the degree of accuracy. The trapezoidal rule is commonly implemented and Equation 4.6 and 4.7 represents how the nodal positions and derivatives are connected [95].

$$U_{n+1} = U_n + \frac{\Delta t}{2}(\dot{U}_n + \dot{U}_{n+1}) \tag{4.6}$$

$$\dot{U}_{n+1} = \dot{U}_n + \frac{\Delta t}{2}(\ddot{U}_n + \ddot{U}_{n+1}) \tag{4.7}$$

These equations can be solved for $\dot{U}_{n+1}$ and $\ddot{U}_{n+1}$ as presented in Equations 4.8 and 4.9.

$$\dot{U}_{n+1} = \frac{2}{\Delta t}(U_{n+1} - U_n) - \dot{U}_n \tag{4.8}$$

$$\ddot{U}_{N+1} = \frac{4}{\Delta t^2}(U_{n+1} - U_n) - \frac{4}{\Delta t}\dot{U}_n - \ddot{U} - n \tag{4.9}$$

By combining Equation 4.8 and 4.9 with the Equation of motion 4.1, Equation 4.10 is yielded where the effective stiffness matrix $K^{eff}$ and the effective load vector $R^{eff}$ is presented in Equation 4.11 and 4.12 respectively.

$$[K^{eff}]U_{n+1} = R^{eff}_{n+1} \tag{4.10}$$

$$K^{eff} = \frac{4}{\Delta t^2}[M] + \frac{2}{\Delta t}[C] + [K] \tag{4.11}$$

$$R^{eff}_{n+1} = R^{ext}_{n+1} + [M]\left(\frac{4}{\Delta t^2}U_n + \frac{4}{\Delta t}\dot{U}_n + \ddot{U}_n\right) + [C]\left(\frac{2}{\Delta t}U_n + \dot{U}_n\right) \tag{4.12}$$

For linear cases, the effective stiffness matrix may be constructed and factored once, followed by forward and backward substitution. For nonlinear material problems, the effective stiffness matrix is a function of the subsequent step $U_{n+1}$ and potentially its time derivatives, which are not known. Thus, the stiffness matrix must be predicted by estimating the succeding step, requiring iterative operations [95]. In scenarios of significant non-linear material properties, it may be difficult for the solution to converge, hence recommendations are made to employ explicit integration for impact reconstructions.

# 5 Objective

## 5.1 Purpose

Purpose of this thesis is to assess the capabilities of the PIPER scalable child HBM and PIPER framework software to be used in an industrial setting as well as for substantial research efforts such as epidemiology simulations. This will be conducted by investigating the sensitivity of the PIPER human body model concerning interaction with the shoulder belt using a parametric study approach where the D-ring position is altered with respect to the H-point in the YZ-plane. In addition, the effect of using belt-positioning boosters with and without high-back will be evaluated in both full frontal and frontal offset loading conditions as recommended by EuroNCAP. Due to limited pediatric threshold data, comparison of injury criteria will be evaluated against thresholds designed for dummies as well as relative differences between various loading conditions and safety setups. A biomechanical comparison with a PMHS study by Lopez-Valdes et al. [68] will additionally be performed, including comparison of kinematic trajectories and measured force exposures.

No physical tests will be conducted during this project. Therefore, verification is limited to available literature and data sources. Limitations are set to one-occupant scenarios. In case of successful verification of the tool, interaction with vehicle interior for one occupant may be complemented. Following research questions have been formulated to capture above mentioned targets.

- *How do changes in the shoulder belt affect the response of the PIPER scalable child HBM in frontal and frontal offset scenarios?*
- *How robust is the PIPER scalable child HBM?*
- *How user-friendly is the PIPER scalable child HBM and the PIPER framework software?*
- *Does the PIPER scalable child HBM reproduce reasonable kinematic behaviour?*
- *Does the PIPER scalable child HBM reproduce reasonable injury criteria values?*

Positioning of the PIPER scalable child HBM will be conducted in the PIPER framework whereas the impact simulations will be performed in the LS-DYNA environment using LS-PrePost interface. Final phase of the project entails data analysis and comparison to findings in the literature review.

# 6 Methods

## 6.1 Feasibility Study

Chiara Giordano et al. evaluated the PIPER scalable child HBM's performances by reproducing three accident reconstructions using simulations. Retrieved data was then compared to the corresponding physical crash-tests accident reconstructions using Q-dummies [6]. In their work, they introduced a methodology for working with both the PIPER scalable child HBM and the framework. Reproduced cases were selected from the CASPER project database where detailed accident data had been collected. Case 2017 was selected as suitable for this feasibility study due to the usage of 3-point seat belts, the age of the child occupant and the usage of a booster cushion which are aligned with the objective of this Master's Thesis project.

The aim of the feasibility study was partly to become acquainted to the PIPER scalable child HBM, the PIPER framework software and the implementation of PIPER in the LS - Dyna environment. Additionally, it could be viewed as an initial robustness, sensitivity and reproducibility test of the PIPER scalable child HBM. Limitations comprised restricted information concerning seat belt data and exclusion of neck positioning due to a an error in the PIPER framework.

### 6.1.1 Background: Case 2017

Child occupant in Case 2017 was a 5 year old boy seated on a Team Tex E2 03 6018 booster cushion. According to the report, the boy did not receive any injuries (MAIS=0). Loading condition for this crash was a fronto-lateral collision involving a Citroen Xsara and a Renault Megan Scenic II.

### 6.1.2 Process

Conducted procedure of the feasibility study has been decomposed to the sections environment and CRS, positioning and scaling of the HBM, pre-positioning simulation and impact simulation. For each segment, the utilized method in [6] will be briefly explained and complemented with potential alterations executed in this reproduction supported with underlying reasoning.

**Environment**

The interior setup consisted of a front and rear seat extracted from the PIPER generic car environment v1.0 where each seat consisted of a cushion and a back geometry as depicted in Figure 6.1. Developed for vehicle impact simulations, this generic model is parameterized with respect to angles, positions and measurements of included components.

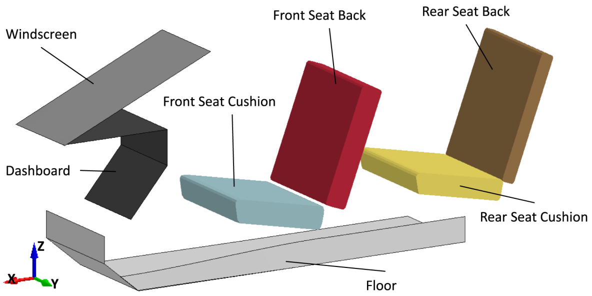

Figure 6.1: *PIPER generic car environment version 1.0 as presented by Giordano et al. [6]. Solely the seat backs and cushions for the front and rear seat respectively were kept for the feasibility simulations.*

A specific model was generated and altered for each scenario in order to provide a realistic scenario in terms of basic measurements. Applied scaling parameters and angles are presented in Table 6.1. Model validation was performed partly by intrusion test concerning the seat cushion as well as comparison to physical accident reconstruction according to CASPER database (CCN 0391) [6].

| **Parameter name** | **Scaling Case 2017** |
|---|---|
| *RSC Scaling X* | 0.8234 |
| *RSC Scaling Y* | 0.6820 |
| *RSC Scaling Z* | 0.8010 |
| *RSC Rotation Y* | -10° |
| *RSB Scaling X* | 1.1000 |
| *RSB Scaling Y* | 0.6820 |
| *RSB Scaling Z* | 1.1003 |
| *RSB Rotation Y* | -14° |
| *FSC Scaling X* | 1.0000 |
| *FSC Scaling Y* | 0.9254 |
| *FSC Scaling Z* | 1.1050 |
| *FSC Rotation Y* | -10° |
| *FSB Scaling X* | 1.0050 |
| *FSB Scaling Y* | 0.9254 |
| *FSB Scaling Z* | 1.0003 |
| *FSB Rotation Y* | -14° |

Table 6.1: Scaling and rotation of seat backs and cushions of the PIPER Environment v1.0. Explanation of abbreviations: RSC - Rear Seat Cushion, RSB - Rear Seat Back, FSC - Front Seat Cushion, FSB - Front Seat Back [6].

During the feasibility study, minor adjustments of the LS-Dyna script were performed concerning the positioning of the rear seat cushion which could be derived from a parametric code error. Giordano et al. [6] conducted a remesh of the back seat in order to portray the real geometry, which was excluded from this feasibility study.

As a part of the CASPER project, two types of CRS were constructed. Group 1 targeted children in the age group 9 months to 2 years old, thus not applicable for this project. Group 2 consisted of a model derived from Jane Indy Racing design where the seat was used for Case 2017. The target group were children in the weight interval of 15-25 kg ranging from 4 to 6 years old, see Figure 6.2.

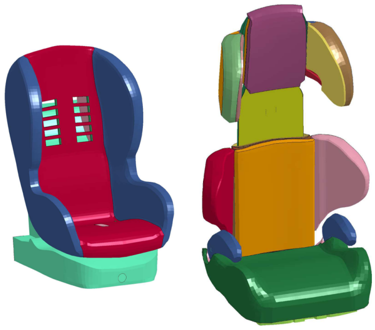

Figure 6.2: *Presentation of the belt positioning booster and high back booster as presented in the accident reconstruction study [6].*

### Scaling and Positioning of Human Body Model

For selected accident reconstruction case, the child occupant was 5 years old and selected as $50^{th}$ where the scaling was facilitated using the interface of the PIPER framework as previously described. Positioning of the child model was performed according to angles provided in Table 6.2 which aimed to imitate the angle of the dummies used in the real accident reconstruction scenarios. Due to erroneous neck-positioning, these were excluded from the simulation.

| Frame Name Relative to World Frame | Angle Case 2017 |
|---|---|
| *Left Hip* | 0 ° |
| *Right Hip* | 0 ° |
| *Left Glenohumeral* | -12° |
| *Left Elbow* | 22 ° |
| *Left Wrist* | 0° |
| *Right Glenohumeral* | -12° |
| *Right Elbow* | 22° |
| *Right Wrist* | 0° |
| *Left Knee* | -13° |
| *Left Ankle* | 0° |
| *Right Knee* | -13° |
| *Right Ankle* | 0° |

Table 6.2: Positioning of the joints in PIPER framework as made by Giordano et al. [6].

### Pre-positioning Simulation

Following the personalization and positioning of the PIPER scalable child HBM in the PIPER framework, the model was exported and imported in the LS-DYNA environment together with the vehicle and CRS model. In order to avoid distortions the vehicle and CRS, which consisted of relatively few of parts, were translated towards the HBM model. Only a minor rotation was conducted on the HBM. As described in [6], the AUTOMATIC_SURFACE_TO_SURFACE was applied between the occupant and the environment as well as in between the environment where the static and dynamic frictions $\mu_s, \mu_d$ were set to 0.1. Gravity was applied to the HBM using the LOAD_Z card. Termination time was set to 300 [ms] and by reviewing the contact between the child and the seat and the child and CRS, suitable phase was selected as the Z-component reached a value of approximately 230 [N] in a downwards direction. Stresses and updated coordinate positions were saved and included in the impact simulation.

### Impact Simulation

Belt geometry was generated using the Belt Fit tool in LS-Prepost where design aimed at maintaining a direct path between between the upper and lower anchorage as can be seen in Figure 6.3. Due to limited information concerning the seat belt properties in Giordano et al. [6], section and material properties from the open source VIVA model was incorporated as can be reviewed in Appendix C [96]. Same material cards was implemented in the final parametric study.

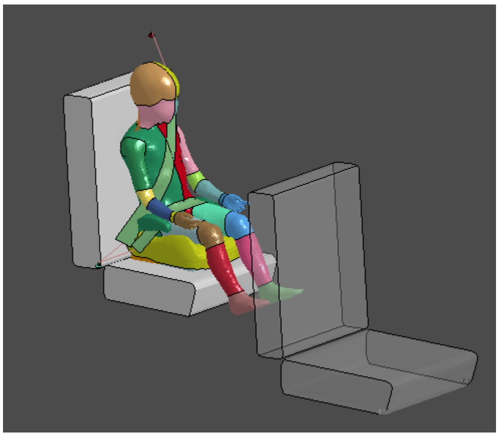

Figure 6.3: *Belt routing of the child HBM following prepositioning simulation.*

Loading curves in the X,Y and Z translational direction as depicted in Figure 6.4 were applied on node sets selected from the seat cushions and backs.

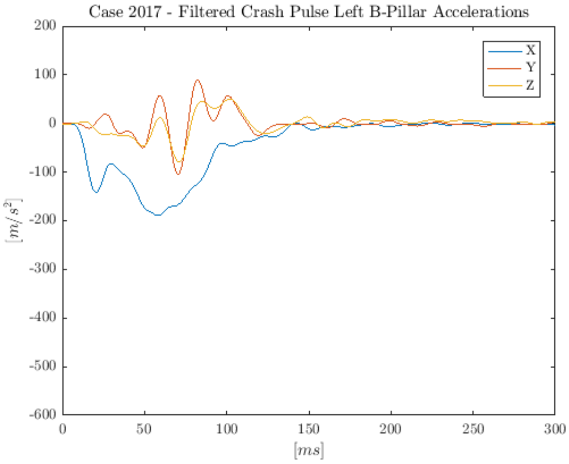

Figure 6.4: *Load curves in translational X, Y and Z directions for Case 2017 as provided by Giordano et al. [6]*

## 6.2 Parameter Study

Objective of this parameter study is to evaluate PIPER:s interaction with shoulder belt by exposing the model to three different the D-ring positions. The borderline values of selected parameters are based on the envelope provided by FMVSS 210 as presented by the UMTRI study [64]. Reason for selecting these angle parameters was to enable comparison between observations made during a static belt fit investigation where trends were identified concerning optimal shoulder belt fit and the D-ring position. Although the extreme values may be more flexible than those provided by European Standards, it allows to provoke the model on both inboard and outboard measurements. Baseline setup was selected as the design position of the vehicle model. This study will also investigate the effect of implementing booster cushions as well as booster seats, which should according to literature provide differences in terms of belt fit, loading and kinematics. Concludingly, two different loading conditions will be evaluated. The test subject has been selected as the baseline PIPER model corresponding to a $50^{th}$ percentile 6 year old. Table 6.3 displays the Test Matrix which contains a total of 18 simulations.

| **Test** | **Dir** | **No Booster** | **Booster** | **High Back Booster** | **D0** | **D1** | **D2** |
|---|---|---|---|---|---|---|---|
| *FINB_D0* | F | X | | | X | | |
| *FINB_D1* | F | X | | | | X | |
| *FINB_D2* | F | X | | | | | X |
| *FIB_D0* | F | | X | | X | | |
| *FIB_D1* | F | | X | | | X | |
| *FIB_D2* | F | | X | | | | X |
| *FIBB_D0* | F | | | X | X | | |
| *FIBB_D1* | F | | | X | | X | |
| *FIBB_D2* | F | | | X | | | X |
| *OINB_D0* | O | X | | | X | | |
| *OINB_D1* | O | X | | | | X | |
| *OINB_D2* | O | X | | | | | X |
| *OIB_D0* | O | | X | | X | | |
| *OIB_D1* | O | | X | | | X | |
| *OIB_D2* | O | | X | | | | X |
| *OIBB_D0* | O | | | X | X | | |
| *OIBB_D1* | O | | | X | | X | |
| *OIBB_D1* | O | | | X | | | X |

Table 6.3: Parametric test matrix. **Dir** represents the loading direction where **F** and **O** denotes full frontal or frontal offset. **D0**, **D1** and **D2** corresponds to the selected parameter angles.

### 6.2.1 Parameter Angles

Upper belt anchorage of the three point belt is denoted as the D-ring position, the inboard lower position as the buckle and outboard lower position as the lap belt anchorage. For this parameter study, the buckle and the lap belt anchorage positions will not be subjected to alterations. Angles of the D-ring position are varied in the YZ-plane where an estimated H-point is set as origin. The Z-coordinate is maintained as fixed whereas the Y-coordinate is altered as presented in Figure 6.5. As humans do not have an H-point, the pelvis sensor of the PIPER scalable child HBM was used to provide an appraisal of this position following the gravity simulation for the model without a belt positioning booster. Based on this position, coordinates for each of the shoulder belt parameters were extracted. Outboard angle **D1** was selected as 32° and the inboard angle **D2** was set to 19°. Baseline angle **D0** was estimated from the vehicle model was determined as 22.3°.

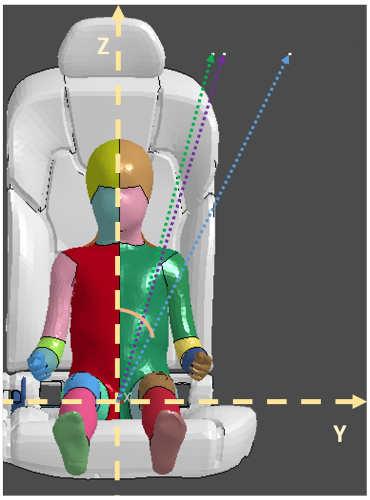

Figure 6.5: *Parameter study setup. Origin was positioned at the estimated H-point position and the angles were based in the frontal YZ-plane where blue arrow represents **D1**, purple the **D0** and green as **D2**.*

### 6.2.2 Restraint Configuration

Simulations were conducted for the three parameters with the child HBM positioned directly on the rear seat of the vehicle as in Figure 6.6, on a booster cushion as in Figure 6.7 or a booster seat as in Figure 6.8. In all of the setups, the rear seat behind the driver was utilized. A pretensioner of 1.5 [kN] with an initial slack reducing force of 0.1 [kN] was incorporated. Equivalent setup was employed for both the frontal impact and offset impact scenarios by simply altering the crash pulse.

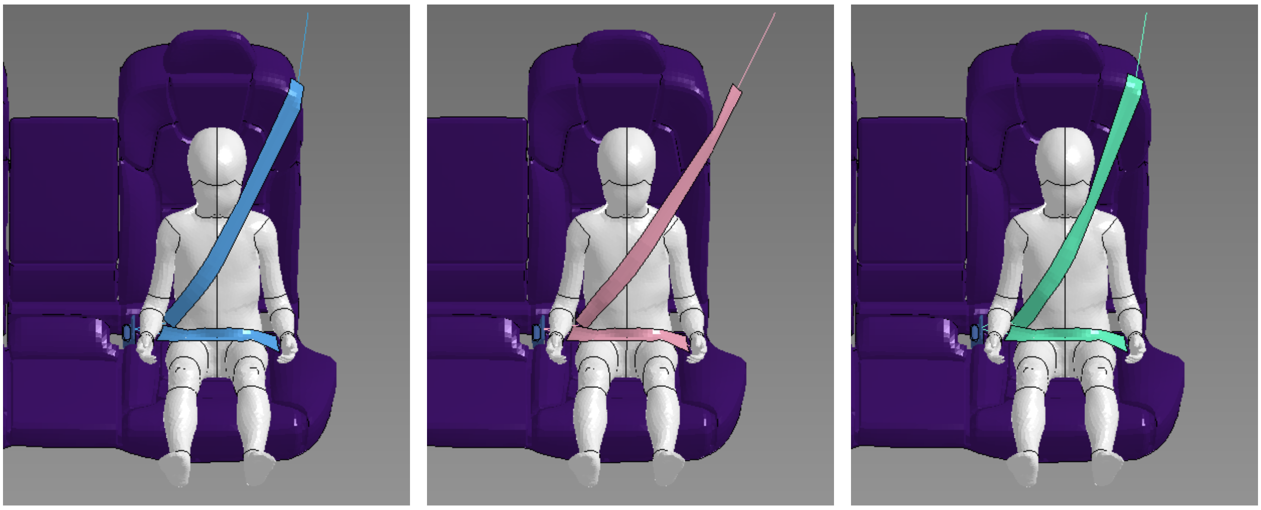

(a) (b) (c)

Figure 6.6: *FINB and OINB test series for Full Width Rigid Barrier (FWRB) and Offset-Deformable Barrier (ODB) crash tests [34].*

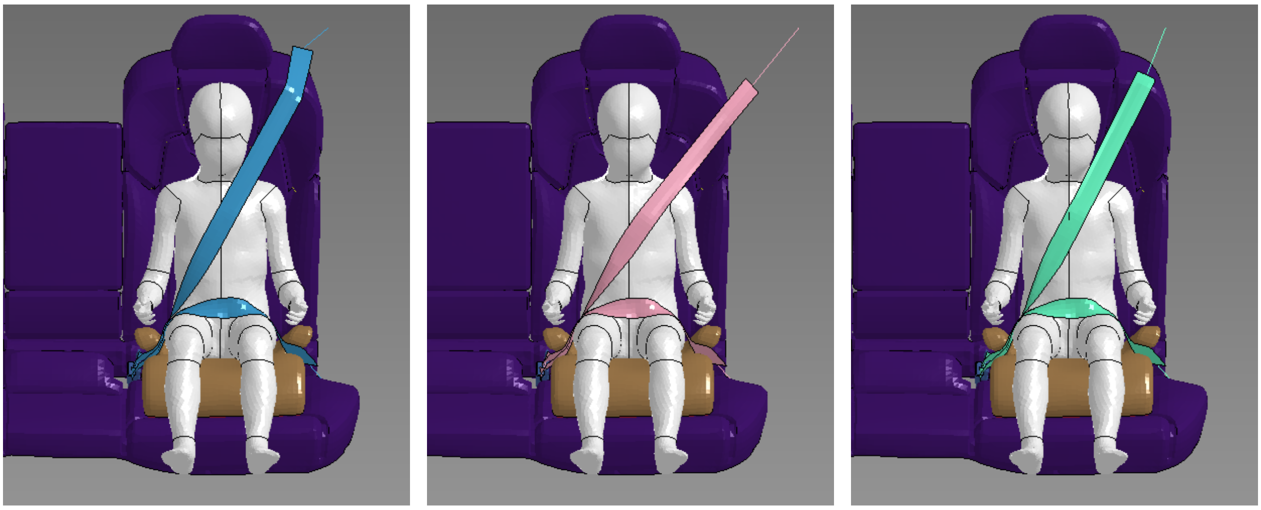
(a) (b) (c)

Figure 6.7: *FIB and OIB test series for FWRB and ODB crash tests [34].*

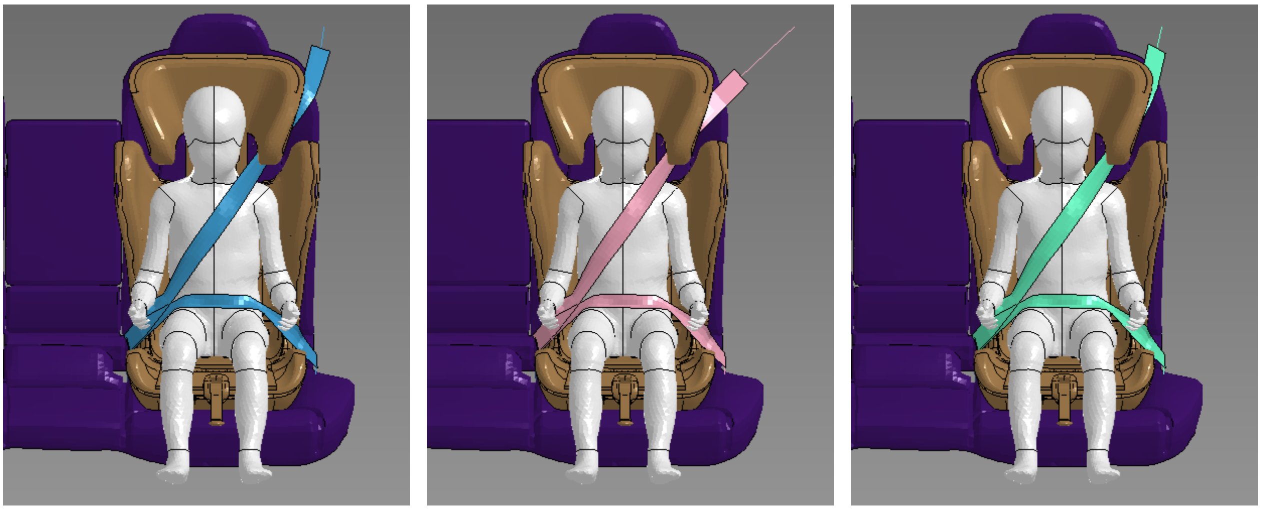
(a) (b) (c)

Figure 6.8: *FIBB and OIBB test series for FWRB and ODB crash tests [34].*

### 6.2.3 Loading Conditions

Loading conditions used in this project comprise the EuroNCAP pulses Full Width Rigid Barrier (FWRB) in Figure 6.9a as well as a 40% Offset-Deformable Barrier (ODB) seen in Figure 6.9b.

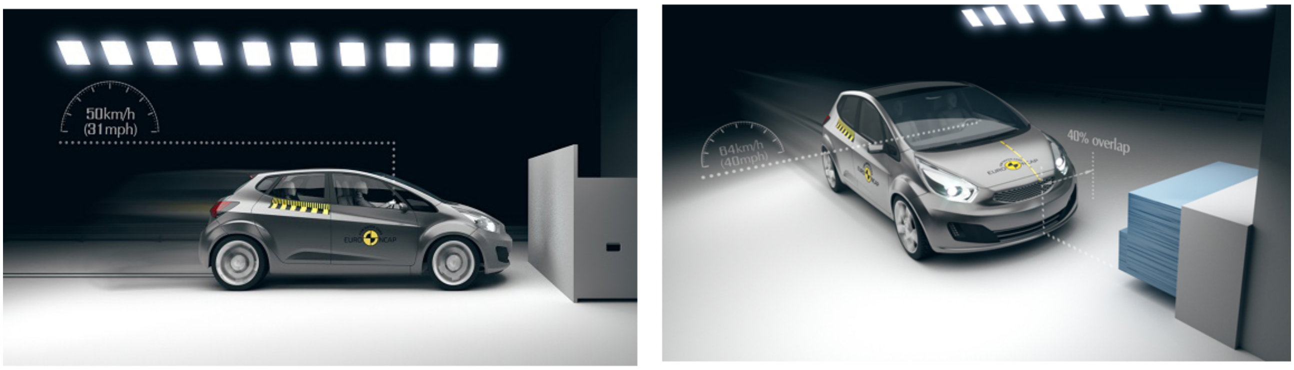

(a)

(b)

Figure 6.9: *Setup for the FWRB crash test in 6.9a and ODB in 6.9b [34]*

.

### Full Width Rigid Barrier Crash Pulse

Figure 6.10 represents a FWRB test crash pulse in the X-translational direction, expressed in terms of [g]. The reconstructed pulse has been utilized for validation of Toyota Yaris Passenger Sedan FE-models in a NCAC project [97]. Although not all directions have been employed, the X-translational deemed sufficient due to the nature of the project as well as being the major direction of impact in full frontal crashes.

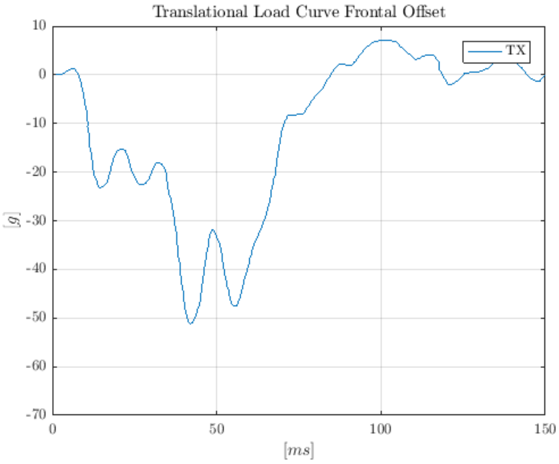

Figure 6.10: *Accelerations in the X-direction, representing the loading of a full frontal crash at 56* $[km/h]$ *or 35* $[mph]$*, reproduced from a NCAC project [97].*

### Offset deformable Barrier Crash Pulse

Figure 6.9b represents a modern large passenger car exposed to a EuroNCAP ODB test crash pulse which will be employed for the frontal offset (40%) parameter study [36]. Here, the pulse is expressed in terms of velocities in $[m/s]$.

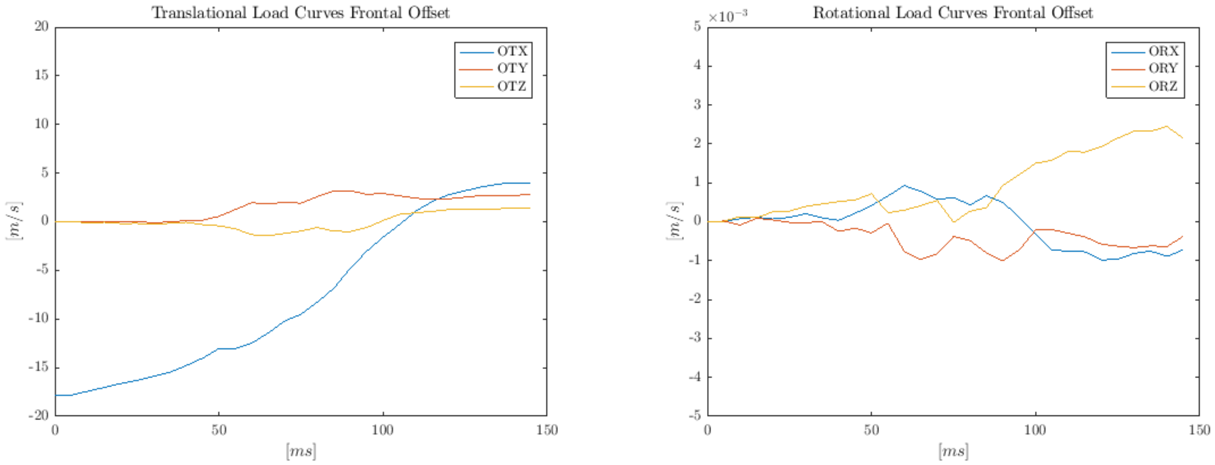

(a) (b)

Figure 6.11: *ODB crash test pulse represented with its translational velocities in 6.11a and rotational velocities in the X, Y and Z-direction in 6.11b.*

# 7 Results - Feasibility Study

Feasibility study conducted on Case 2017 did not reach normal termination due to instability issues with interpolation nodes in the neck. A visual comparison between the kinematics of the model as performed by Giordano et al. [6] and the feasibility reconstruction has been demonstrated in Figure 7.1, initially displaying similar kinematic behaviour. Discrepancies can be found in a relatively higher position of the shoulder belt for the reproduced simulations as well as increased forward planar movement of the CRS in comparison to the original simulation. Such differences could be derived from different belt properties as well as different simulation procedures.

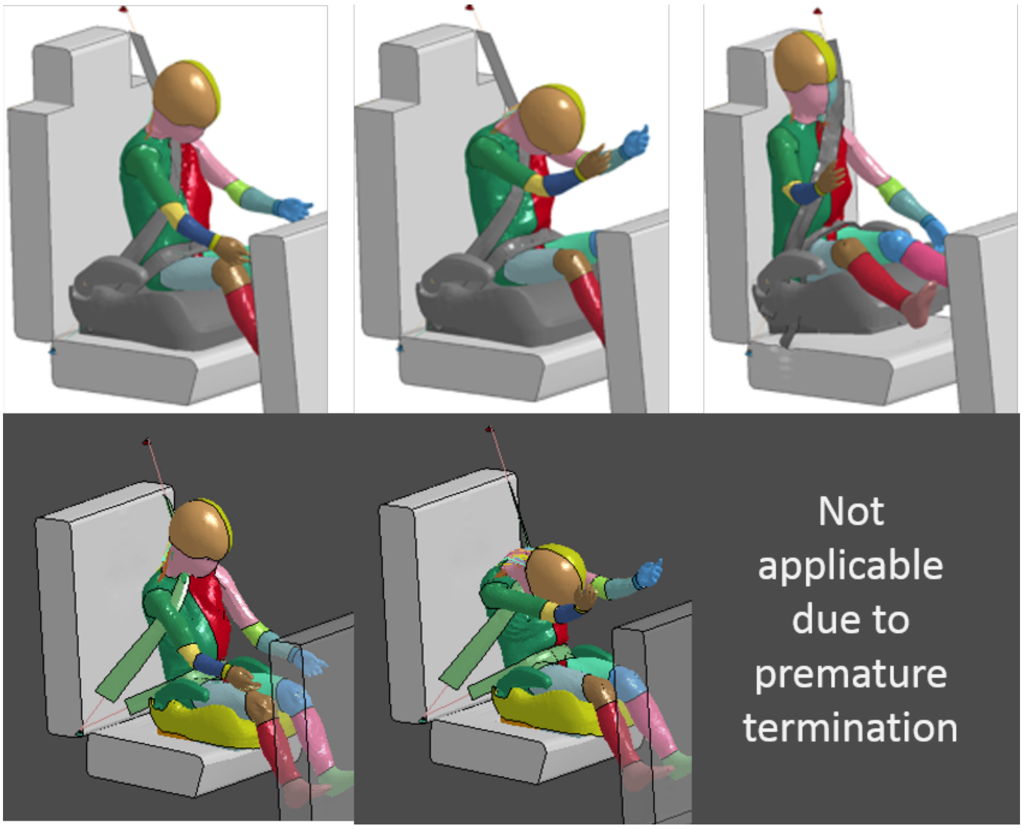

Figure 7.1: *Comparison between the simulations conducted by Giordano et al. [6] and performed resimulation, captured at 70, 96 and 217 [ms]. Due to premature termination, it was not possible to compare the concluding kinematic response.*

Figure 7.2 stratifies the linear acceleration extracted at the virtual head sensor from the original accident reconstruction simulation whereas Figure 7.3 comprises retrieved accelerations from current simulation prior to termination. For each of the original result charts, the red curve correspond to the dummy measurements of the physical reconstruction and the red values corresponds to the PIPER scalable child HBM values. X, Y and Z acceleration graphs have been combined into one plot for the virtual reconstructions. Early acceleration evaluation will be conducted, although it is not possible to make conclusive remarks as the simulation did not succeed. However, indications of potential error sources may be observed when investigating the different accelerations. It has been assumed that the acceleration measurements of the original simulation were extracted at designated virtual sensors.

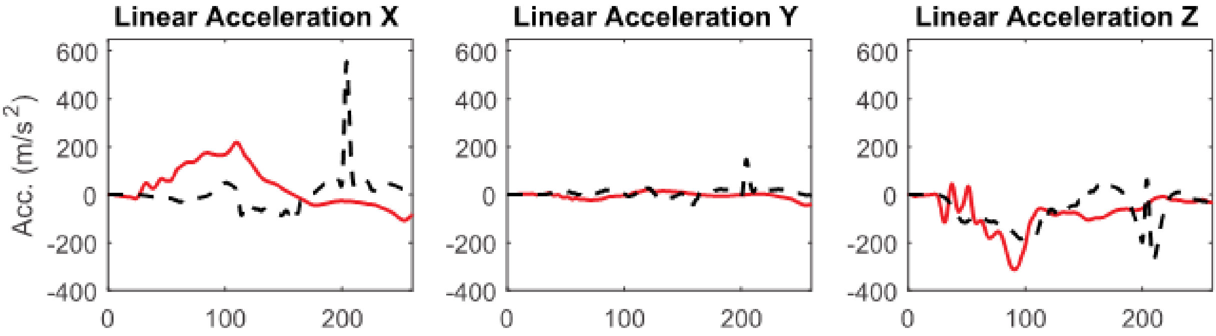

Figure 7.2: *Linear head accelerations as presented by Giordano et al. [6]. Red curve corresponds to the ATD values measured during the physical reconstruction whereas the black dashed line represents the PIPER scalable child HBM measurements.*

X-acceleration appears to strive towards similar values at 100 [ms] although the progress differs between the two. Peak Z-accelerations are approximately twice as high for the reconstructed simulation than for the original simulation.

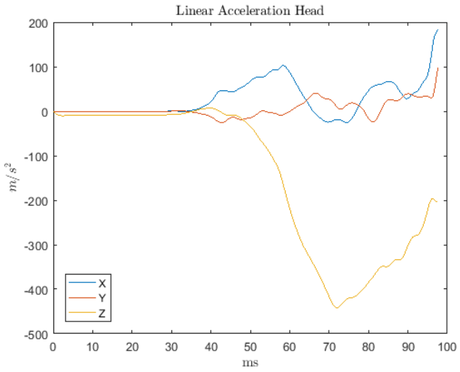

Figure 7.3: *Linear accelerations measured at the virtual head sensor during the re-simulation. Notice the comparably shorter time axis as the simulation did not proceed to designated termination time.*

Figure 7.4 demonstrates the thorax acceleration retrieved from the original simulation whereas Figure 7.5 corresponds to the re-simulation measurements respectively.

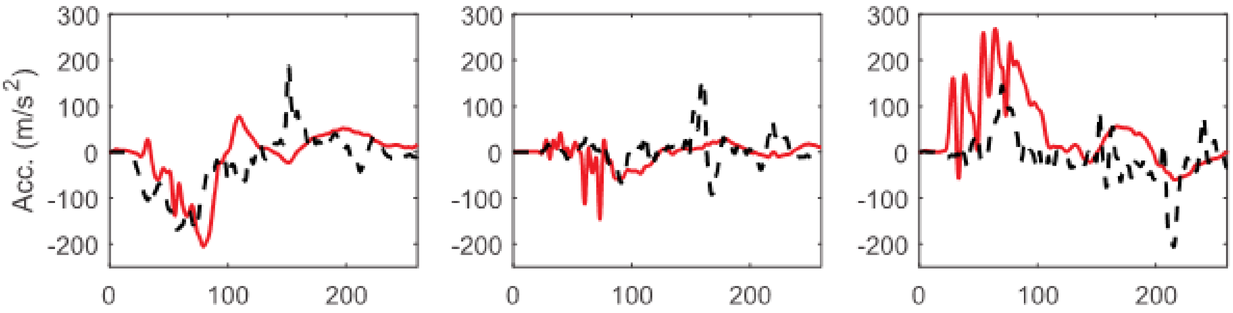

Figure 7.4: *Linear chest accelerations as presented by Giordano et al. [6]. Red curve corresponds to the ATD values measured during the physical reconstruction, whereas the black dashed line represents the PIPER scalable child HBM measurements.*

As observed, the X-acceleration peak is positioned at similar time index for both the simulations although the re-run possessed a magnitude more than twice as high. In contrast, the Z-acceleration was lowered for the resimulation and the pre-peak phase was positioned later than for the original simulations. Magnitude of the Y-acceleration was in addition higher for the re-simulation.

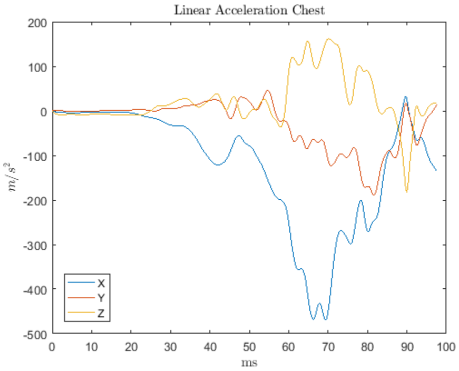

Figure 7.5: *Linear accelerations measured at the virtual chest sensor during the re-simulation. Notice the comparably shorter time axis as the simulation did not proceed to designated termination time.*

Figure 7.6 and Figure 7.7 conclude the acceleration data extracted from virtual sensors of the original and reconstructed simulations respectively, where the measurements are positioned at the pelvis.

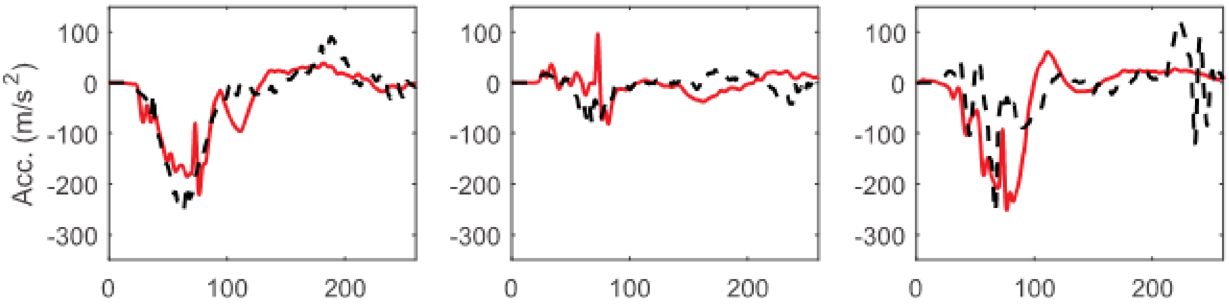

Figure 7.6: *Linear pelvis accelerations as presented by Giordano et al. [6]. Red curve corresponds to the ATD values measured during the physical reconstruction, whereas the black dashed line represents the PIPER scalable child HBM measurements.*

Similarly to previous observations, the X-acceleration of the reconstructed simulation exhibits a slightly different trend with an intermediate raise prior to the maximum peak which is of significantly higher magnitude than the original simulation. However, largest incongruities were found for the Z-acceleration which contained a peak magnitude almost ten times as high as the the original simulation.

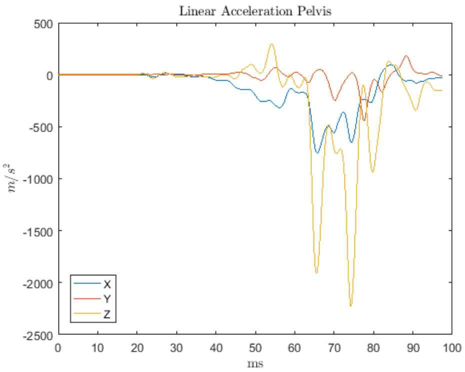

Figure 7.7: *Linear accelerations measured at the virtual pelvis sensor during the re-simulation. Notice the comparably shorter time axis as the simulation did not proceed to designated termination time.*

Figure 7.8 and Figure 7.9 correspond to accelerations by the CRS for each configuration. Data from the reconstructed simulation were extracted for each part of the CRS.

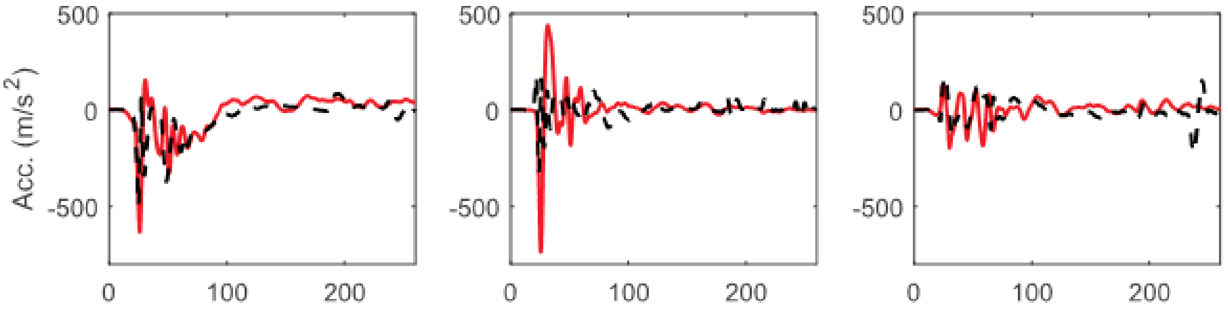

Figure 7.8: *Linear CRS accelerations as presented by Giordano et al. [6]. Red curve corresponds to the ATD values measured during the physical reconstruction, whereas the black dashed line represents the PIPER scalable child HBM measurements.*

By comparing the different setups, it appears as if the accelerations associated to the CRS are fairly equivalent considering available data.

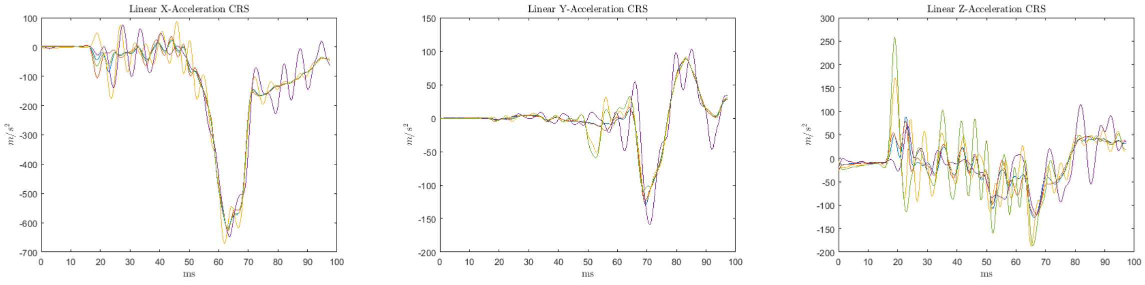

(a) (b) (c)

Figure 7.9: *Linear accelerations measured for each of the CRS components are presented where 7.9a portrays the X-accelerations, 7.9b depicts the Y-accelerations and concludingly 7.9c corresponds to the Z-accelerations.*

Major differences in measured accelerations concerns partly the X-accelerations and partly the Z-accelerations which in general tended to be higher for the reconstruction simulation than the original simulation. Dissimilar simulation procedures such as different strategies in pre-positioning and impact simulations as well as different belt properties could act as sources for discrepancies. Potential errors could occur during the stress and strain initialization for the impact simulations. Behaviour such as larger excursions in the X-direction due to CRS motion and increased belt slack could also be further investigated in order to explain these variations.

# 8 Results - Parameter Study

Crash simulations with FE models are complex problems, especially when employing material nonlinearities, high accelerations and severe deformations. In LS-Dyna, the term ”Error termination” refers to premature ending of a simulation whereas ”Normal termination” implies that the simulation was able to finish at the designated termination time. This parameter study included 18 simulations of relatively severe impacts where 17 simulations were able to achieve normal termination. Baseline model of the frontal impact booster cushion (FINB_D0) terminated early due to negative volume in the neck area. However, the simulation was able to proceed through the crash curve's peak and was thus included in the data assembly, although consideration of premature ending should be kept in mind.

## 8.1 Kinematic Analysis

Head impact is the most common injury type for children in car accident regardless of loading condition, where the main injury mechanism is believed to be contact with the interior car environment. Planes have been used as boundaries for the front seat and side structure such as the door and window as can be visualized in Figure 8.1. By utilizing planes as thresholds, although it does not fully represents the actual profile of the interior structures, it simplifies the simulation environment which allows for faster simulations.

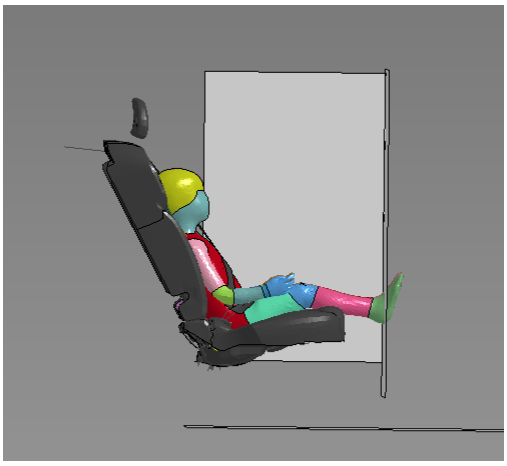

Figure 8.1: *Positioning of front and side planes which represent spatial thresholds for the front seat and the side structures.*

Resulting interaction between the PIPER scalable child HBM and the designated planes have been presented in Table 8.1. Each of the simulations exposes the child to interaction between the frontal plane and the feet. This interaction can be more or less amplified throughout the simulations depending on the employed restraint support system and occasionally include lower extremities up to knee-level. This approach is in particular noted when utilizing the high-back booster which positions the child in an increasingly anterior position. In the lateral view, the high-back booster have repeatedly been found to interact with the side plane, especially for the OIBB test series. Upper extremities such as the hands and arms have been noted to interact with the side plane as well.

However, the most important observation concerning the kinematic behaviour associated with each setup is the head excursions, where two of the tests have exposed the child's head to interaction with the vehicles interior side structure. Parameter **D1** for both the FWRB and ODB pulse when employing the backless booster have resulted in excessive lateral excursions.

Visual Analysis

| **Test** | **Interference with Frontal Plane** | **Interference with Side Plane** |
|---|---|---|
| *FINB_D0* | Feet, Fingers | No |
| *FINB_D1* | Feet, Fingers | Right Hand |
| *FINB_D2* | Feet | Minor Contact with Fingers |
| *FIB_D0* | Feet, Fingers | Right Hand, Forearm |
| *FIB_D1* | Feet, Hands | Head (at 154 ms), Right Hand, Arm |
| *FIB_D2* | Feet | Right Arm |
| *FIBB_D0* | Feet, Legs to knee, Hands | Upper SSBB, Head SSBB |
| *FIBB_D1* | Feet, Legs to knee, hands | Right Arm |
| *FIBB_D2* | Feet, Legs to knee, hands | No |
| *OINB_D0* | Feet | No |
| *OINB_D1* | Feet | No |
| *OINB_D2* | Feet | No |
| *OIB_D0* | Feet | Right Arm |
| *OIB_D1* | Feet | Head (138 ms), Right Hand, Arm, Left Fingers |
| *OIB_D2* | Feet | Right Forearm, Hand |
| *OIBB_D0* | Feet, Legs to knee | Upper SSBB, Head SSBB |
| *OIBB_D1* | Feet, Legs to knee, | Right Arm, Left hand, Upper SSBB and Head SSBB |
| *OIBB_D2* | Feet, Legs to knee, hands | Upper SSBB, Head SSBB |

Table 8.1: Interaction of body parts with the frontal and side planes have been assembled for each test, where the planes correspond to estimated positions of the front seat and side door structures respectively. SSBB denotes the Side Structures Boosters with Back. Initial penetration with feet on the frontal plane was prevalent for all test setups.

During shoulder belt loading, optimal loading path according to literature is over the ribcage across the mid sternum and centered over the clavicle in proximity to the D-ring. This parameter study has positioned the child occupant behind the driver's seat, hence the right clavicle subjected to loading. Figure 8.2 highlights the skeletal structures associated with this assessment, namely the rib cage, sternum, clavicles and the sternoclavicular joint which connects the sternum and the clavicles. Following sections will compare the belt loading of the skeletal parts for each of the restraint scenarios.

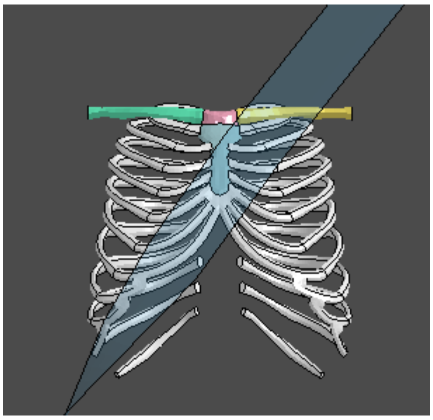

Figure 8.2: *Illustration of skeletal parts associated with shoulder belt loading. Blue represents the sternum, white structure comprise the ribcage including intercoastal cartilage. The yellow and green structures portray the right and left clavicle meanwhile the pink structure represents the sternoclavicular joint which connects the clavicles to the sternum.*

### Frontal and Offset Impact No Booster

Initial belt positions of the scenario without a booster have been depicted for the FINB and OINB test series in Figure 8.3. For the belt parameters **D0** and **D2**, the belt covers essentially the entire sternum and progresses across the rib cage, covering the inboard right clavicle and partially the sternoclavicular joint. For the parameter **D2**, the belt covers the lower sternum but leaves a segment of the mid sternum and the entire upper sternum unexposed to belt loading. In addition, the right clavicle is loaded increasingly outboard, borderlining the shoulder joint.

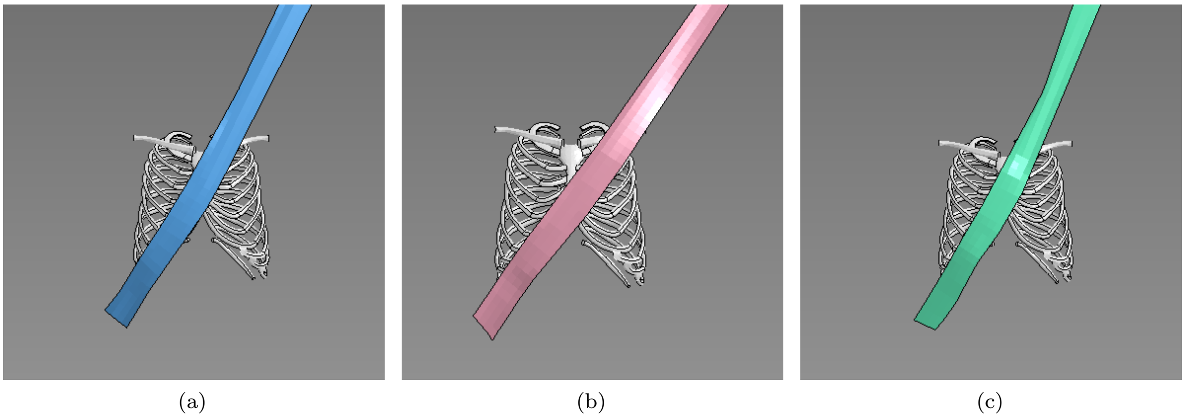

(a) (b) (c)

Figure 8.3: *Subfigure 8.3a refers to the initial baseline routing whereas subfigures 8.3b and 8.3c correspond to the parametric variations of the initial positions without a restraint support respectively. This setup is applicable for both the FINB test series as well as the OINB test series.*

Subsequently at 76 [ms], as can be visualized in Figure 8.4, for all of the parameters in the Frontal Impact scenarios the belt has slided inwards to cover the left ribcage, above the sternum progressing over the left clavicle. Loading occurs anterior of the neck, and for the narrow angles presented by **D0** and **D1** in subfigures 8.4a and 8.4c, the belt has glided upwards the arm pit.

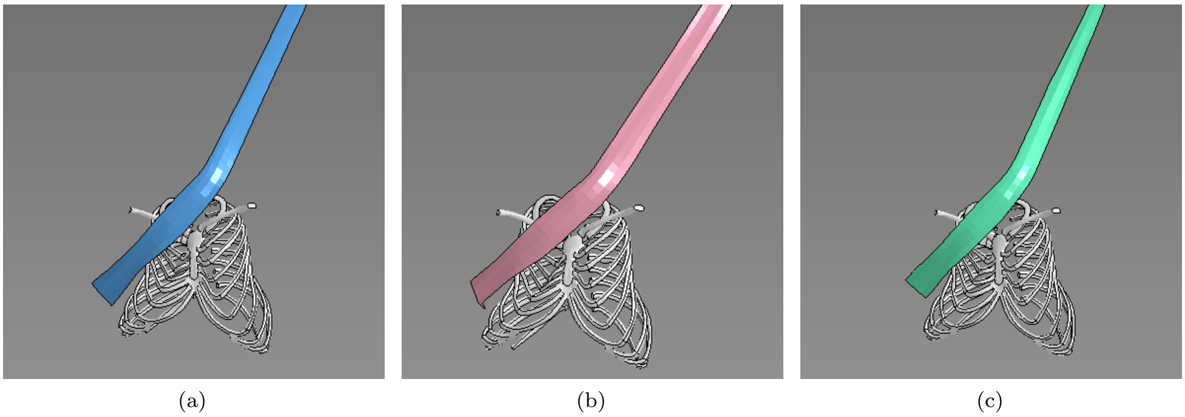

(a) (b) (c)

Figure 8.4: *Subfigures 8.4a, 8.4b and 8.4c represents the loading of the shoulder belt for the frontal impact test series at 76 [ms].*

Each of the cases composing the FINB series, roll-out of the occupant occurred during the recoil phase at the end of the crash pulse as can be seen in Figure 8.5. Roll-out is here defined as a sliding beneath the shoulder joint which allows the occupant to be ejected towards the middle seat.

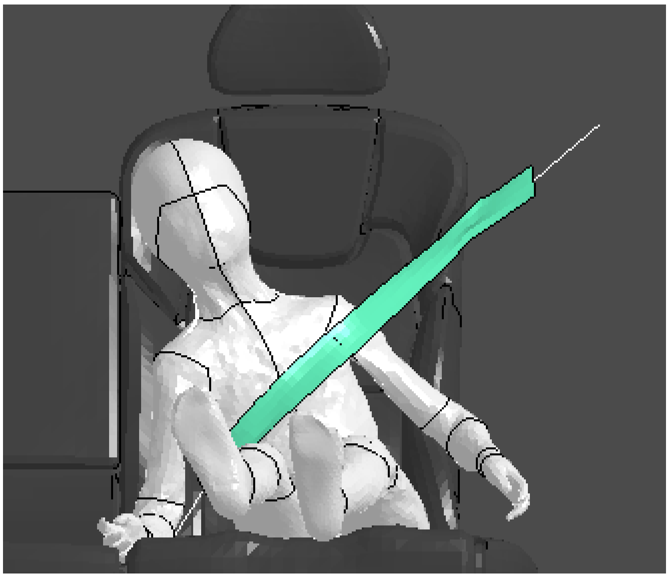

Figure 8.5: *For the FINB test series, roll-out indications have been witnessed during the post-peak acceleration where the shoulder belt has slided off the shoulder joint.*

Similar trends can be envisioned for the OINB series where the belt has slided up along the left ribcage, above the sternum and across the left clavicle, proceeding to load the neck. Positioning on the left clavicle is slightly more inwards for parameter **D1** in subfigure 8.6b in comparison to the remaining two scenarios. Unlike the FINB-setup, no roll-out was identified. Instead, the belt followed the recoil of the child occupant which was rotationally amplified due to the angular velocities of the vehicle.

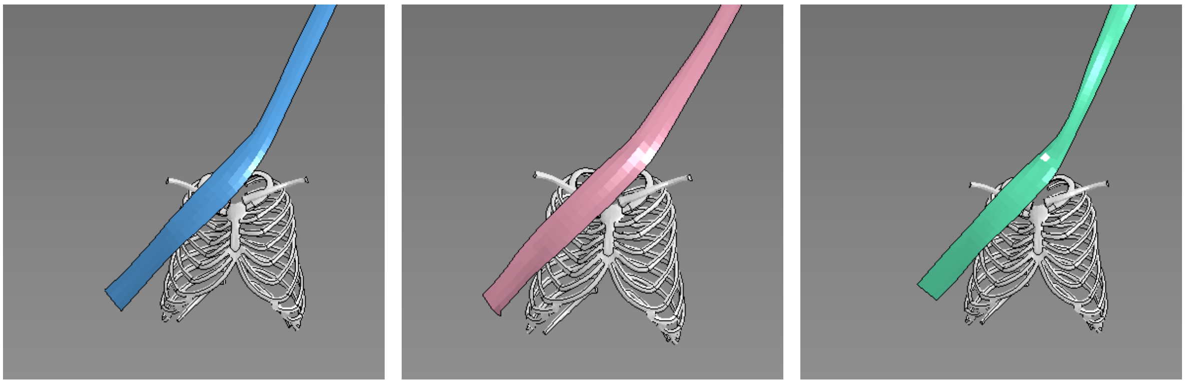

(a) (b) (c)

Figure 8.6: *Subfigures 8.6a, 8.6b and 8.6c depict the impact of shoulder belt loading during offset impact at 76 [ms].*

Lap belt interaction with pelvis was additionally assessed in order to investigate if the D-ring position or the booster setup possessed an influence on proper lap belt fit. Figure 8.7 depicts initial lap belt position with respect to the hemipelvises as well as the lumbar and thoracic spine at initial time step. For all of the booster less configurations, the lap belt was positioned too high with respect to the anterior superior iliac spine (ASIS).

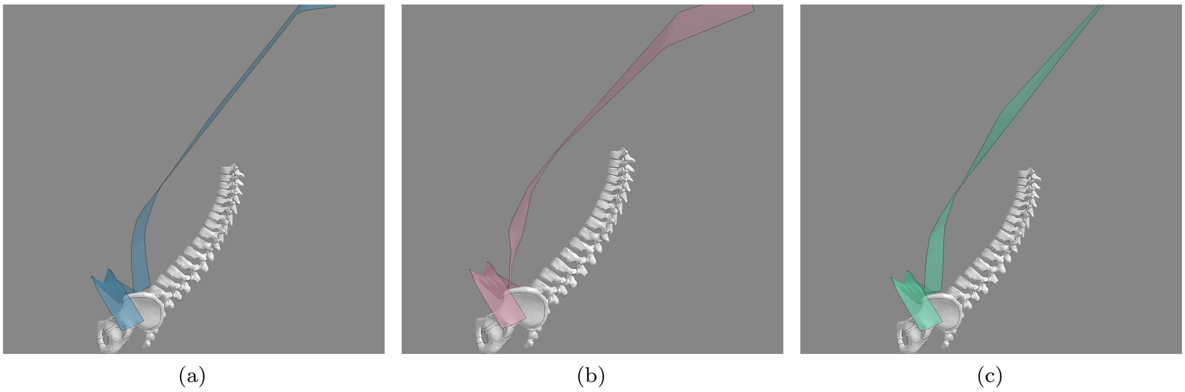
(a) (b) (c)

Figure 8.7: *Initial lap belt position for both the full frontal barrier and the ODB impact pulse where 8.7a, 8.7b and 8.7c correspond to* ***D0****,* ***D1*** *and* ***D2****.*

Figure 8.8 represents the lap belt routing at approximately 80 [ms] for the FWRB scenarios. For all three scenarios the child was subjected to submarining, resulting in abdominal loading due to non-existing or minimal interaction between lap belt and pelvis. Tilting of pelvis can be observed in comparison to the initial position seen in Figure 8.7. Small variations between the different positions could be noted such as a flatter webbing for the inboard and outboard angles in Figure 8.8b and 8.8c in comparison to the baseline model.

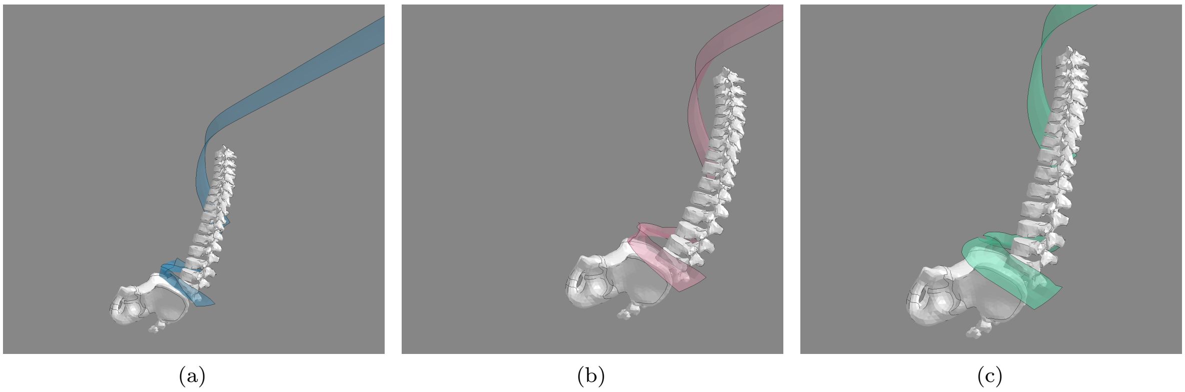
(a) (b) (c)

Figure 8.8: *Belt position at approximately 80 [ms] during the frontal impact scenario without booster, where 8.8a, 8.8b and 8.8c represent the parameters* ***D0****,* ***D1*** *and* ***D2****.*

Lap belt interactions during the ODB crash pulse were captured at approximately 116 [ms], as been visualized in Figure 8.9. In comparison to the FWRB crash pulse, both the tilting of pelvis as well as the abdominal loading is slightly less distinct for the ODB scenarios.

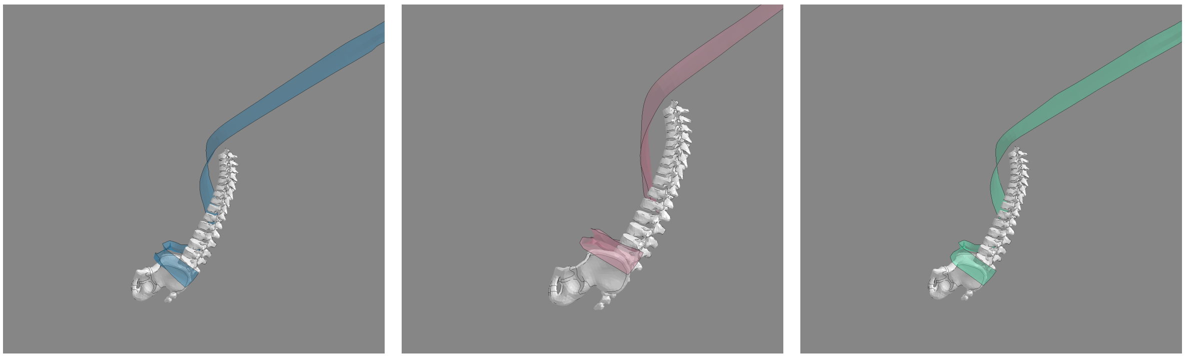

(a) (b) (c)

Figure 8.9: *Lateral view of lap belt interaction with pelvis for the no booster ODB-setup where 8.9a, 8.9b and 8.9c denotes the parameters **D0**, **D1** and **D2**.*

However, by reviewing the ODB lap belt interaction from a lateral perspective as in Figure 8.10 it becomes apparent that the lap belt is above the iliac crest, thus loading of the abdomen is prevalent. Small variations between the parameters can be noted for the most outboard angle **D2** demonstrated in Figure 8.10b which portrays a slightly more tilted pelvis around the X-axis.

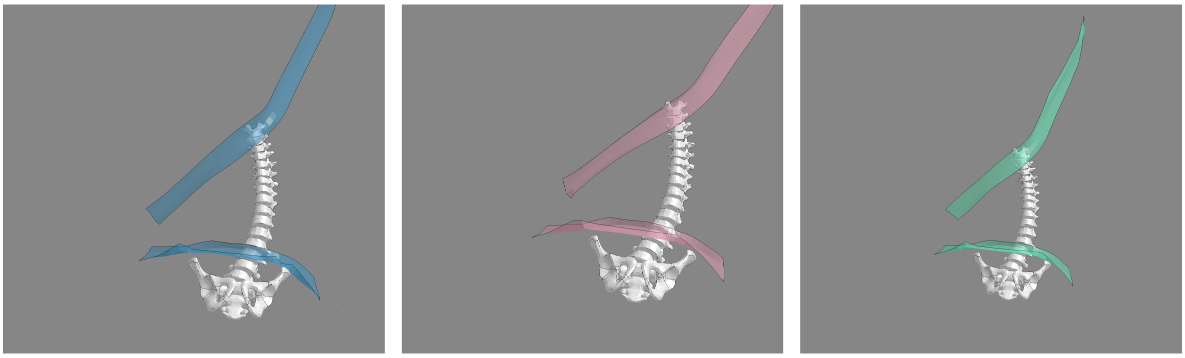

(a) (b) (c)

Figure 8.10: *Frontal view of no booster configuration employing ODB-pulse at approximately 116 [ms] where 8.10a, 8.10b and 8.10c correspond to the parameters **D0**, **D1** and **D2** respectively.*

### Frontal and Offset Impact Booster Cushion

During the FIB and OIB test series, the occupant was placed on a belt positioning booster, which according to literature is the most suitable restraint assisting system for a 6 year old child, thus optimal for the baseline PIPER child HBM. Initial belt positioning with respect to the skeletal loading structures for the shoulder belt have been demonstrated in Figure 8.11 for both FWRB and ODB loading conditions.

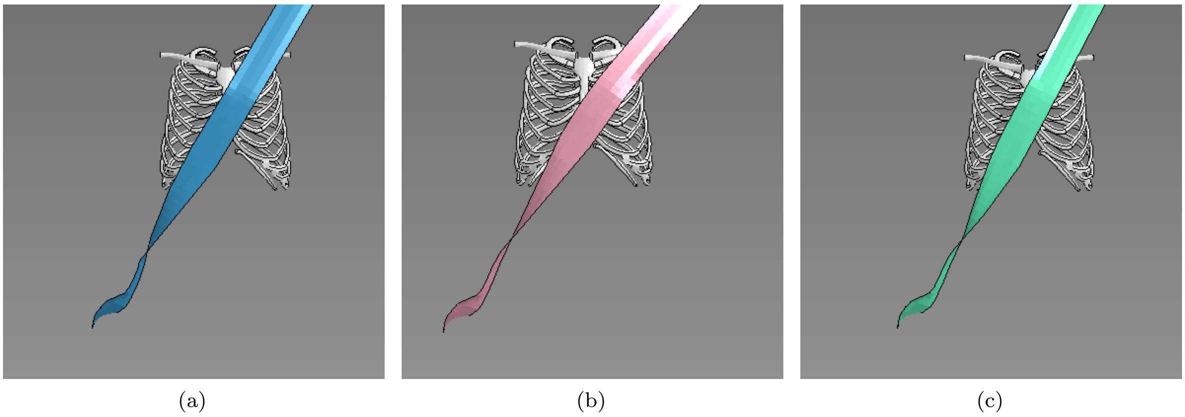
(a) (b) (c)

Figure 8.11: *In subfigure 8.11a to the left, the baseline shoulder belt routing when employing a belt-positioning booster is depicted. Subfigures 8.11b and 8.11c represent the corresponding loading for belt angles **D1** and **D2** respectively.*

For the **D1** parameter representing the outwards envelope of D-ring angular position with respect to an estimated H-point, the child occupant rolled out of the belt and experienced a head interaction with the side plane. Interaction with the lateral plane can be visualized in Figure 8.12, demonstrating a significant surpassing of the boundary threshold.

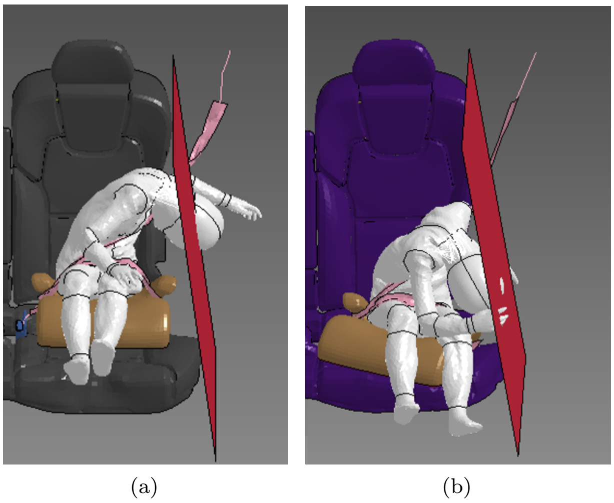
(a) (b)

Figure 8.12: *For parameter **D2**, the child occupant was exposed to head impact with the lateral side structure of the vehicle. In this figure, the frontal impact scenario has been depicted in 8.12a and the offset scenario in 8.12b. Although similar occurrence was witnessed for the offset scenario, it was slightly less prominent than for the frontal case.*

Figure 8.13 enables visualization of the belt loading at 76 [ms] for the frontal impact booster conditions. Meanwhile the baseline model **D0** presented in Figure 8.13a portrays a belt interaction which loads the rib cage, sternum and right clavicle, the variation **D1** resulted in an outwards sliding of the belt towards the shoulder joint and beneath. This created a momentum effect, centered slightly beneath the shoulder joints, which generated a rotation of the child's upper torso. Due to the lowered belt fixation point of the upper arm, the child rotates over the belt. Prior to the impact with the side structure, the head collides with the child's thighs. Parameter **D2** acted more similar to the baseline although a slightly increased tendency of neck loading may be visualized. Twisting of the belt webbing in Figure 8.13c implies that the area of loading is reduced, amplifying the pressure acting on the neck structure.

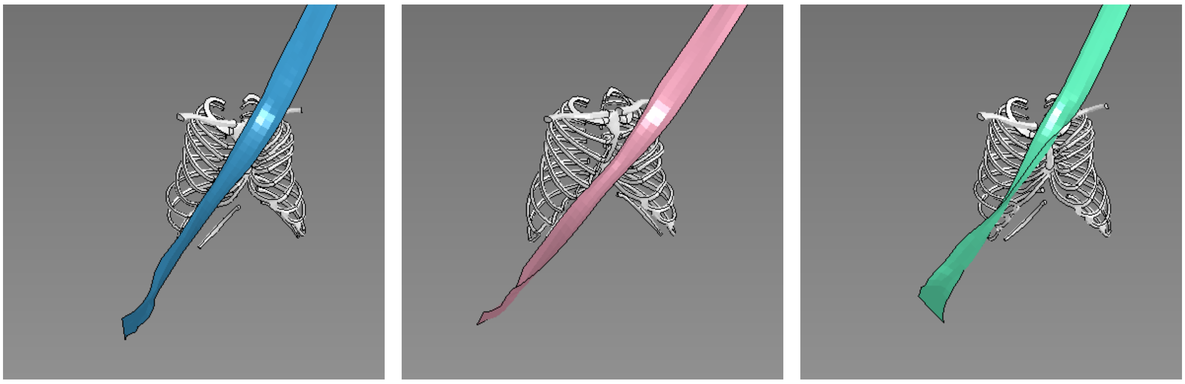
(a) (b) (c)

Figure 8.13: *Frontal impact loading at 76 [ms] is presented in subfigures 8.13a, 8.13b and 8.13c respectively.*

Similar appearances were identified for the OIB test series where parameter **D0** in Figure 8.14a maintained a relatively stable load path whereas the second scenario in Figure 8.14b caused the child to act similar as the occupant of FIB_D2. Hence, indicating that the outboard seat belt position in combination with the elevated center of gravity creates a rotational axis for which the occupant rolls out of the belt despite different loading conditions. Parameter **D2** in Figure 8.14c for the offset scenario depicted similar belt placement on the rib cage as the baseline version, and the webbing appears to lay flatter on the torso in contrast to corresponding FWRB scenario.

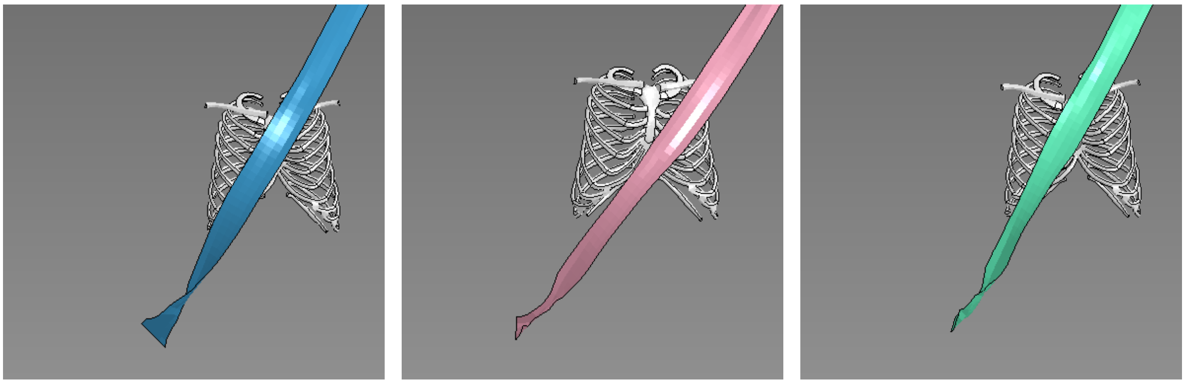
(a) (b) (c)

Figure 8.14: *Offset impact loading at 76 [ms] is visualized in sub figures 8.14a, 8.14b and 8.14c respectively.*

Despite a flatter webbing, an ejecting force was internalized for the belt positioning booster as can be seen in Figure 8.15, causing the booster cushion and the occupant to be thrown diagonally backwards in an inwards motion.

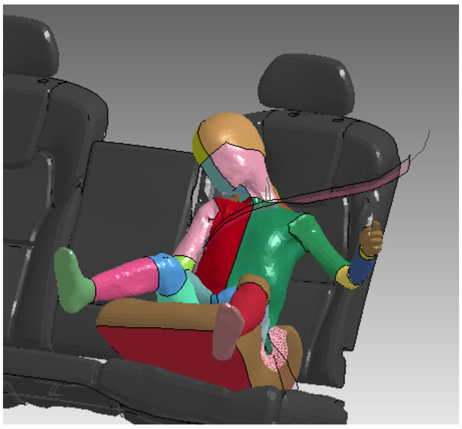

Figure 8.15: *During the rebound phase of the crash pulse, the belt positioning booster and the occupant were ejected in a YZ oriented motion.*

Interaction between the belt setup and the booster allowed for a rotational movement in the XY-plane where the rotation initiated from the inboard belt guide meanwhile the shoulder belt pulled the right shoulder backwards. Thus, exposing the occupant's spine and pelvis for counteracting angular inertia as can be seen in Figure 8.16. A simple slipring model comprising of 1-D elements did allow for slippage through the buckle.

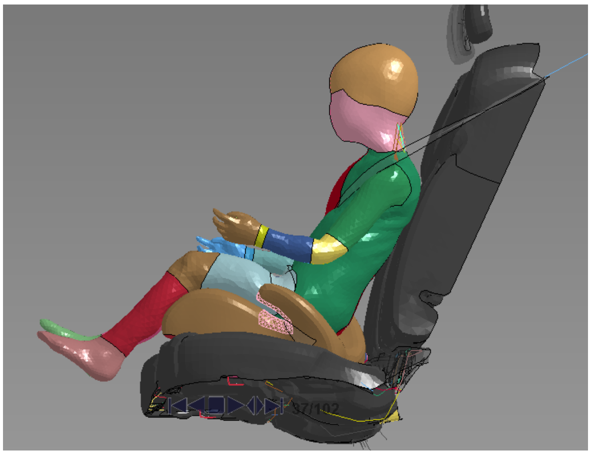

Figure 8.16: *Rotational kinematics derived from interaction between the belt guides and the belt configuration.*

In Figure 8.17, the lap belt routing with respect to the pelvis as well as the lumbar and thoracic spine have been visualized at initial time step for both loading conditions using the belt positioning booster. Although the belt appears to be positioned relatively high, a larger portion of the belt is increasingly proximal to the ASIS than the configurations without a booster.

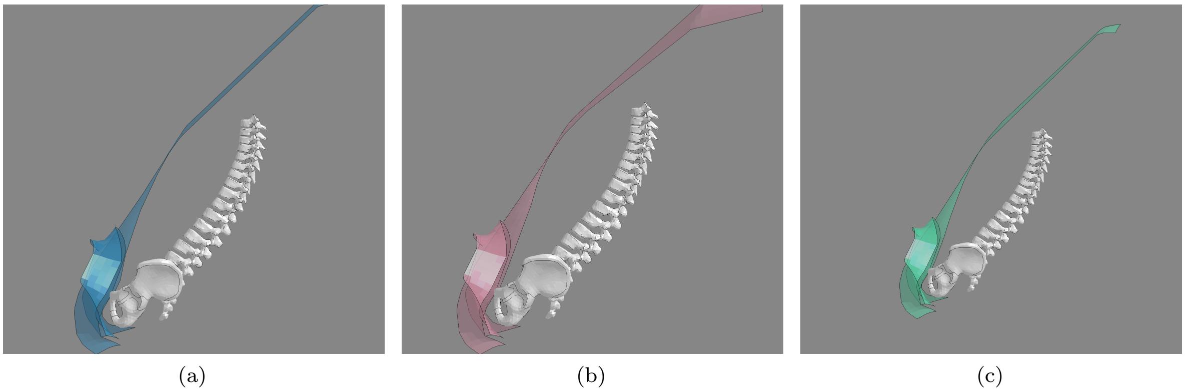
(a) (b) (c)

Figure 8.17: *Initial positions for the booster scenarios where the parameters **D0**, **D1** and **D2** are represented by 8.17a, 8.17b and 8.17c correspondingly.*

In contrast to the setup without a booster, all of the frontal impact booster configurations displayed engagement of the pelvis during lap belt loading as demonstrated in Figures 8.18c and 8.19c. Similar time step of 80 [ms] was utilized for all frontal comparisons of lap belt interaction. By increased fixation of the pelvis, variations of the shoulder belt with respect to the spine became more ostensible.

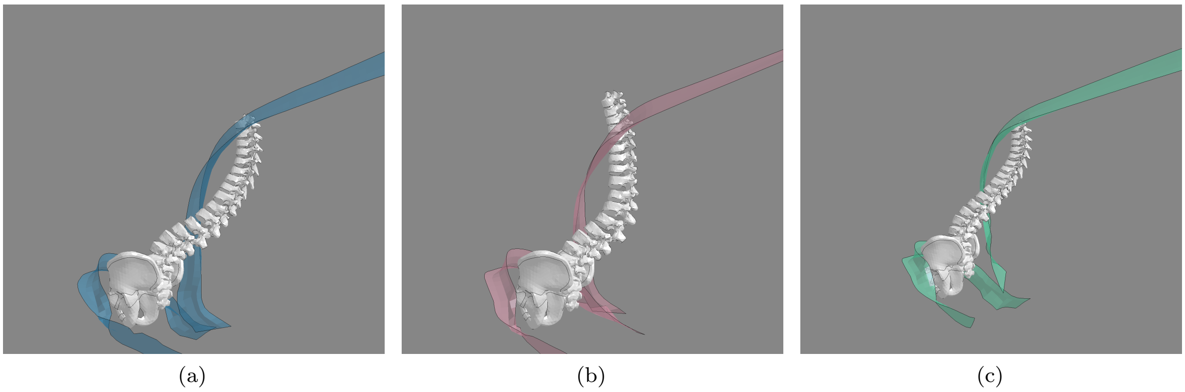
(a) (b) (c)

Figure 8.18: *Lateral perspective of seat belt interaction for full frontal barrier pulse where 8.18a, 8.18a and 8.18a embody parameters **D0**, **D1** and **D2**.*

Outboard angle demonstrated a shoulder belt interaction positioned over the lower thoracic spine around T9 as can be seen in Figures 8.18b and 8.19b in comparison to its more inboard counterparts. For the baseline model, the shoulder belt was positioned in proximity to T6 as observed in Figures 8.18a and 8.19a meanwhile for the inboard angle, the belt was positioned around T4. Notable distortion of the belt was visible for the outboard and inboard angles.

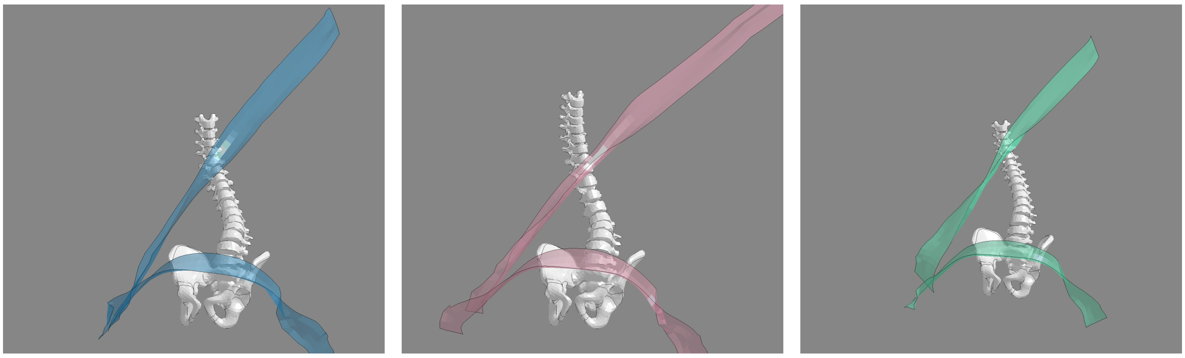

(a) (b) (c)

Figure 8.19: *Frontal view displaying the seat belt routing for the booster setup in the full frontal loading condition where **D0**, **D1** and **D2** are presented in 8.19a, 8.19b and 8.19c.*

Figures 8.20 and 8.21 portray the belt interaction for the booster setup employing the ODB-pulse at 116 [ms]. Similar to the full frontal simulations, the pelvis was activated for the three scenarios indicating that submarining was avoided for all cases of the belt-positioning booster.

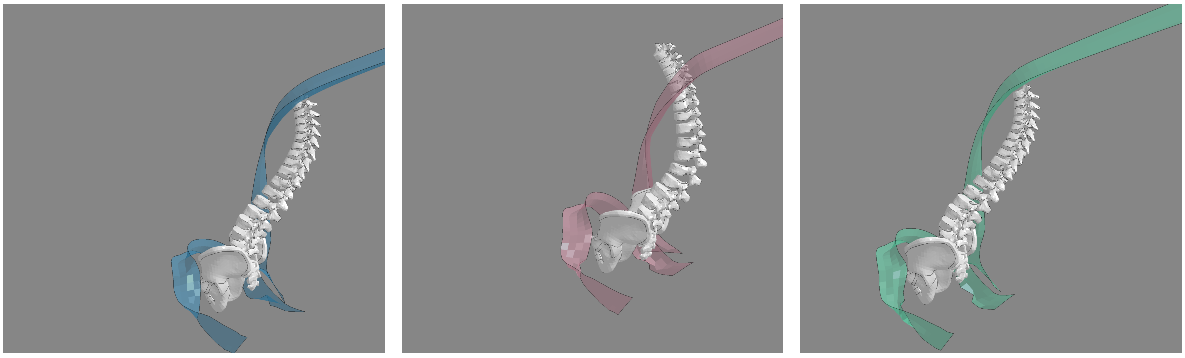

(a) (b) (c)

Figure 8.20: *Side-view of ODB-scenario for booster setup where **D0**, **D1** and **D2** were represented by 8.20a, 8.20b and 8.20c*

In comparison to the frontal counterparts, the shoulder belt was positioned higher with respect to the spine for the inboard and baseline angles whereas the outboard D-ring belt routing was maintained across T9. For the baseline setup, the belt was positioned over vertebra T3 meanwhile the inboard angle was positioning slightly more towards T2. Discrepancies between rotation of the spine was noted between the outboard angle in Figure 8.21b in comparison to the inboard and baseline angle in Figures 8.21a and 8.21c.

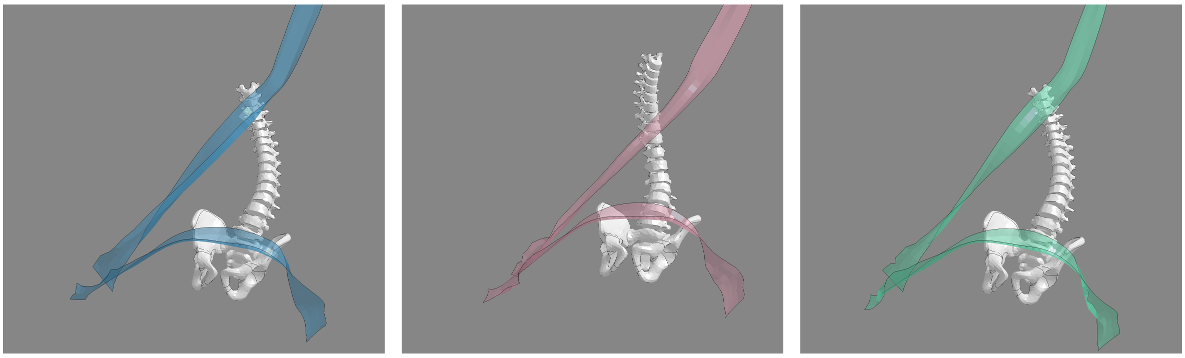
(a) (b) (c)

Figure 8.21: *Anterior perspective of the booster configurations in the ODB scenarios where 8.21a, 8.21a and 8.21a correspond to the parameters **D0**, **D1** and **D2** respectively.*

### Frontal and Offset Impact Booster Seat

Final configuration utilized the booster seat, where the observed initial seat belt loadings on the skeletal structure for the FWRB and ODB impact scenarios are presented in Figure 8.22.

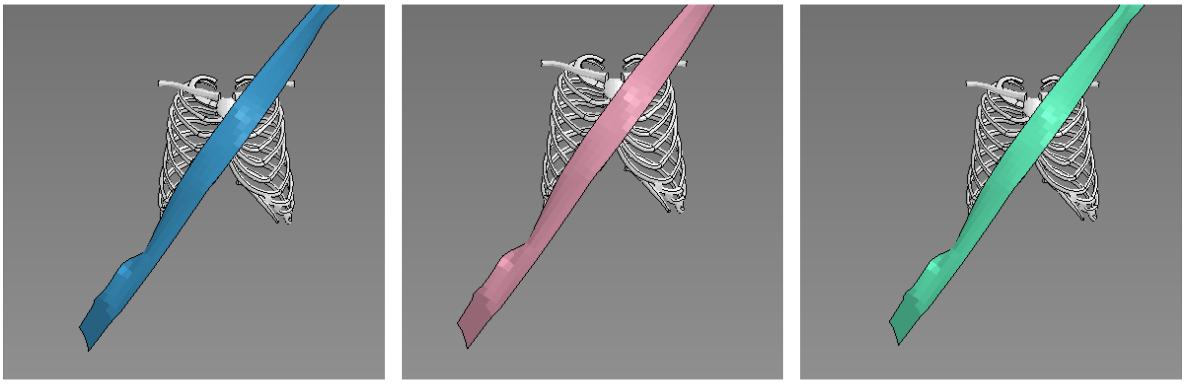
(a) (b) (c)

Figure 8.22: *Position of the initial belt routing with respect to skeletal anatomy of the thorax for parameter **D0** in 8.22a, **D1** in 8.22b and **D2** in 8.22c.*

As a result of including an integrated belt guide for the booster seat, the variation of the shoulder parameter was estimated to become less apparent. In the initial positioning, the different parametric scenarios loaded approximately similar skeletal structures, including the lower and upper sternum and partially the upper sternum. The rib cages were loaded along with an inwards position on the left clavicle. During the pretensioning and acceleration phase, parameter **D2** in Figure 8.23b managed to approximately maintain this position at 70 [ms], although a slight outwards rotation into the belt could be noted. For both the baseline parameter and the narrow belt parameter in Figure 8.23a and 8.23c respectively, the belt had glided across the sternum with only a small portion covering the upper sternum, complemented with loading of the sternoclavicular joint and left rib cage. For the baseline and the inboard angle setup, the web had become increasingly twisted in comparison to the outboard angle. A stronger V-projection of the clavicles can be seen for those configurations in comparison to the outboard angle where the right clavicle protrudes meanwhile the left clavicle is relatively fixated by the belt.

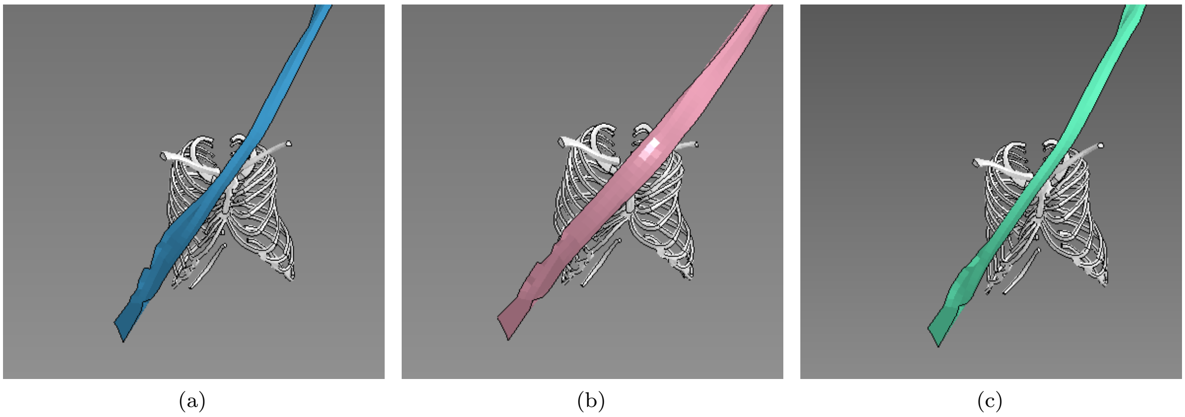
(a) (b) (c)

Figure 8.23: *Shoulder belt loading at 70 [ms] for the frontal crash scenario using the high-back booster for parameter* ***D0*** *at 8.23a, parameter* ***D1*** *at 8.23b and* ***D2*** *at 8.23c.*

Figure 8.24 presents the corresponding belt routing at 70 [ms] for the ODB crash pulse. All of the configurations maintain a relatively centered position, comprising mid and upper sternum, the inboard left clavicle including the sternoclavicular joint. The inboard and baseline angles neglected the left rib cage and the inboard angle in Figure 8.24c covered minimal sternal area out of the three configurations. In contrast to the frontal impact, the webbing for all configurations managed to maintain relatively flat.

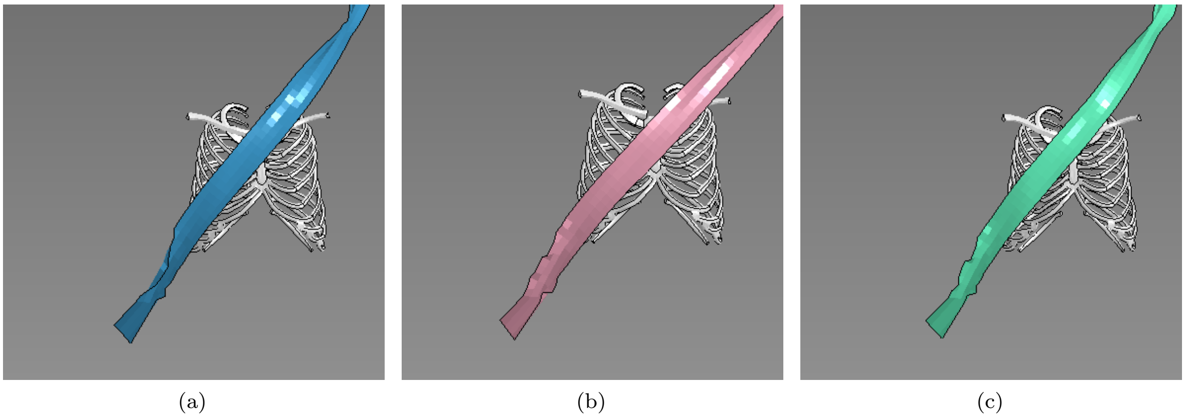
(a) (b) (c)

Figure 8.24: *Shoulder belt loading at 70 [ms] for the ODB pulse operating the high-back booster for parameter* ***D0*** *at 8.24a, parameter* ***D1*** *at 8.24b and* ***D2*** *at 8.24c.*

A majority of the scenarios involving high-back booster resulted in excessive head interaction between PIPER scalable child HBM and the upper side structures of the booster as exemplified in Figure 8.25. This behavior was observed for both loading conditions, although more prominent for the FWRB scenarios and was less severe for the most outboard D-ring position. It should be noted that the contact between the belt and the booster was not optimal, but the observations may still be included as indicative.

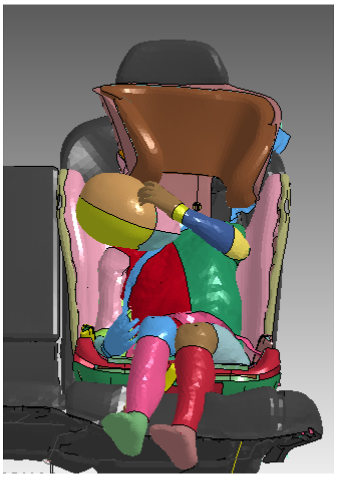

Figure 8.25: *Undesirable head interaction with the side-flanks of the high-back booster in a frontal crash pulse for the most inboard D-ring position* ***D2****.*

Initial belt position with regards to the thoraco-lumbar spine and the pelvis for the high-back booster is depicted in Figure 8.26 where 8.26a, 8.26b and 8.26c represent the parameters **D0**, **D1** and **D2** respectively.

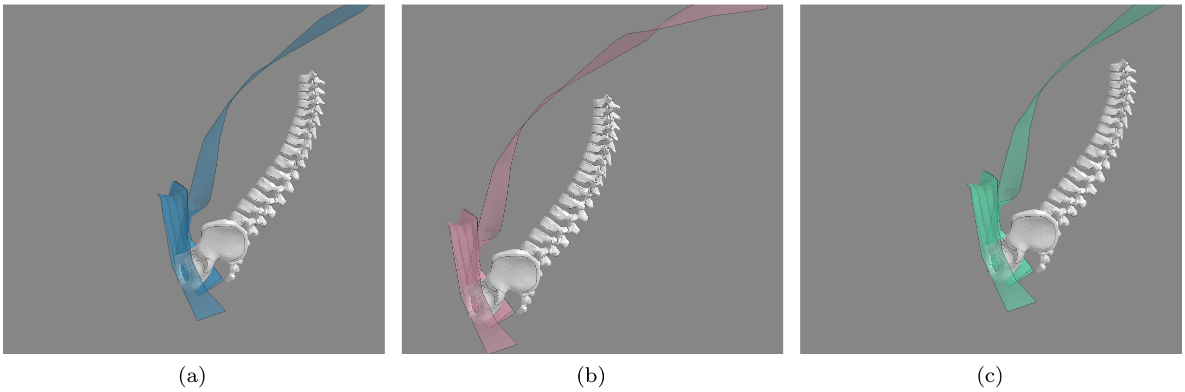

(a) (b) (c)

Figure 8.26: *Belt position in relation to the pelvis and thoraco-lumbar spine at time 0 [ms] comprising both loading conditions. Here D0, D1 and D2 are represented 8.26a, 8.26b and 8.26c correspondingly.*

Figures 8.27 and 8.28 visualize the belt interaction from two viweing directions at approximately 80 [ms]. Analogous to the booster condition, the three parameters did not exhibit any submarining behaviour.

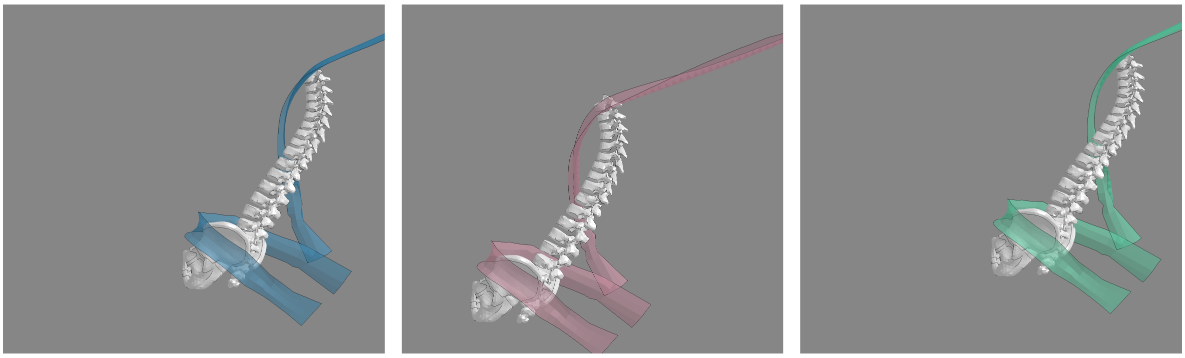
(a) (b) (c)

Figure 8.27: *Lateral view of belt interaction during frontal high-back booster scenarios where D0, D1 and D2 are represented by 8.27a, 8.27a and 8.27a congruently.*

Baseline and inboard parameters **D0** and **D2** in Figures 8.28a and 8.28c displayed similar behaviour with a twisting of the diagonal belt surpassing the vertebrae T3-T4. For the outboard parameter, the belt was positioned slightly higher than its corresponding booster scenario, surpassing the T5-T6 vertebrae. In addition, rotations of the thoraco-lumbar spine is less varied between the more inboard and outboard angles than for the booster simulations.

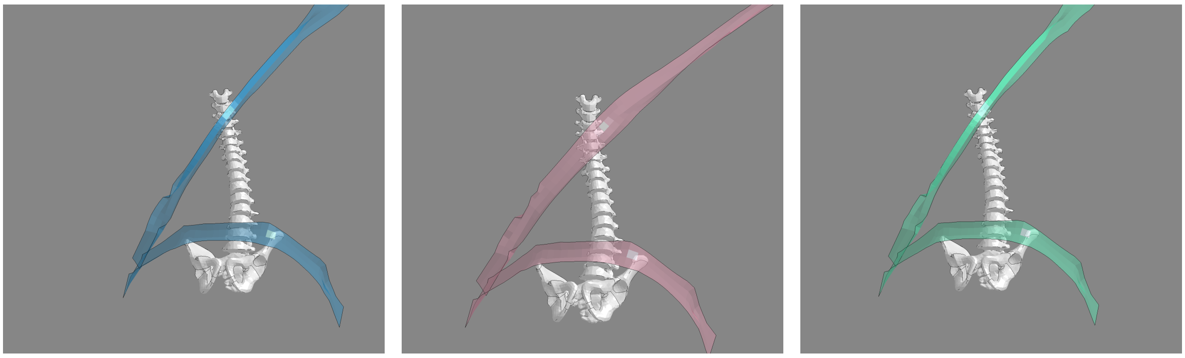
(a) (b) (c)

Figure 8.28: *Frontal perspective for the high-back booster exposed to full frontal rigid barrier pulse where 8.28a, 8.28b and 8.28c demonstrated the parameters **D0**, **D1** and **D2** at approximately 80 [ms].*

Concluding the belt interaction with respect to anatomy, Figures 8.29 and 8.30 demonstrate the relative position for the high-back booster configuration subjected to the ODB crash pulse at approximately 116 [ms]. As described for the other simulations employing belt positioning booster or the high-back booster, no submarining was identified during the peak acceleration as the pelvis was engaged by the lap portion of the seat belt.

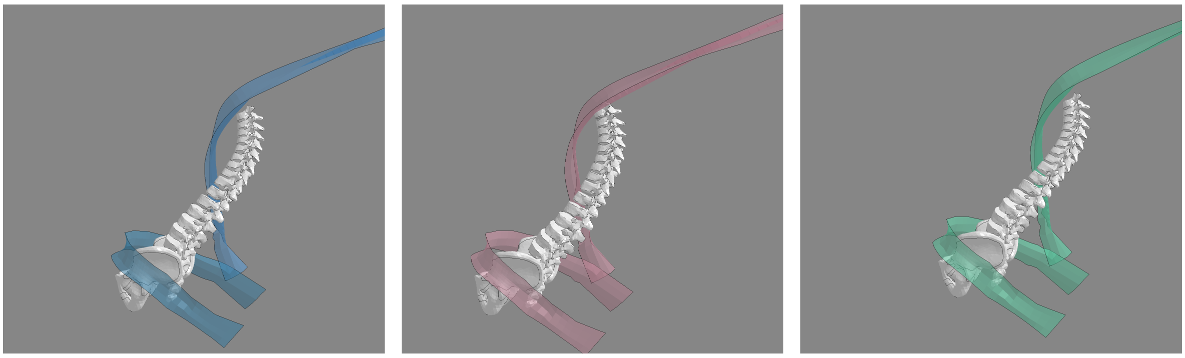
(a) (b) (c)

Figure 8.29: *Lateral perspective of the belt interaction with pelvis and thoraco-lumbar spine for the high-back booster scenarios exposed to ODB-pulse. Here the parameters D0, D1 and D2 were presented by 8.29a, 8.29b and 8.29c accordingly.*

Similar to the preceding simulations of the high-back booster for the full frontal crash scenario, less variation among the parameters was observed when comparing to the booster simulations. In general, the shoulder belt was positioned higher in contrast to the frontal loading condition. A slight difference can be seen between the inboard angle in Figure 8.30b and the baseline angle in Figure 8.30b as the inboard angle is positioned marginally higher where both surpasses the T2-T3 vertebrae. The outboard angle in Figure 8.30c covers the T3-T4 vertebrae.

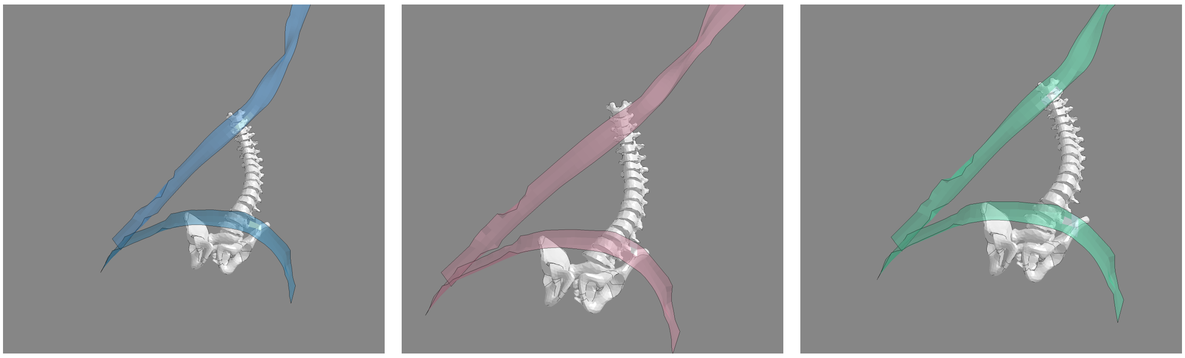
(a) (b) (c)

Figure 8.30: *Frontal view of high-back booster ODB-pulse at approximately 116 [ms] where 8.30a, 8.30a and 8.30a correspond to the parameters **D0**, **D1** and **D2** subsequently.*

## 8.2 Trajectory Comparison

As the development team behind the PIPER scalable child HBM prioritized validation with post mortem human subjects (PMHS), a trajectory comparison was conducted between the baseline frontal booster configuration and trajectories scaled from a frontal sled test using a PMHS with an anthropometry of a 10 year old performed by Lopez-Valdes et al. in [68]. Purpose of this evaluation was to assess the validity of the observed behaviour by the PIPER scalable child HBM. Kinematic excursions from the PMHS sled test were scaled to that of a 6 year old in order to be comparable to a Hybrid III 6 ATD. The PMHS was positioned on a belt-positioning booster and tested for impacts speeds of 29 km/h and 48 km/h, incorporating two different belt setups. One belt configuration comprised a force limiter as well as a pretensioner whereas the other setup for similar impact speed attained no EM systems. As can be seen in Figure 8.31, the behaviour of head impact with the upper abdomen was observed for both the baseline PIPER simulation and the PMHS subjected to a 48 km/h impact speed with energy management systems incorporated into the seat belt. Similar behavior was not witnessed for the Hybrid III 6 year old that was exposed to same experiment as the PMHS. For the high impact PMHS test without EM systems, the head impact with abdomen was more prominent. Simulations conducted within this project included pretensioner as the belt EM system, and the impact speed for the full frontal barrier test was approximately 56 km/h. Innate incongruities between the setups should also be noted as the full frontal barrier simulations were subjected to a pulse sampled from a physical crash test with a vehicle, meanwhile the PMHS test employed a sled system.

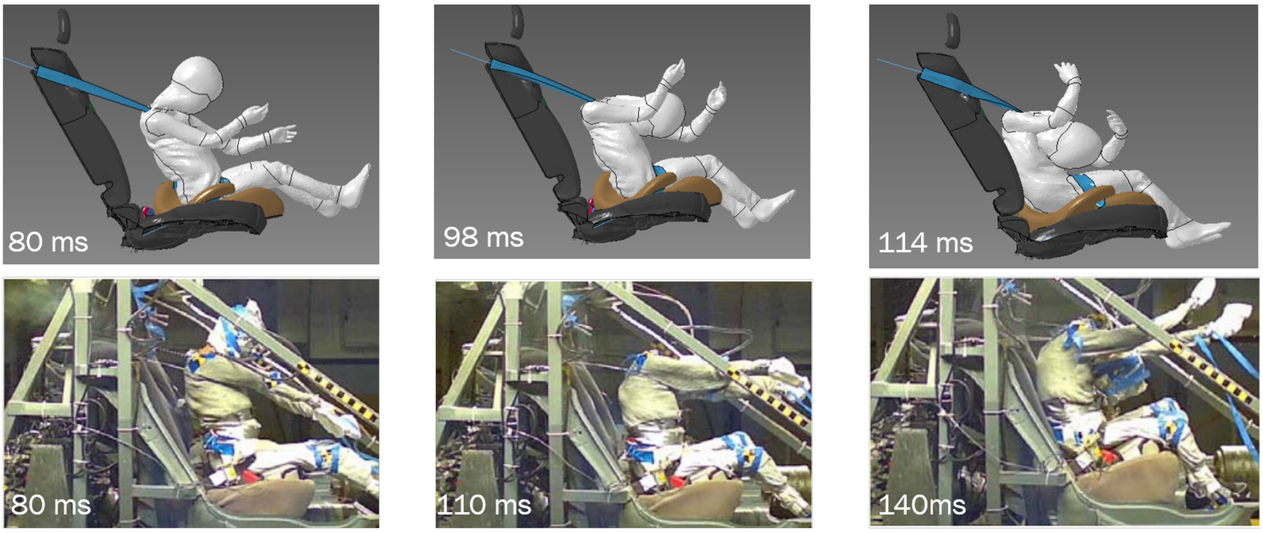

Figure 8.31: *Visual comparison between the full frontal barrier simulation using the PIPER scalable child HBM on a booster and the frontal sled test using a PMHS with a 10 year old anthropometry by Lopez-Valdes et al. [68]. Main discrepancies between the experimental designs include an utilized force limiter for the depicted PMHS scenario as well as differences in impact speed, where 48 km/h and 56 km/h where used for the PMHS and PIPER respectively.*

Sampling of the frontal and lateral excursions for the executed simulations have been exemplified in Figure 8.32 for the full frontal crash scenarios using belt positioning booster. Subfigure 8.32a visualizes the tracing of the head, chest and pelvis virtual accelerometers in the XZ-plane and subfigure 8.32b demonstrates the corresponding sideway kinematics in the YZ-plane. For this evaluation, emphasis was placed on the frontal head excursion as such data was available from the PMHS-evaluation by Lopez-Valdes et al. [68] in a comparable manner.

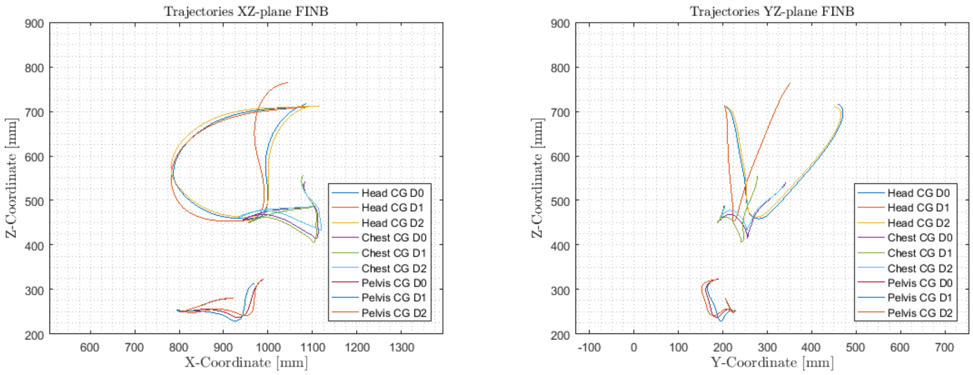

(a) (b)

Figure 8.32: *Here, 8.32a depicts frontal trajectories of the belt-positioning booster setup and 8.32b portrays equivalent lateral trajectories.*

In order to assess whether the magnitude of the head excursion trajectories was within reasonable ranges, maximum distances in the XZ-plane was estimated for the PMHS test during the high-severity impact speeds by Lopez-Valdes et al. [68] and then compared to the maximum excursions of the PIPER simulations. Both belt configurations with and without energy management systems were included in order to generate a frame of references. Extraction of maximum X and Z directions was executed according to Figures 8.33 and 8.35.

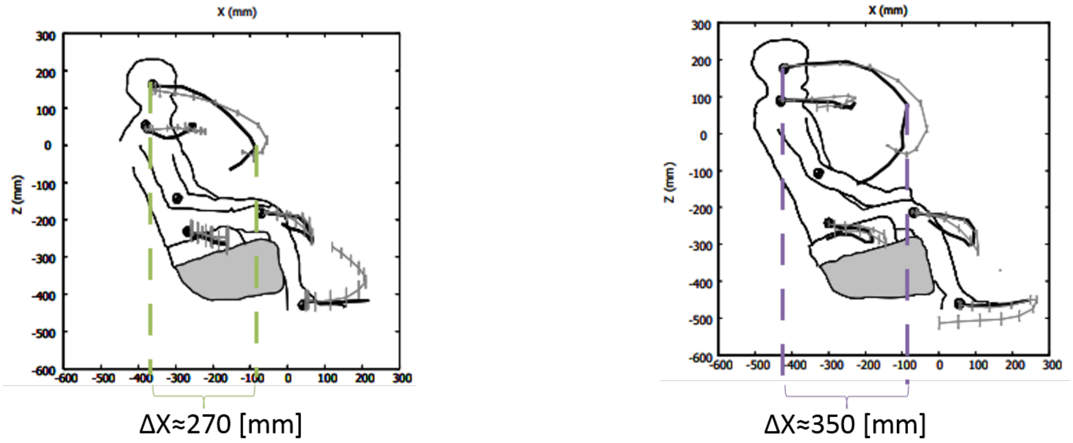

(a)

(b)

Figure 8.33: *Image to the left 8.33a represents the high-severity PMHS scenario with belt energy management systems such as load limiter and pretensioner whereas the right image 8.33b portrays the high-severity PMHS test without belt related energy management systems as presented by Lopez-Valdes et al. [68].*

Figure 8.34 visualizes the maximum X-displacement with respect to the initial relative position for each of the test configurations, starting with the baseline parameter **D0** followed by parameters **D1** and **D2** for each group of simulations. Upper parallel line corresponds to the maximum horizontal displacement measured for the PMHS without seat belt energy management systems whereas the lower line included such systems, as reported by Lopez-Valdes et al. [68]. Observations should be made concerning the differences in impact speed and experimental setup, hence direct comparison is not possible. However, it may provide insights for future kinematic evaluations.

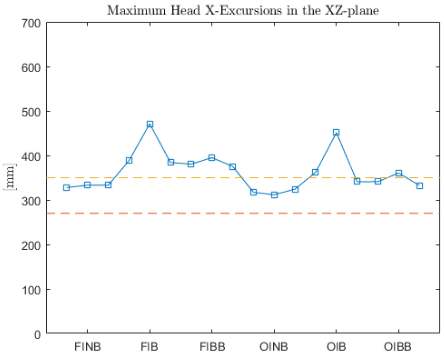

Figure 8.34: *Maximum horizontal excursions of the head CG have been plotted for each of the experimental setup where the **F** and **O** symbolizes loading conditions, **NB** implies no booster configuration where **B** and **BB** represent the booster and high-back booster scenarios respectively. Upper parallel line indicates maximum displacement for the PMHS without force limiter and pretensioner, meanwhile the lower dashed line represents excursions with energy management appliances as describes by Lopez-Valdes et al. [68].*

Upper values for the different loading conditions were found among the belt assisting devices, peaking at the booster cushion setup at the most outboard angle **(FIBD1,OIBD1)** for both crash pulses. This is consistent with the observed roll-out behaviour. In addition, a small peak was noted for the most outboard angle of the booster seat scenarios for both loading conditions. Similarly, minor excursions were found for the no-booster setup. Figure 8.35 represents the maximum Z-displacement for the high severity PMHS sled tests as reported by Lopez-Valdes et al. [68].

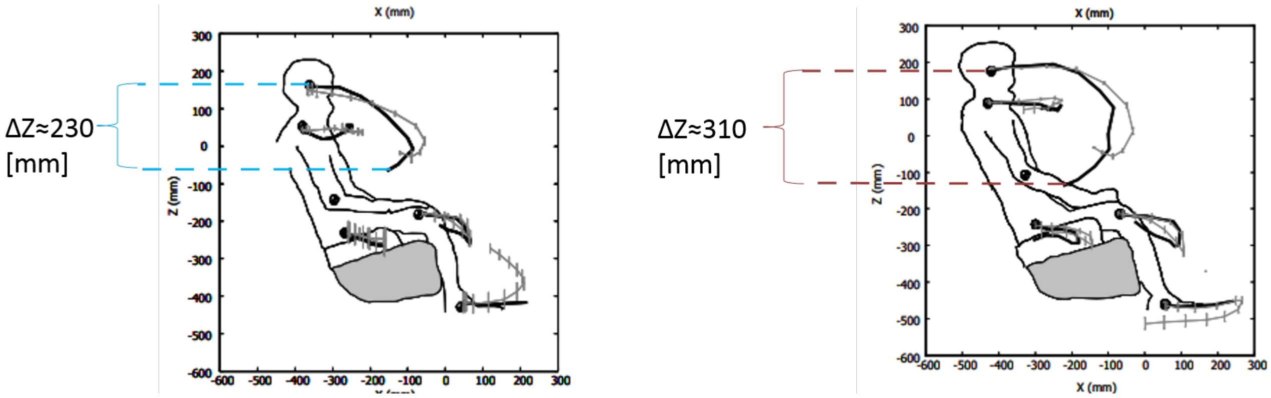

(a) (b)

Figure 8.35: *Picture to the left 8.35a corresponds to the high severity experiment utilizing belt energy management systems whereas the right image 8.35b corresponds to the PMHS test without belt energy management systems, as presented by Lopez-Valdes et al. [68].*

In comparison to the X-trajectories, the maxmimum Z-displacements were considerably lower with respect to the PMHS sled tests conducted by Lopez-Valdes et al. [68], as can be seen in Figure 8.36. As described for the horizontal excursions, the outboard angle of the belt-positioning booster configurations were notably higher in relation to the more inboard angles. However, the FWRB booster seat had the uppermost Z-translations which could be deemed consistent with the interaction between the head and the upper side structures of the high-back booster as noted during the visual analysis. In addition, the vertical displacements were lower for the ODB crash pulse than for the full frontal rigid barrier pulse.

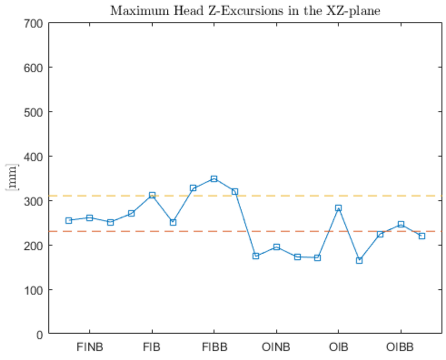

Figure 8.36: *Maximum vertical translations of the head CG have been plotted for each of the experimental setup where the* ***F*** *and* ***O*** *symbolizes loading conditions,* ***NB*** *implies no booster configuration where* ***B*** *and* ***BB*** *represent the booster and high-back booster scenarios respectively. Upper parallel line indicates maximum Z-displacement for the PMHS without force limiter and pretensioner, meanwhile the lower dashed line represents excursions with energy management appliances, as stated by Lopez-Valdes et al. [68].*

### 8.2.1 Linear and Angular Accelerations

Linear and angular accelerations have been sampled at the three virtual sensors positioned in the head, chest and pelvis. The maximum accelerations have been filtered according to SAE recommendations and visualized for each configuration in Figures 8.37 and 8.38 respectively where the different lines corresponds to each parameter. For the linear head accelerations, which are used to calculate the global head injury criteria, the outboard angle of the frontal high-back booster setup was distinguished as having the highest peak. Small variations were noted for the booster cushion configurations where the baseline parameter **D0** was slightly lower than its companions. No variation was noted for the no booster setup with respect to linear head accelerations. Larger variations were observed for the chest and pelvis accelerometers, where the pelvis accelerometer data was significantly higher than the remaining. Peak values for the linear chest accelerometer were identified for the high-back frontal impact booster, meanwhile maximum pelvis recordings could be observed for the baseline and outboard angle parameters during the ODB booster accelerations.

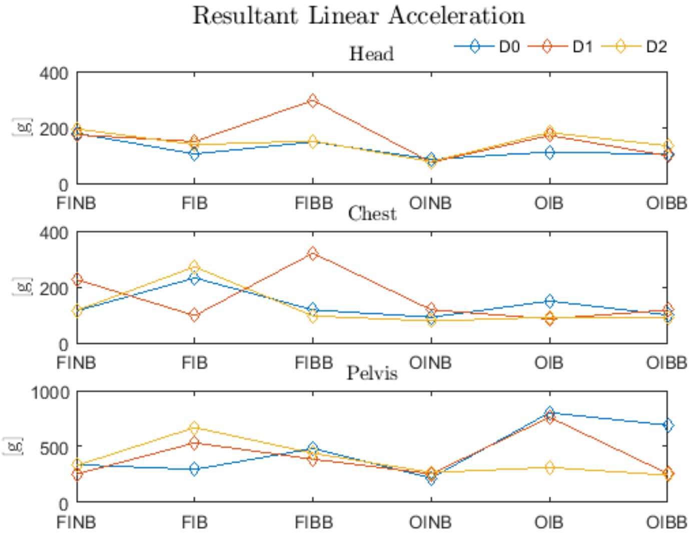

Figure 8.37: *Maximum linear accelerations of the head, chest and pelvis have been plotted for each of the experimental setup where the **F** and **O** symbolizes loading conditions, **NB** implies no booster configuration where **B** and **BB** represents the booster and high-back booster scenarios respectively.*

Although a larger data set would be required for full validation of values, measured linear accelerations and $HIC_{15}$ from the PMHS trial and corresponding Hybrid III 6 year old can be found in Table 8.2 as presented by Lopez-Valdes et al. [68] in order to act as potential indicators of reasonable values. PMHS data has been scaled from the original test subject which was a cadaver with the anthropometric measurements of a 10 year old. As the $HIC_{15}$ was not scalable, the unscaled values have been included for further comparison. When associating linear head acceleration from the PIPER model with the listed data, some correspondences could be found for the **FIB** baseline model, as well as the **OINB**, **OIB** and **OIBB** configurations. Remaining values were observed to be significantly higher, although dissimilarities in impact speeds should be considered. Main differences are however observed for the trend between the different sensor measurements where the PMHS investigation portrays a less or equal relationship between the head against the chest and pelvis measurements. On the contrary, the PIPER scalable child HBM measurements demonstrate a substantial increase for the pelvis and chest measurements in relation to the head accelerations. Emphasis should additionally be placed on the fact the the PMHS study did not evaluate ODB crash pulses.

| **Accelerations** | **With EM systems** | | **No EM systems** | |
|---|---|---|---|---|
| *[g]* | *HIII 6 YO* | *PMHS scaled* | *HIII 6 YO* | *PMHS scaled* |
| *Head* | 46.0±2.4 | 104.2 | 65.0±0.9 | 107.5 |
| *T1* | N/A | 51.7 | N/A | 74.9 |
| *Mid-Spine* | 29.0±1.7 | 57.7 | 55±1.7 | 105.5 |
| *Pelvis* | 46.0±4.2 | 70.5 | 53±1.7 | 87.1 |
| *HIC15* | 203.0±22. | 368.0 (not scaled) | 457.0±19 | 481.0 (not scaled) |

Table 8.2: Extracted acceleration measurements and $HIC_{15}$ values as reported by Lopez-Valdes et al. [68]. As previously mentioned, the PMHS values are scaled from the test subject with an anthropometry of a 10 year old. This scaling was however not applicable for the $HIC_{15}$ calculations, hence the original values of the PMHS was included for comparison.

Measured maximum angular displacements for the three sensors presented in Figure 8.38 displayed similar behaviour as the linear accelerations with comparatively higher chest and pelvis accelerations than head accelerations. Slight behavioral variations could be observed in comparison to the linear accelerations, such as the smaller discrepancies for the booster ODB impact scenario.

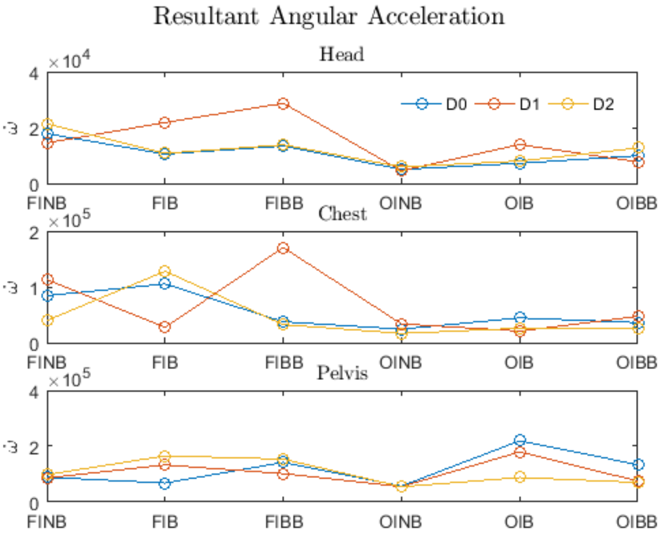

Figure 8.38: *Maximum angular accelerations of the head, chest and pelvis have been plotted for each of the experimental setup where the* ***F*** *and* ***O*** *symbolize loading conditions,* ***NB*** *implies no booster configuration where* ***B*** *and* ***BB*** *represent the booster and high-back booster scenarios respectively.*

### 8.2.2 Global Head Injury Criteria

Linear head accelerations were filtered according to SAE recommendations prior to calculating the resultant and corresponding HIC values during a 15 [ms] window. These $HIC_{15}$ values have been presented for each configuration in Figure 8.39.

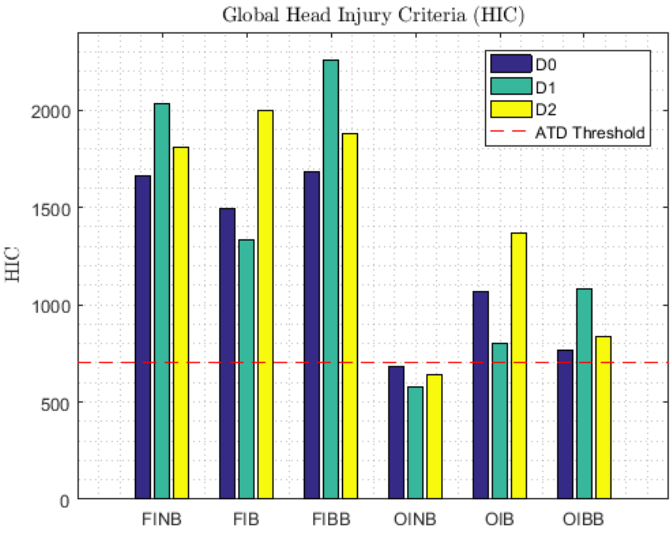

Figure 8.39: *Calculated $HIC_{15}$ values for each simulation setup where the dashed line indicates the severe injury threshold of 700 for Q6 ATD:s.*

Although some parallels can be drawn from the linear head accelerations, discrepancies are found to be of greater magnitude between each parameter than that of the linear accelerations. As the $HIC_{15}$ value is based on the integral of the acceleration, these dissimilarities may be explained by that the measured accelerations are momentous meanwhile the $HIC_{15}$ values is calculated during a larger time window. Observations should be made that some of the FWRB simulations estimated $HIC_{15}$ twice that of the injury threshold for Q6 ATD:s. Although measurements on dummies and HBM:s may not be equivalently comparable, the discrepancies are substantial. As a reference, major $HIC_{15}$ values of the PMHS frontal sled as conducted by Lopez-Valdes et al. [68] measured below 500. Although these values were observed at a lower impact speed (48 [km/h] versus 56 [km/h]) without belt energy management systems, the differences in $HIC_{15}$ values are approximately 480 against 1300 when comparing the baseline frontal impact booster configuration.

### 8.2.3 Upper Neck Tension Forces

Due to existing definitions of coordinate systems in the PIPER scalable child HBM, upper neck Z-forces were extracted between the C2-C3 vertebrae, filtered according to SAE guidelines and presented in Figure 8.40. Commonly, the tensile forces are measured in proximity to the atlanto-occipital joint and could be expected to be higher than forces measured at the C2-C3 joint. Limits are set based on thresholds provided by EuroNCAP protocols for assessment of child occupants protection [34], where the subordinate dashed line represents the upper limit for receiving maximum score. Values within the range between the green and red line are scored according to a scale, where the red line and above equals zero score rating. Although a complete comparison can not be conducted due to differences in measurement points, it can be observed that the frontal crash scenarios reached relatively high forces with the associated expectancy of potentially higher values for the actual measurement point. As can be observed from the presentation, the booster seat reaches the highest score on vertical neck loading, accompanied by the most inboard angle of the booster cushion. On the contrary, the ODB impact pulse achieves relatively low values and would potentially be able to reach top scores. The main outlier is the outboard angle for the high back-booster.

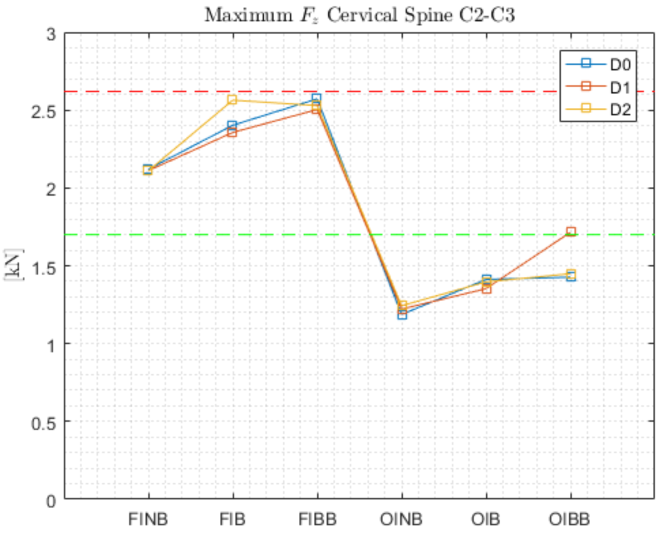

Figure 8.40: *Maximum neck $F_z$ extracted at the C2-C3 vertebrae.*

### 8.2.4 Chest Deflection

For these simulations, chest deflections were estimated using the nodal accelerometers positioned at the lower, mid and upper sternum. Resultant distances were measured towards the defined chest accelerometer positioned at the T6 vertebrae, as can be visualized in Figure 8.41.

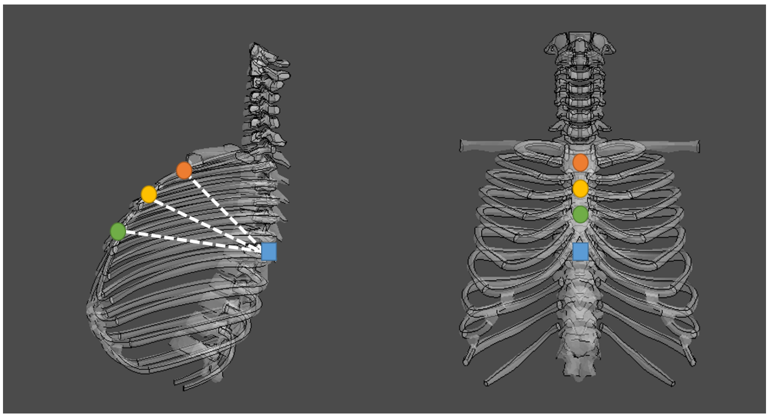

Figure 8.41: *Lateral and frontal view of virtual accelereometers employed for measuring the chest deflections. Blue square corresponds to the chest accelerometer at vertebra T6. Sternum comprises three nodal accelerometers where the green represents the lower sternum, yellow the mid-sternum and red the upper sternum.*

By studying the chest deflection as a function of time, a kinematic behaviour could be observed as exemplified in Figure 8.42. A small displacement was noted derived from the pretensioner acting on the shoulder belt. Subsequently, a plateau or a local minimum was in general identified as the crash pulse peaks causing a significant compression of the chest. Further compression was generally noted when the head impacted the rib cage and abdomen. A concluding deflection could be observed when the child occupant's back was pressed against the seat back cushion, adding to the posterior pressure from the head.

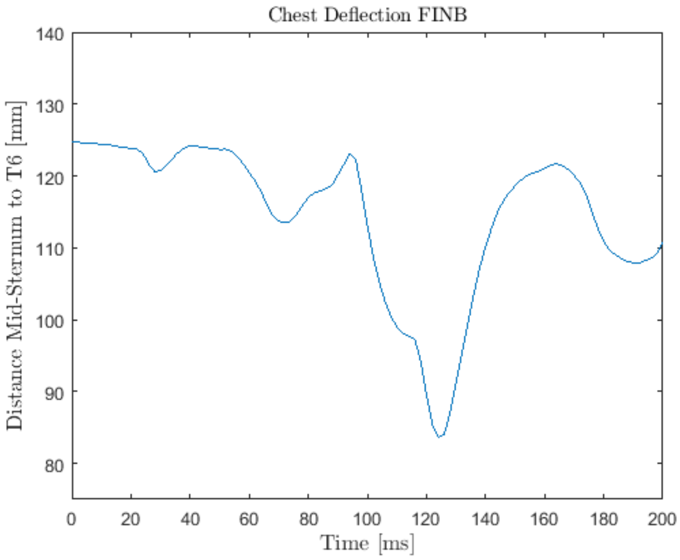

Figure 8.42: *Chest deflection as a function of time, exemplified by the* ***FINB*** *baseline model. A small plateu follows the pretensioner and belt slack reducing force. Second plateu appears during the deceleration as the belt couples the occupant to the vehicle. Subsequently, the third plateu depicts the head impact to the chest and concludingly, the final minimum occurs when the seat's back is pushed against the back of the occupant.*

Maximum chest deflection for each configuration has been depicted in Figure 8.43. Similar to the $HIC_{15}$, compressions equal to the lower threshold or below receive maximum scores which declines in the area between the green and red dashed lines. At the upper line or above, the rating scores equates zero. Based on the protocol, the mid-sternum measurement point is the closest to the Q6-dummy chest load cell. When studying the mid-sternum maximum displacement, all of the FWRB crash scenarios ranges above the upper limit. Although this is prevalent for both the upper and lower sternum a part from a few exceptions, varying relative differences between the parameters can be observed where for instance the outboard angle of **FIB** demonstrates larger deflection at the lower sternum in comparison to the mid-sternum. A majority of the parameters at the FWRB crash scenarios peak at the mid-sternum. Variations are of greater magnitude between the ODB crash pulse scenarios where the outboard angle of **OIB** peaks at the lower sternum whereas a majority of the parameters reach higher values at the upper-sternum than the mid-sternum. In general, the ODB cases achieve lower values than the FWRB scenarios, although most parameters traverse the upper threshold.

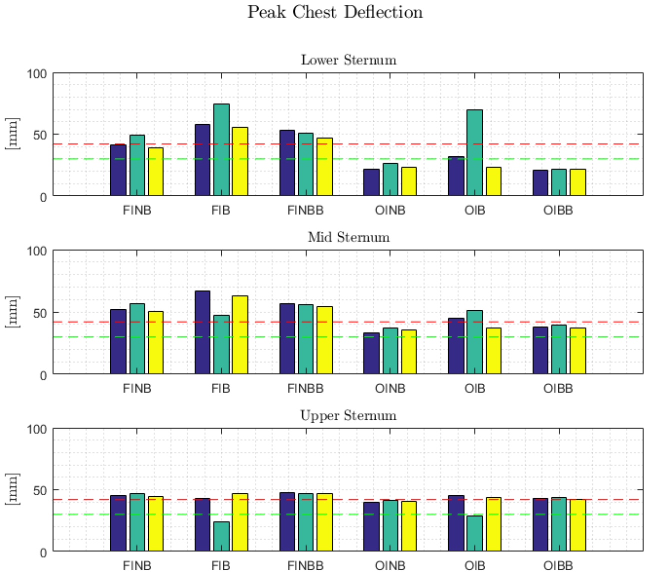

Figure 8.43: *Absolute chest deflection in [mm] where the upper and lower limits are based on the Euro NCAP child occupant protection rating [34].*

Normalized chest deflections have been calculated using the initial chest distance portrayed in Figure 8.44. For both loading conditions, compressions of approximately 60 % were observed for the outboard angle at the booster configuration. Apart from this peak, the relative differences between the different sternum measurements points are smaller for the FWRB impact scenarios. Meanwhile, an increasing trend from lower to upper sternum in chest deflection can be seen for the ODB setupds.

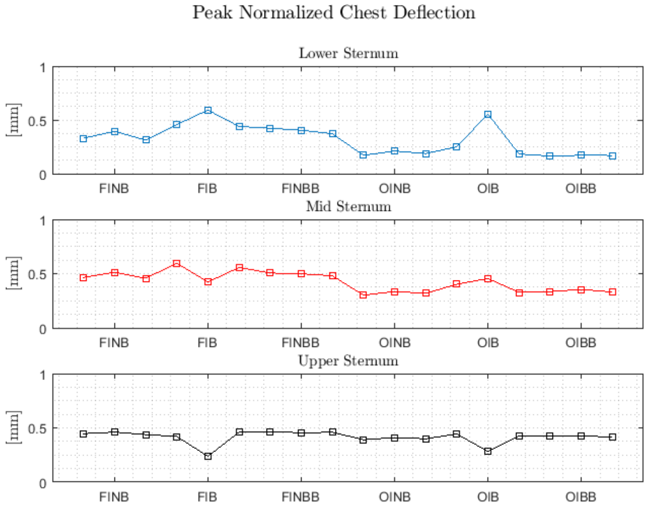

Figure 8.44: *Normalized chest deflection measured at the lower, mid and upper sternum.*

### 8.2.5 Simulation Metrics

Basic simulation parameters such as mass scaling, energy balance and hourglass energy ratio were evaluated for the PIPER child scalable occupant model. Assessments of the mass scaling did not reveal any unreasonable addition where the maximum mass added was observed for the trunk with an addition of approximately 25 g.

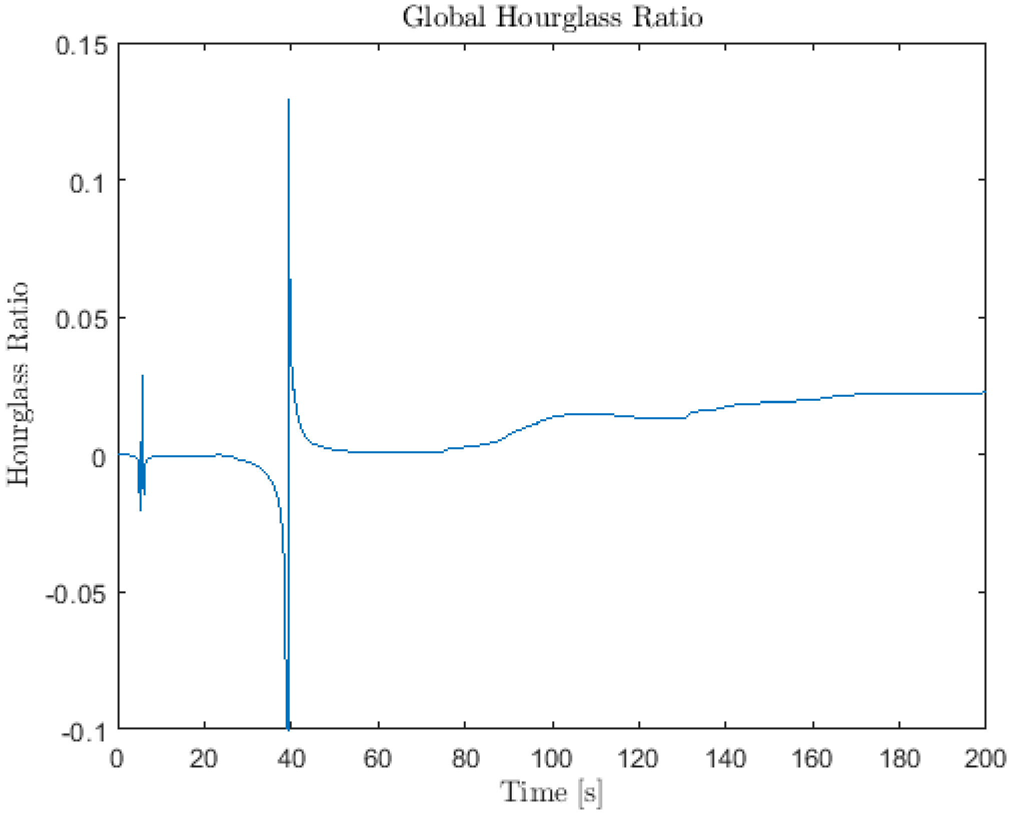

Figure 8.45: *Global hourglass ratio depicted for the simulation setup FINB. A part from initial extreme values, the remainder keeps below 5 %.*

A review of the energy balance equated remained equal a part from an initial dip derived from the 1D-element belt structure when subjected to the pretensioner.

The hourglass ratio did not succeed the recommended threshold of 5 % when conducting a global review of the entire model, including the environment as visualized in Figure 8.45. However, when reviewing the hourglass ratio by subparts, three parts consisting of the right Humerus, right Scapula and the ground substance found inbetween the vertebrae of the cervical spine reached high levels of hourglass energy ratios as depicted in Figure 8.46.

The right humerus achieved hourglass energy ratios of approximately 3000 % in Figure 8.46a, 1600 % for the right scapula in Figure 8.46b and 14000 % for the ground substance of the intervertebral discs in the neck. Further investigations should evaluate if these values are aligned with the validation data, or if the modelling technique in terms of hourglass cards should be reviewed.

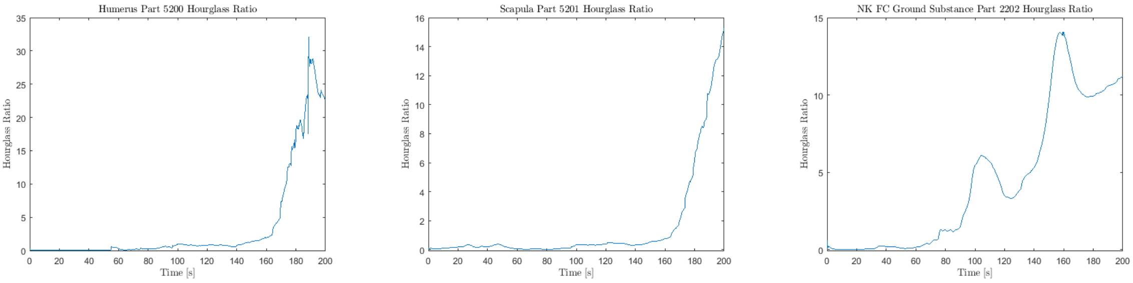

(a) (b) (c)

Figure 8.46: *Figure 8.46a depicts the hourglass ratio of the right Humerus, 8.46b corresponds to the right Scapula and the 8.46c represents hourglass ratio for the intervertebral ground substance of the cervical spine.*

# 9 Discussion

This discussion will analyze the reported results in the perspective of the stated research questions. Stratification in the analysis has been conducted based on the aim of the research questions in combination with the processed data.

- *How do changes in the shoulder belt affect the response of the PIPER scalable child HBM in frontal and frontal offset scenarios?*
- *How robust is the PIPER scalable child HBM?*
- *How user-friendly is the PIPER scalable child HBM and the PIPER framework software?*
- *Does the PIPER scalable child HBM reproduce reasonable kinematic behaviour?*
- *Does the PIPER scalable child HBM reproduce reasonable injury values?*

## 9.1 Sensitivity of the PIPER Child Scalable HBM

Assessment of the sensitivity of the PIPER child scalable HBM has been addressed at three stages where the major classification encompass different loading conditions. Subsequent step is categorization based on belt assisting systems comprising the booster, high-back booster and no booster setup. Concluding differentiation involved translation of the D-ring position which generates an envelope of angles ranging from $19 - 32[^\circ]$, including a baseline angle of $22.3[^\circ]$. Kinematic behavior derived from each of these stages will be discussed in the following subsections.

### 9.1.1 Sensitivity Towards D-ring Position

Envelope of selected angles was based on an UMTRI static belt study conducted by Reed et al. [64] covering the range as recommended by the FMVSS regulations. The most inboard and outboard angles were selected in order to provoke behavioral variations, whereas the baseline model was selected as the design position of the vehicle. It could be argued that disparities of larger magnitude could be observed if a midpoint in between the extreme angles would have been selected. However, this configuration enables evaluation whether the PIPER model is able to capture both smaller and larger alterations in the shoulder belt position.

**Sensitivity D-ring Position - No Booster Scenarios**

As the interior vehicle environment is relatively large in comparison to the the 6 year old child occupant, no major differences were expected between the different parameters as the model was positioned low with regards to the shoulder belt. This resulted in that the shoulder belt crossed the rib cage comparatively high, reducing the distance between the shoulder belt and the neck, even for the more outboard **D2** angle. Initial belt-routing could not be fully straightened as this would have generated complications for the shoulder belt interaction with the neck structure. Instead, final straightening was conducted using the pretensioner.

Initial belt routing in relation to the sternum, rib cage and clavicles portray minimal differences between the **D0** and **D2** parameters where both exhibit an inboard belt interaction meanwhile the **D1** parameter covers less of the sternum and is positioned increasingly outboard on the clavicle. For the FWRB conditions, a small discrepancy could be identified at the end of the simulation during the rebound phase where the **D2** parameter was slightly more rotated outwards to the D-ring with a larger left arm movement with respect to the configurations with smaller angles. In addition, the shoulder belt was positioned in closer proximity to the neck for the inboard angles than that of the **D2** parameter, as could be expected. Evaluation of trajectories for the **FINB** test series demonstrated no significant differences inbetween the parameters. A slight increase in X-excursion was observed for the **D1** and **D2** relative the baseline parameters in Figure 8.34 meanwhile a minor increase of the Z-displacement was noted for the outboard angle comparative to the remaining FINB parameters as can be seen in Figure 8.36.

When observing the effect on the upper thorax with respect to literature which encourages neck loading over roll-out, observed kinematic behaviour may not be as undesirable as expected. However, the whole body kinematics is dependent on the full configuration as well as potential interdependencies between the two belt portions. Upon reviewing the engagement of pelvis by the lap belt, it becomes apparent that the child occupant is exhibiting submarining behaviour and therefore its abdomen is loaded by the lap belt. A minor variation could be observed in terms of flattening of the belt web between the different parameters, but the main implications of this aspect will be further discussed when evaluation PIPER's sensitivity towards different booster configurations.

Analogous to the FWRB simulations without booster, the ODB displayed small variations between the parameters for the kinematic analysis. Setup with the **D1** parameter exhibited a slight engagement of the sternum during loading and the left arm was the main behavioral difference in comparison to the increasingly inboard angles. In addition, increased shoulder belt routing close to the neck was observed for the inboard and baseline angles meanwhile the **D1** shoulder belt had a lesser degree of contact area. An indication of increased outboard rotation of the child occupant was noted when studying the frontal view of spine and pelvis interaction with the belt in Figure 8.10b. Horizontal displacement in terms of trajectories depicted similar levels as the FWRB simulations, a part from a minor decrease of the outboard angle parameter. In contrast, the vertical head trajectories were significantly lower with a slight peak noted for the **D2** scenario.

### Sensitivity D-ring Position - Booster Cushion Scenarios

The booster cushion will elevate the child, imitating the height of an adult. Hence, the potential effects of the shoulder belt variations were expected to be of greater magnitude for this configuration, supported by findings in literature [64]. Belt routing at initial time step depicts a relatively centered shoulder belt position for the baseline model with respect to the upper thorax. Simultaneously, the **D1** parameter is almost beneath the sternum and positioned at the outboard clavicle meanwhile the **D2** parameter is rather similar to the baseline model with a slightly more inboard position on the sternum and clavicle.

Both the FWRB and the ODB crash pulse employing the booster configuration exhibit the largest spread in kinematic behavior among the parameters. Meanwhile the baseline position is close to ideal in terms of shoulder belt interaction, the heightened center of gravity of the child occupant in combination with the outboard angle causes the child to roll out during the acceleration peak for both the frontal and offset loading conditions. Hence, this setup encompasses both the optimal behaviour in terms of loading as well as the worst kinematic behavior. Roll-out prevalent during the FWRB crash pulse was more severe than that of the ODB scenario, but for both configurations the child was rotating around the diagonal belt, hitting its head onto the thighs before bouncing into the side-plane representing the door and window. No contact was placed between the plane and the child's head, therefore such interaction would not be detected in the head injury evaluation. For the inboard angle, the belt was in closer proximity to the neck and during the FWRB-pulse the shoulder belt became twisted.

Lap belt engagement of pelvis was observed for all of the booster setup parameters regardless of loading conditions. In comparison to the parameters of the no booster condition, larger variations in positioning over the thoraco-lumbar spine were observed. In the frontal crashes, the **D0** parameter was positioned across T6 vertebra where the **D1** and **D2** parameters differed 3 vertebrae lower and 2 vertebrae higher respectively. Notable differences were witnessed for the ODB-crash pulse as the discrepancy between the baseline model and the inboard angle was significantly reduced, diverging with approximately half of a vertebra. The baseline parameter was also positioned relatively higher, covering the T3 vertebrae. However, the outboard angle maintained similar position anterior to the T9 vertebrae irrespective of crash-pulse. Increased differences were observed for the ODB scenarios between the more inboard parameters which fixated the spine in comparison to the increasingly outboard rotated spine associated with the **D1** angle.

No variations were observed for the frontal **D0** and **D2** parameters in terms of horizontal excursions, and a small difference was notable for the same parameters pending the ODB crash pulse where the most inboard angle exhibited slightly smaller maximum X trajectory. In contrast, the outboard angle experienced a significantly larger maximum X-excursion following the roll-out behaviour where the relative difference between the inboard angles and the outboard angle was of greater magnitude for the ODB condition. This may be derived from the similar shoulder belt routing with respect to the thorax and thoraco-lumbar spine.

Vertical head displacement was substantially larger for the outboard angle than the remaining angles for both loading conditions. Minor dissimilarities were noted between the baseline and inboard parameters where the discrepancies between the loading conditions were of greater altitudes. Relative differences between the more inboard angles and the roll-out angles were greater for the ODB-pulse than the FWRB-pulse, although similar trends were observed for both setups.

**Sensitivity D-ring Position - Booster Seat Scenarios**

As the booster seat included in these simulations possessed an integrated D-ring for the shoulder belt, less variations between the parameters were expected since the alterations in D-ring positions could be attenuated by the enforced belt routing. Initial shoulder belt routing with respect to the rib cage, sternum and clavicles depicted less variations than the remaining booster configurations. Nevertheless for the FWRB-pulse, an increased twisting of the shoulder belt was found for the inboard and baseline parameters which increased loading obliquely positioned over the sternum apart from a small area in the upper left corner. In contrast, the belt webbing was maintained relatively flat for the outboard angle which covered a larger part of the sternum although neglecting the lower and the upper left corner. Less twisting was observed for the ODB-crash pulse where a larger portion of the belt covered the upper and mid sternum as well as the sternoclavicular joint meanwhile the D1 parameters maintained a path across the inboard right clavicle.

Similar to the booster configuration, simulations conducted in the high-back booster allowed for proper pelvis and lap belt interaction. Differences between the baseline and inboard angle with respect to the thoracolumbar spine were close to non-existing and the outboard angle maintained a higher position in proximity to the inboard angles when comparing to the backless booster simulations.

In terms of maximum trajectories, a small increase in horizontal excursion was noted for outboard D-ring position in comparison to the more inboard angles for both loading conditions. The FWRB **D0** and **D1** parameters were at similar altitude, and for the ODB counterparts a minor deflection could be noticed for the inboard parameter. Comparatively, the vertical displacement was slightly more prominent than the horizontal excursions, in particular for the frontal loading conditions.

### 9.1.2 Sensitivity Towards Belt Assisting Devices

Subsequent analysis will discuss the sensitivity of PIPER to capture differences with seat belt interaction between booster configurations comprising the no booster, booster cushion and booster seat scenarios. As previously discussed, undesirable kinematic behaviours such as roll-out, submarining and head impact with side structures have been observed across the simulations.

For the configuration without any booster cushion, behaviour such as late roll-out was detected for all of the simulations. Late roll-out has here been defined as falling out of the belt in an inboards manner during the rebound phase. Even though this may not be as hazardous as the peak roll-out which occurs during the maximum acceleration, it could still induce harm in terms of collision with other passengers or not properly restrain the occupant in the event of a subsequent crash. Penetration of the shoulder belt into the seat's back during the simulations was observed for the FWRB **D0** and **D2** parameters as exemplified in Figure 9.1. This behaviour was not observed for the outboard angles although similar kinematic behaviour was experienced by the occupant combined with a comparatively high position of the shoulder belt which attenuates the outboard angle affect with respect to the child's CG, hence indicating that this may not necessarily influence the results in a significant manner. However, this must be further investigated. A physical parallel could be drawn by suggestions made by Reed et al. [64] that seat belt interaction with back rest needs to be investigated as this may effect the performance of the restraint system, in particular for narrow D-ring to H-point angles. Similar belt penetrations were observed for the **D0** and **D2** parameters of the ODB-crash pulse. Due to the nature of the ODB-pulse, the simulations did not reach a late roll-out with respect to time although it may be implied prior to termination of the simulations.

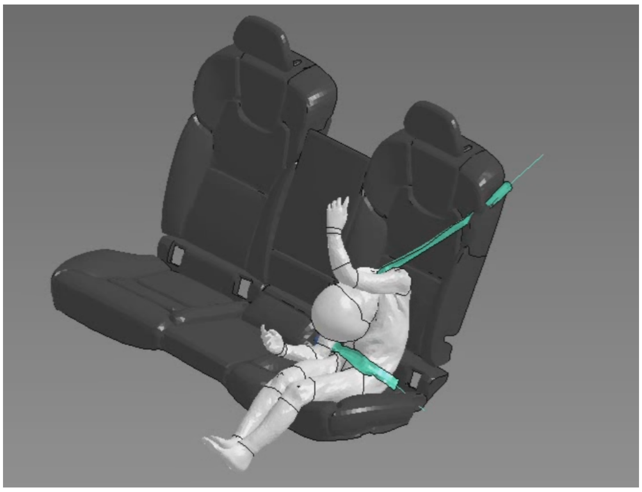

Figure 9.1: *Observed penetration of the shoulder belt after contact with the back rest of the seat.*

In terms of trajectories, the no booster scenarios depicted similar altitude for both loading conditions and had the lowest X-excursions out of the three variations. Variations between the loading conditions were observed for the vertical displacement where the ODB-crash scenario had lesser Z-excursions than the FWRB. For both loading conditions, although especially for the ODB scenario, the maximum Z trajectory was similar for the no booster scenario as well as the backless booster scenario apart from the outboard parameter of the booster condition. As the rear seat is relatively large in relation to the 6 year old occupant, the child was positioned moderately low with respect to the adult seat belt geometry. As the trajectories in the XZ-plane for the rear seat only portrayed better values in comparison to the belt assisting devices correlated to the increased neck and arm pit loading of the shoulder belt. Investigation of the lap belt interaction demonstrated both submarining and abdominal load for all of the no booster parameters regardless of loading condition. The edge of the interior seat cushion corresponded to the mid calves of the child and the knee angle was significantly wider than the booster cushion and booster seat configurations, forcing the legs to become almost straight. For the booster cushion and booster seat on the other hand, the knee passed the booster's edge which facilitated a natural bend similar to that of an adult positioned in the rear seat.

A majority of the simulations exhibited head impact to the thoraco-abdominal region, mainly targeting the lower rib cage. Visual comparison between a PMHS study as published by Lopez-Valdes et al. [68] and the baseline booster cushion model confirmed that this behaviour might be realistic, especially considering that PIPER development team has prioritized validation against PMHS studies. The booster setup, which according to literature is one of the optimal belt assisting devices, encompassed the biggest diversity in terms of kinematic behaviour. It captured both one of the optimal positions in terms of shoulder belt routing in relation to the upper thorax yet containing one of the worst behaviour with an early roll-out of the belt. Maximum head trajectories for the inboard and baseline parameters were found above the threshold from the PMHS experiment without seat belt energy management systems for both loading conditions although the ODB was found to be slightly below the FWRB. Sources for discrepancies could be found in differences between the experimental sled and the virtual car environment, usage of a generic seat belt and retractor model as well as different impact speeds. Outboard parameters of the booster scenarios are markedly peaking which is related to the roll-out behaviour. Despite relatively high horizontal excursions for the FWRB and ODB booster and high back booster configurations, none of the setups interacted with the frontal plane. However, with respect to the lateral plane, the **D1** parameter caused the child to first impact its head onto the thighs and then bounce into the side plane. As no comparative data was included in the PMHS study for lateral excursions. These graphs were not included in the report, but can be found in Appendix B.

Since the booster cushion is according to a growing body of research one of the optimal belt assisting tools for a 6 year old, indications of such non-optimal behavior would be both interesting and important to evaluate. From a physical point of view, the center of gravity of a child is elevated when positioned on a booster but it is not integrated with the booster itself. Therefore the baseline angle may be optimally routed, while for an outboard D-ring position it would lower the belt thus facilitating the roll-out behavior. As the HBM is more flexible than a physical ATD and issues concerning belt interaction with the stiffer dummy geometry have been highlightened in literature, perhaps such behaviour would not have been possible to detect with the golden standard physical crash test. The extreme D-ring positions are selected based on the envelope provided by the FMVSS which was intended to provoke the model's behaviour. It would however be interesting to vary this parameter with a higher resolution in order to evaluate at what angle this behavior stops and how often this would be found in existing vehicles. However, it is important to note that further kinematic evaluations are required to fully evaluate the validity of this behaviour where alternative comparisons to ATD:s could be performed. If this behaviour would prove to be valid, it could act as an argument to enforce testing of the child booster cushions and similar devices in an actual vehicle environment rather than a test bench. Differences between the loading conditions were noted for the vertical displacement which could be related to the different characteristics of the ODB-pulse. Similar to the horizontal excursions, both loading conditions peaked for the **D1** roll-out parameter.

Large displacements of the booster cushion and corresponding high pelvis acceleration are most likely derived from the simulation setup rather than physical reasons, as such behaviour would be captured during physical crash tests. Reasons for this could be related to initial stress and strains imposed on the impact simulation, too low friction coefficient in the contact between the booster and the rear seat cushion as well as excessive initial belt slack, in particular for the lap belt which is not connected to a retractor. Belt routing under the belt guides of the booster cushion was not trivial, thus improved belt routing could potentially reduce the jumping behaviour of the booster cushion.

As expected, the high-back booster portrayed only a slight variation in terms of the outboard angles with respect to the horizontal and vertical displacements. For the X-trajectories, the frontal excursions were of similar magnitude as the backless booster, but they were in general higher in vertical displacement. This behaviour could be derived from the head impact with the side-structures for all of the high-back booster simulations. Although a complete evaluation of the high-back booster could not be conducted as certain parts of the booster did not achieve contact with the shoulder belt following sliding out of the integrated D-ring, it was still deemed sufficient to recognize a potential concern which requires further evaluation. Shoulder belt glided out of the integrated D-ring for all of the high-back booster simulations during the FWRB, but did not glide out during the ODB-pulse.

## 9.2 Injury Biofidelity of the PIPER Scalable Child HBM

Due to scarce data concerning pediatric injury criteria, only a few metrics have been selected as initial assessment of the PIPER scalable child model's injury biofidelity. Designated metrics were the global head injury criteria (HIC), upper neck forces and chest deflection. Resultant linear and angular accelerations have in addition been reviewed.

### 9.2.1 Comparison of Accelerations

Upon comparing the data from the PMHS study as conducted by Lopez-Valdes et al. [68] with maximum resultant linear accelerations measured from the simulations, it was observed that for the **FIB** baseline scenario, all of the **OINB** parameters, the baseline **OIB** configuration and the baseline and outboard angles of the **OIBB** setup contained potentially similar values. Acceleration measurements for mentioned simulations ranged from $77.21 - 111$ [g] meanwhile the scaled PMHS values for the high severity crash pulse were 104.2 [g] and 107.5 [g]. Following considerations should however be kept in mind when comparing the data; different experimental/simulation setup, lower crash pulse for the PMHS study, different EM system, potentially different material properties for belt and cushion, repeated crash tests of one PMHS, limited data set due to only one PMHS, scaling of PMHS data, no ODB-pulse was evaluated for the PMHS and potentially different booster cushions were employed. Although bias and error sources are most likely present, the data can still act as an indicator whether simulation measurements appear reasonable with the aim to further evaluate full body kinematics of the PIPER scalable child model. Upper range of linear head accelerations comprised values from $134 - 296.5$ [g] spread out on different simulation configurations excluding the ODB-pulse no booster setup and peaking at the high-back booster scenario. Potential reasons for this observed peak could be excessive head and chest interaction with the upper head structure and the back of the high-back booster. When comparing the measured data from the ATD with the scaled PMHS, the Hybrid III 6 year old was significantly underestimated the accelerations at approximately 46 [g] and 65 [g] with and without EM-systems respectively.

Mid-spine measurements were selected for comparison with the virtual chest accelerometer of the PIPER model positioned at the T6 vertebra. Significant difference was noted between the scaled PMHS experiment with and without EM-systems 57.7 [g] and 105.5 [g]. Maximum chest accelerations of the PIPER model ranged between $78.2 - 320$ [g], peaking at the **FIBB** setup where similar reason could be derived as for the increase in head accelerations. For the belt-positioning booster scenario, the **D0** and **D2** parameters were increased in comparison to the head accelerations, meanwhile the **D1** parameter associated with the roll-out behavior was significantly lower. Similar behaviour was seen for **D1** parameter of the ODB-pulse booster scenarios, although it was now accompanied by the **D2** parameter. In general, the chest accelerations were relatively high in comparison to the head acceleration when relating to the PMHS experiment employing the EM-systems. In the PMHS study, the Hybrid III 6 year old underestimated the accelerations by approximately 50 %.

For the PIPER's pelvis accelerations, all of the measured values were higher than the head accelerations which indicates a trend that does not appear in the PMHS study as reported by Lopez-Valdes et al. [68]. Pending the simulations, maximum linear pelvis accelerations varied from $218.7 - 802$ [g]. Peaks were found for the **D0** and **D1** parameters. During the visual analysis, excessive vertical displacement were observed for the **OIB** although it was not apparent how two of the parameters could diverse from the inboard angle by approximately 450 [g]. By certainty, the slack in lap belt could be reduced, but this factor would not explain a discrepancy of this magnitude. Considering the generally high pelvis acceleration, sources of simulation errors that could potentially influence such behaviour could be initial stress/strain values following the positioning simulation, inadequate contact settings between model and environment, initial slack in belt and material properties of the belt. However, as this as been observed for all of the simulations, it could potentially be related to material properties, accelerometer constraints and position, stiffness properties or contacts in the PIPER scalable child HBM. Further evaluation employing both physical tests concerning ODB-pulses as well additional PIPER evaluations should be conducted before proper conclusions could be drawn.

### 9.2.2 Global Head Injury Criteria

As previously discussed, it appears as if the PIPER scalable child HBM overestimates the $HIC_{15}$ values, in particular for the FWRB-pulse. For the FWRB-pulse, the values ranged between approximately $1300 - 2200$ meanwhile the ODB-pulse was measured in the $600 - 1300$ interval. Considering the fact that no contact was applied between the model and the kinematic boundary planes, the primary head impact occurred between the child and its thorax. Subsequently, as the thorax of a child is not stiff enough to generate skull fractures, presented $HIC_{15}$ values are unlikely. Secondary head impact could occur from the upper structure of the high-back booster. Nevertheless, the secondary impact would not explain the relatively small differences between booster conditions when reviewing average statistics. During the outboard booster conditions where the pediatric occupant rolled-out and experienced head impact with thighs constituted some of the lower $HIC_{15}$, which would contradict existing impact scenarios as principle cause for such elevated values.

Recordings from the PMHS-study as reported by Lopez-Valdes et al. [68] extracted during the high severity crash pulse revealed $HIC_{15}$ measurements of 368 and 481 with and without belt EM-systems correspondingly. Although these values are documented from one test subject in a slightly lower impact speed with a different environment, and even though these values have not been scaled from a 10 year old to a 6 year old it could still indicate that these $HIC_{15}$ estimations are out of range. An average 6 year old would be expected to have an increase in $HIC_{15}$ due to a proportionally larger head and a weaker neck structure than that of an average 10 year old, yet discrepancies of such magnitude appear unreasonable.

Previously discussed limitations in the simulation setup may influence the accelerations, yet further evaluations should be conducted on the ability of PIPER to calculate $HIC_{15}$. Recommendations are to extend the validation of the neck, both in terms of moments and forces during full kinematic behaviour as well as evaluating the stiffness and material properties. One of the components with substantially high hourglass ratio is the **2202 NK_FC_Ground Substance_3D** which is found in the intervertebral discs, a property which should be evaluated whether the increased stiffness is aligned with actual material properties. Biofidelic range of movement of the neck should in addition be further investigated, in particular the combination of rotation and flexion. Concludingly, future validation should aim to compare PIPER's performance with high severity crash pulses.

### 9.2.3 Neck $F_z$

$F_z$ between the C2-C3 vertebrae was compared to the EuroNCAP neck tension thresholds for the Q6 ATD. Larger discrepancies were found in between the booster configurations and loading conditions rather than the different belt parameters apart from the **D2** parameter which peaked for the FWRB booster without back and the **D1** parameter for the ODB high-back booster. Acknowledgements should be made about the differences in quality between the sampled FWRB pulse and the fully equipped ODB pulse. High tensile forces were found for the FWRB configurations. Less tensile forces for the no booster conditions could potentially be derived from the fact that the shoulder belt was positioned higher on the small occupant. In general, highest values were measured for the booster seat which could be a results of impact from the upper head and back structure of the booster. Almost all of the ODB-values were below the critical area, indicating that the model was able to capture differences in loading condition. Although these values could not be considered equivalent as the measurement points differs between the Q6 dummy and the C2-C3 vertebrae location of the PIPER model, the FWRB measurements are on the higher end. Further research should be assigned in order to evaluate if these values are biofidelic and that the neck-model does not overestimate the tensile loading.

### 9.2.4 Chest Deflection

Chest deflection over time links the chest compression with the kinematic behaviour of the occupant model where belt loading, head impact with thorax and final added compression made by interaction with the seat could be visualized. Absolute peak chest deflections showed that the compression in general was above thresholds set by the EuroNCAP for the Q6 dummy. As the pediatric rib cage is more flexible than that of an adult due to a larger portion of cartilaginous tissue material, the chest compression may not necessarily imply rib fracture. It would however be interesting to continue working on the model of the lungs in order to assess thresholds for pneumothorax which is according to literature more prevalent among children. By measuring at the lower, mid and upper sternum, relative differences could be observed between the shoulder belt parameters, although the mid sternum measurements were able to capture critical areas for the FWRB pulse. In contrast, the upper sternum portrayed on average the highest chest deflections which could potentially be a result of a different shoulder belt loading during the rotational movement. Findings in literature have addressed the issue with capturing true chest compression of ATD:s as the shoulder belt slides of the deflection sensor. Results of the ODB-crash pulse could therefore indicate a potential opportunity to portray the actual maximum deflection as more measurement points are available.

## 9.3 Robustness of the PIPER Child Scalable HBM and the PIPER Personalization Framework

Out of the 18 simulations, 17 simulations were able to reach normal termination time. The remaining simulation, **FIB_D0**, was able to capture the maximum acceleration peak and terminated during the rebound phase, hence the results were included although this deficiency should be kept in mind. In general, a majority of the simulations required manual processing in terms of belt routing to avoid termination due to negative volume mainly located in the neck region. This project aimed to assess the current status of the PIPER scalable child model, therefore no alterations of the model's properties have been conducted. Explanations have not been found on why the **FINB_D0** did not reach full termination due to negative volume in the neck as the shoulder belt routing was considered to be close to optimal. Supplementary to negative volume, NaN and shooting nodes were identified as common simulation issues where some were addressed by changing the LS-Dyna binary. During the feasibility study which contained the only specimen of a scaled $50^{th}$ percentile 5 year old, shooting interpolation nodes in the neck were expressed as the reason for not being able to reach normal termination.

Further investigations should evaluate different ages and sizes of the PIPER child scalable HBM within given range to estimate if this is a structural problem in the model.

Scaling and positioning of limbs were facilitated by a user friendly environment. Neck positioning module was reportedly malfunctioning, hence this was not applied. However, after positioning the elbow of both a 6 year old and a 5 year old PIPER child, problems occurred as the final model's ulnar and radius were translated backwards and penetrated the model's skin on the interior side of the elbow. Further investigations should address this problem and evaluate if this occurs in additional body parts for other joints. In addition, the smoothing of solid elements using Kriging in a box was somewhat problematic to optimize and during the final sessions it was not possible to evaluate the quality of the elements due to a problem with the software.

# 10 Conclusions

## 10.1 Evaluation of the PIPER Scalable Child HBM

The PIPER scalable child HBM is a great initiative which takes an important step in order to contribute to the gap of virtual models that can assess pediatric safety aspects in motor vehicle crash scenarios. With this in mind, it is important to address the lack of data on pediatric injury tolerances and kinematic behaviour which is required to validate these substantial efforts.

Analysis of the kinematic behaviour did find promising abilities for the PIPER scalable child model to respond to varying input configurations. Undesirable belt behaviours such as submarining, roll-out and interaction with both the belt geometry as well as the child safety equipment were observed during the span of 18 parametric simulations. Although demonstrating positive indications, further evaluation of the kinematic responses should be conducted to generate a larger validation data set, in particular for high-severity crash pulses. In addition, findings of this project support HBM as a complementary tool to the physical crash test.

Limitations were observed in terms of injury criteria, where the main focus assessed the commonly used $HIC_{15}$. The PIPER scalable HBM model appeared to overestimate these values. In combination, research should additionally address appropriate biofidelic values as most of the data is gathered from dummy ATD:s or scaled from adults values. Concludingly, further validation of the neck's range of motion and the high tensile neck forces would be beneficial.

## 10.2 Future Work and Recommendations

Endorsements for further evaluations of the PIPER model have been assembled in this section. For instance, recommendations are to conduct the ODB loading conditions with the child seated behind the passenger front seat as this may produce different belt interaction behaviour. By using a more advanced belt setup and corresponding energy management systems, unstable behaviour observed with the booster cushion may be attenuated.

Similar parametric setup would be interesting to execute while scaling the child occupant in terms of age and size in order to evaluate the efficiency of the safety systems for a population. Investigations could potentially address interdependencies between the shoulder belt and the lap belt. Variations of the D-ring position could comprise higher resolutions in the YZ-plane as well as adding variations in positions within the XZ-plane. Such information could be used to optimize devices addressing shoulder belt fit. Complementary, effects of altering the buckle position could in addition be assessed. For this study, analyses were conducted on the excursions in the XZ-plane. Next step could be to include lateral excursions as well.

Pending improved positioning, it would be interesting to test the PIPER's ability to evaluate deliberate missuse in terms of non optimal belt routing or behaviour associated with children.

If the kinematic behaviours identified in this project prove to be valid, it could be an important argument to extend the current CRS regulation to include testing in actual vehicles instead of simply using a standardized test bench. Additional benefits could be to perform virtual assessments when designing CRS together with different vehicles, thus including safety systems from a pediatric perspective for a larger population which is not confined to an average child or age group.

# Appendix A: Validation Matrix Of PIPER Scalable Child HBM

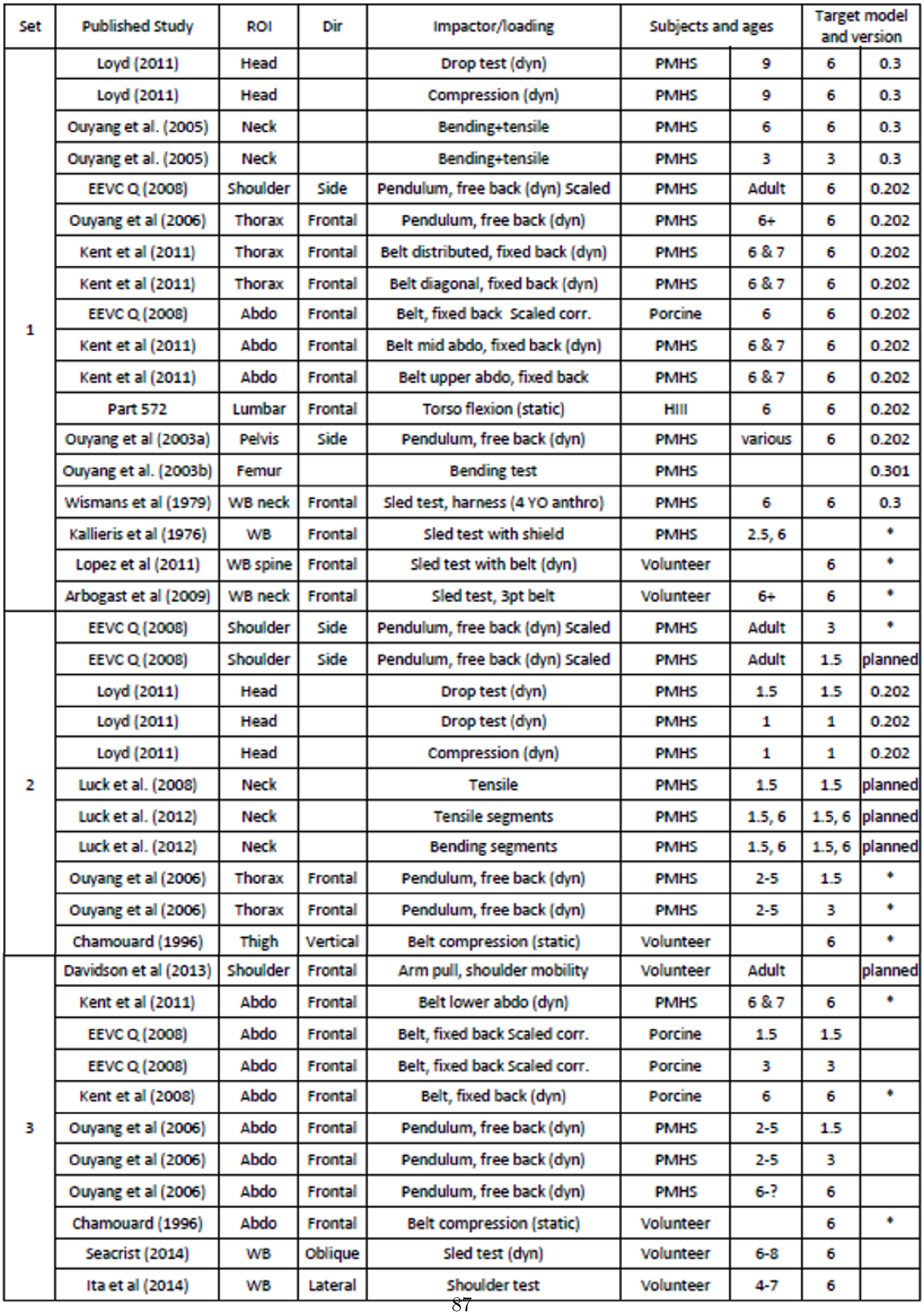

| Set | Published Study | ROI | Dir | Impactor/loading | Subjects and ages | | Target model and version | |
|---|---|---|---|---|---|---|---|---|
| 1 | Loyd (2011) | Head | | Drop test (dyn) | PMHS | 9 | 6 | 0.3 |
| | Loyd (2011) | Head | | Compression (dyn) | PMHS | 9 | 6 | 0.3 |
| | Ouyang et al. (2005) | Neck | | Bending+tensile | PMHS | 6 | 6 | 0.3 |
| | Ouyang et al. (2005) | Neck | | Bending+tensile | PMHS | 3 | 3 | 0.3 |
| | EEVC Q (2008) | Shoulder | Side | Pendulum, free back (dyn) Scaled | PMHS | Adult | 6 | 0.202 |
| | Ouyang et al (2006) | Thorax | Frontal | Pendulum, free back (dyn) | PMHS | 6+ | 6 | 0.202 |
| | Kent et al (2011) | Thorax | Frontal | Belt distributed, fixed back (dyn) | PMHS | 6 & 7 | 6 | 0.202 |
| | Kent et al (2011) | Thorax | Frontal | Belt diagonal, fixed back (dyn) | PMHS | 6 & 7 | 6 | 0.202 |
| | EEVC Q (2008) | Abdo | Frontal | Belt, fixed back Scaled corr. | Porcine | 6 | 6 | 0.202 |
| | Kent et al (2011) | Abdo | Frontal | Belt mid abdo, fixed back (dyn) | PMHS | 6 & 7 | 6 | 0.202 |
| | Kent et al (2011) | Abdo | Frontal | Belt upper abdo, fixed back | PMHS | 6 & 7 | 6 | 0.202 |
| | Part 572 | Lumbar | Frontal | Torso flexion (static) | HIII | 6 | 6 | 0.202 |
| | Ouyang et al (2003a) | Pelvis | Side | Pendulum, free back (dyn) | PMHS | various | 6 | 0.202 |
| | Ouyang et al. (2003b) | Femur | | Bending test | PMHS | | | 0.301 |
| | Wismans et al (1979) | WB neck | Frontal | Sled test, harness (4 YO anthro) | PMHS | 6 | 6 | 0.3 |
| | Kallieris et al (1976) | WB | Frontal | Sled test with shield | PMHS | 2.5, 6 | | * |
| | Lopez et al (2011) | WB spine | Frontal | Sled test with belt (dyn) | Volunteer | | 6 | * |
| | Arbogast et al (2009) | WB neck | Frontal | Sled test, 3pt belt | Volunteer | 6+ | 6 | * |
| 2 | EEVC Q (2008) | Shoulder | Side | Pendulum, free back (dyn) Scaled | PMHS | Adult | 3 | * |
| | EEVC Q (2008) | Shoulder | Side | Pendulum, free back (dyn) Scaled | PMHS | Adult | 1.5 | planned |
| | Loyd (2011) | Head | | Drop test (dyn) | PMHS | 1.5 | 1.5 | 0.202 |
| | Loyd (2011) | Head | | Drop test (dyn) | PMHS | 1 | 1 | 0.202 |
| | Loyd (2011) | Head | | Compression (dyn) | PMHS | 1 | 1 | 0.202 |
| | Luck et al. (2008) | Neck | | Tensile | PMHS | 1.5 | 1.5 | planned |
| | Luck et al. (2012) | Neck | | Tensile segments | PMHS | 1.5, 6 | 1.5, 6 | planned |
| | Luck et al. (2012) | Neck | | Bending segments | PMHS | 1.5, 6 | 1.5, 6 | planned |
| | Ouyang et al (2006) | Thorax | Frontal | Pendulum, free back (dyn) | PMHS | 2-5 | 1.5 | * |
| | Ouyang et al (2006) | Thorax | Frontal | Pendulum, free back (dyn) | PMHS | 2-5 | 3 | * |
| | Chamouard (1996) | Thigh | Vertical | Belt compression (static) | Volunteer | | 6 | * |
| 3 | Davidson et al (2013) | Shoulder | Frontal | Arm pull, shoulder mobility | Volunteer | Adult | | planned |
| | Kent et al (2011) | Abdo | Frontal | Belt lower abdo (dyn) | PMHS | 6 & 7 | 6 | * |
| | EEVC Q (2008) | Abdo | Frontal | Belt, fixed back Scaled corr. | Porcine | 1.5 | 1.5 | |
| | EEVC Q (2008) | Abdo | Frontal | Belt, fixed back Scaled corr. | Porcine | 3 | 3 | |
| | Kent et al (2008) | Abdo | Frontal | Belt, fixed back (dyn) | Porcine | 6 | 6 | * |
| | Ouyang et al (2006) | Abdo | Frontal | Pendulum, free back (dyn) | PMHS | 2-5 | 1.5 | |
| | Ouyang et al (2006) | Abdo | Frontal | Pendulum, free back (dyn) | PMHS | 2-5 | 3 | |
| | Ouyang et al (2006) | Abdo | Frontal | Pendulum, free back (dyn) | PMHS | 6-? | 6 | |
| | Chamouard (1996) | Abdo | Frontal | Belt compression (static) | Volunteer | | 6 | * |
| | Seacrist (2014) | WB | Oblique | Sled test (dyn) | Volunteer | 6-8 | 6 | |
| | Ita et al (2014) | WB | Lateral | Shoulder test | Volunteer | 4-7 | 6 | |

Figure 10.1: *Validation Material for the PIPER Scalable Child HBM as presented by Beillas et al. [84].*

# Appendix B: Frontal and Lateral Trajectories

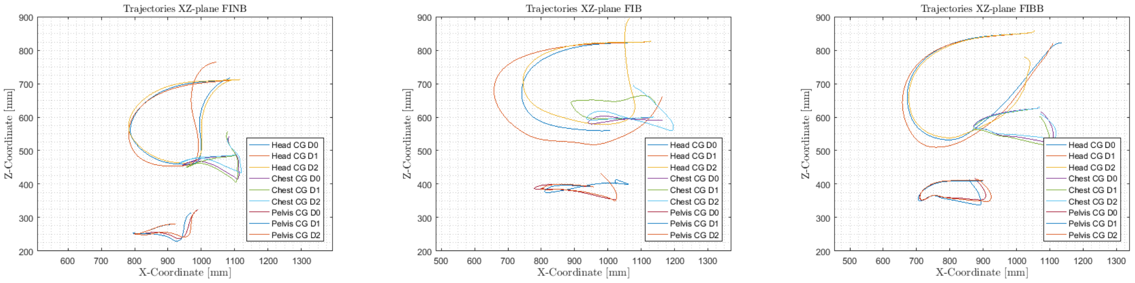

(a) (b) (c)

Figure 10.2: *Frontal trajectories in the XZ-plane depicted for* ***FINB*** *in 10.2a,* ***FIB*** *in 10.2b and* ***FIBB*** *in 10.2c.*

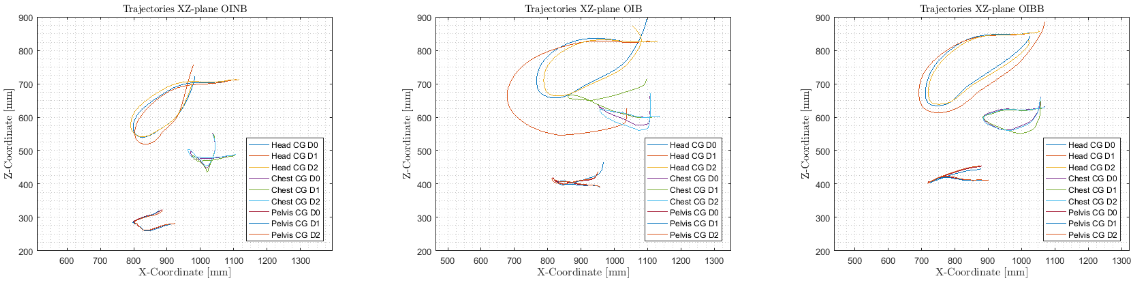

(a) (b) (c)

Figure 10.3: *Frontal trajectories in the XZ-plane visualized for* ***OINB*** *in 10.3a,* ***OIB*** *in 10.3b and* ***OIBB*** *in 10.3c*

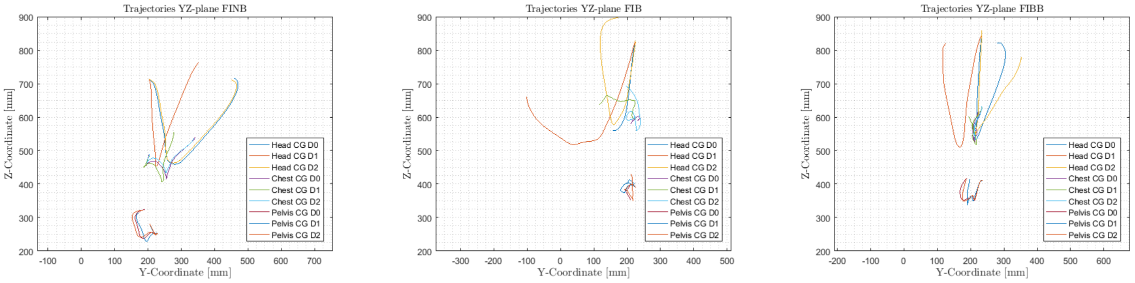

(a) (b) (c)

Figure 10.4: *Lateral trajectories in the YZ-plane portrayed for* ***FINB*** *in 10.4a,* ***FIB*** *in 10.4b and* ***FIBB*** *in 10.4c*

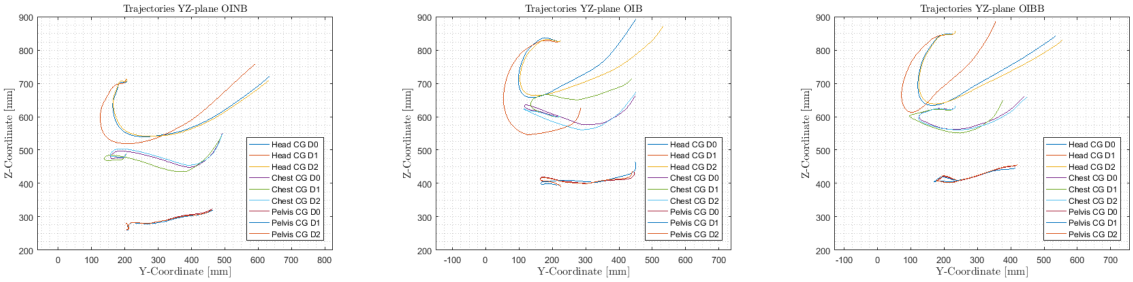

(a) (b) (c)

Figure 10.5: *Lateral trajectories in the YZ-plane demonstrated for* ***OINB*** *in 10.5a,* ***OIB*** *in 10.5b and* ***OIBB*** *in 10.5c*

# Appendix C: Belt Material and Section Cards

data.txt

```
$# LS-DYNA Keyword file created by LS-PrePostR V4.5.4 - 04Nov2017
$# Created on May-27-2018 03:05:00
$$$$$$$$$$$$$$$$$$$$$$$$$$$$$$$$$$$$$$$$$$$$$$$$$$$$$$$$$$$$$$$$$$$$$$$$

                                                2018-05-03
                                Reconstructed Belt Properties
                                                Based on:
                        ViVA - Virtual Vehicle-safety Assessment:
        OpenSource Human Body Models addressing gender diversity



$$$$$$$$$$$$$$$$$$$$$$$$$$$$$$$$$$$$$$$$$$$$$$$$$$$$$$$$$$$$$$$$$$$$$$$$
$#                                                                         title
Belt_1D
$#     pid     secid       mid     eosid      hgid      grav    adpopt      tmid
    970105    970106     30003         0         0         0         0         0
$#                                                                         title
Belt_2D
$#     pid     secid       mid     eosid      hgid      grav    adpopt      tmid
    970106    970105     30002         0         0         0         0         0
BELT_1D
$#   secid      area     thick
    970106       0.0       0.0
BELT_1D
$#     mid      mpul     llcid     ulcid      lmin       cse      damp         e
     300035.50000E-4     10001     10001       1.0       0.0       0.0       0.0
BELT_2D
$#   secid    elform      shrf       nip     propt   qr/irid     icomp     setyp
    970105         9    0.8333         1       1.0         0         0         1
$#      t1        t2        t3        t4      nloc     marea      idof    edgset
       1.2       1.2       1.2       1.2       0.0       0.0       0.0         0
BELT_2D
$#     mid        ro        ea        eb         -      prba      prab         -
     300029.26000E-6      2.48       0.0       0.0       0.0       0.0       0.0
$#     gab         -         -       cse        el       prl    lratio      damp
       0.0       0.0       0.0       0.0       0.0       0.0       0.0      0.05
$#    aopt       flc       fac       ela      lnrc      form     fvopt    tsrfac
       0.0       0.0       0.0       0.0       0.0         0         0       0.0
$#  unused    rgbrth     a0ref        a1        a2        a3        x0        x1
                 0.0         0       0.0       0.0       0.0       0.0       0.0
$#      v1        v2        v3         -         -         -      beta    isrefg
       0.0       0.0       0.0       0.0       0.0       0.0       0.0         0
```

# References

(1) (WHO), W. H. O. Ten strategies for keep children safe on the road., `http://www.who.int/roadsafety/week/2015/Ten_Strategies_For_Keeping_Children_Safe_on_the_Road.pdf`, (accessed: 28.05.2018).

(2) Brolin, K.; Stockman, I.; Andersson, M.; Bohman, K.; Gras, L.-L.; Jakobsson, L. Safety of children in cars: A review of biomechanical aspects and human body models. *International Association of Traffic and Safety Sciences* **38** (**2015**), 92–102.

(3) Reed, M. P.; Klinich, K. D. Predicting vehicle belt fit for children ages 6-12. *Traffic Injury Prevention* **17** (**2016**), 58–64.

(4) Project, P. Vision., `http://piper-project.org/vision#eid`, (accessed: 15.05.2018).

(5) Bohman, K.; Arbogast, K. B.; Loeb, H.; Charlton, J. L.; Koppel, S.; Cross, S. L. Frontal and oblique crash tests of HIII 6-year-old child ATD using real-world, observed child passenger postures. *Traffic Injury Prevention* **19** (**2018**), PMID: 29584494, S125–S130.

(6) Giordano, C.; Li, X.; Kleiven, S. Performances of the PIPER scalable child human body model in accident reconstruction. *PLoS ONE* **12** (**2017**), 91–114.

(7) Burdi, A. R.; Huelke, D. F.; Snyder, R. G.; Lowrey, G. H. Infants and children in the adult world of automobile safety design: Pediatric and anatomical considerations for design of child restraints. *Journal of Biomechanics* **2** (**1969**), 267–280.

(8) Yoganandan, N.; Kumaresan, S.; Pintar, F. A.; Gennarelli, T. A. *Accidental Injury 2nd Edition*, Nahum, A. M., Melvin, J. W., Eds.; Springer: New York, 2002; Chapter 21, pp 550–587.

(9) Swearingen, J. J.; Young, J. W. *Determination of Centers of Gravity of Children, Sitting and Standing.* Tech. rep. AM 65-23; FEDERAL AVIATION AGENCY - Office of Aviation Medicine Civil Aeromedical Research Institute, 1965.

(10) Arbogast, K. B.; Maltese, M. R. *Accidental Injury 3d Edition*, Yoganandan, N., Nahum, A. M., Melvin, J. W., Eds.; Springer: New York, 2015; Chapter 22, pp 643–697.

(11) Giedd, J. N.; Blumenthal, J.; Jeffries, N. O.; Castellanos, F. X.; Liu, H.; Zijdenbos, A.; Paus, T.; Evans, A. C.; Rapoport, J. L. Brain development during childhood and adolescence: a longitudinal MRI study. *Nature Neuroscience* **2** (**2008**), 861–863.

(12) Margulies, S.; Coats, B. *Pediatric Injury Biomechanics*, Crandall, J. R., Myers, B. S., Meaney, D. F., Schmidtke, S. Z., Eds.; Springer: New York, 2013; Chapter 4, pp 157–190.

(13) Bain, A. C.; Meaney, D. F. Tissue-Level Thresholds for Axonal Damage in an Experimental Model of Central Nervous System White Matter Injury. *Journal of Biomechanical Engineering* **122** (**2000**), 615–622.

(14) Meaney, D. F.; Smith, D. H. Biomechanics of Concussion. *Clinics in Sports Medicine* **30** (**2011**), 19–vii.

(15) Yeates, K. O.; Kaizar, E.; Rusin, J.; Bangert, B.; Dietrich, A.; Nuss, K.; Wright, M.; Taylor, G. H. Reliable Change in Postconcussive Symptoms and Its Functional Consequences Among Children With Mild Traumatic Brain Injury. *Pediatrics Adolescent Medicine* **166** (**2012**), 615–622.

(16) McKinlay, A. Controversies and outcomes associated with mild traumatic brain injury in childhood and adolescences. *Child Care Health Development* **36** (**2010**), 3–21.

(17) Of Orthopaedic Surgeons, A. A. Orthoinfo - Spine Basices., `https://orthoinfo.aaos.org/en/diseases--conditions/spine-basics/`, (accessed: 09.06.2018).

(18) Kumaresan, S.; Yoganandan, N.; Pintar, F. A.; Maiman, D. J.; Kuppa, S. Biomechanical Study of Pediatric Human Cervical Spine: A Finite Element Approach. *Journal of Biomedical Engineering* **122** (**1999**), 60–71.

(19) Huelke, D. F.; Mackay, G. M.; Morris, A.; Bradford, M. Car Crashes and Non-Head Impact Cervical Spine Injuries in Infants and Children. *SAE International* (**1992**), DOI: `https://doi.org/10.4271/920562`.

(20) Weber, K. *Accidental Injury 2nd Edition*, Nahum, A. M., Melvin, J. W., Eds.; Springer: New York, 2002; Chapter 20, pp 523–549.

(21) Staff, H. Reviewed by: Adam Husney, MD - Family Medicine and Kathleen Romito, MD - Family Medicine E. Gregory Thompson, MD - Internal Medicine Martin J. Gabica, MD - Family Medicine. Broken Rib in Children: Care Instructions., `https://myhealth.alberta.ca/Health/aftercareinformation/pages/conditions.aspx?hwid=bu1140`, (accessed: 09.06.2018).

(22) Stürtz, G. Biomechanical Data of Children. *Proceedings of the 24th Stapp Car Crash Conference, Troy, MI* **October** (**1980**).

(23) McElhaney, J.; Roberts, V. L.; Alem, N. M. A porous block model for cancellous bones. *Proceedings of the 24th Stapp Car Crash Conference, Troy, MI* **November** (**1970**).

(24) Parent, D. P. Scaling and optimization of thoracic impact response in pediatric subjects., Master Thesis, Mechanical and Aerospace Engineering, University of Virginia., 2008.

(25) Ouyang, J.; Zhao, W.; Xu, Y.; Chen, W.; Zhong, S. Thoracic impact testing of pediatric cadaveric subjects. *The Journal of Trauma* **61** (**2006**), 1492–500.

(26) Kroell, C. K.; Schneider, D. C.; Nahum, A. M. Impact Tolerance and Response of the Human Thorax II. *18th Stapp Car Crash Conference (1974)* **Technical Paper 741187** (**1974**), DOI: `https://doi.org/10.4271/741187`.

(27) Ivarsson, J.; Okamoto, M.; Takahashi, Y. *Pediatric Injury Biomechanics*, Crandall, J. R., Myers, B. S., Meaney, D. F., Schmidtke, S. Z., Eds.; Springer: New York, 2013; Chapter 3, pp 87–156.

(28) Reed, M. P.; Ebert-Hamilton, S. M.; Klinich, K. D.; Manary, M. A.; Rupp, J. D. Effects of vehicle seat and belt geometry on belt fit for children with and without belt positioning booster seats. *Accident Analysis and Prevention* **50** (**2013**), 512–522.

(29) Demetriades, D.; Karaiskakis, M.; Velmahos, G. C.; Alo, K.; Murray, J.; Chan, L. Pelvic Fractures in Pediatric and Adult Trauma Patients: Are They Different Injuries? *The Journal of Trauma: Injury, Infection, and Critical Care.* **54** (**2003**), 1146–1151.

(30) Gennarelli, T. A.; Wodzin, E. AIS 2005: A contemporary injury scale. *International Journal of the Care of the Injured* **37** (**2006**), 1083–1091.

(31) Board, S. T. S. Surface Vehicle Recommended Practice - Calculations Guidelines for Impact Testing., version J1727; SAE International, 24 pp.

(32) Ommaya, A. K.; Yarnell, P.; Hirsch, A. E.; Harris, E. H. Scaling of Experimental Data on Cerebral Concussion in Sub-Human Primates to Concussion Threshold for Man. *11th Stapp Car Crash Conference* (**1967**), https://doi.org/10.4271/670906.

(33) Eppinger, R.; Sun, E.; Kuppa, S.; Saul, R. *Supplement: Development of Improved Injury Criteria for the Assessment of Advanced Automotive Restraint Systems - II.* Tech. rep.; National Highway Traffic Safety Administration (NHTSA): National Transportation Biomechanics Research Center (NTBRC) and Vehicle Research  Test Center (VRTC), 2000.

(34) NCAP, E. *Assessment Protocol - Child Occupant Protection.* Tech. rep., Version 7.2.1; European New Car Assessment Programme, 2017.

(35) Chou, C. C.; Lin, Y. S.; Lim, G. G. An Evaluation of Various Viscous Criterion Computational Algorithms. *International Congress  Exposition* (**1993**), DOI: `https://doi.org/10.4271/930100`.

(36) NCAP, E. Offset deformable barrier frontal impact testing protocol., version 7.1.2; European New Car Assessment Programme (Euro NCAP), 27 pp.

(37) Viano, D. C.; Parenteau, C. S. Fatalities of Children 0–7 Years Old in the Second Row. *Traffic Injury Prevention* **9** (**2008**), PMID: 18570145, 231–237.

(38) Bohman, K.; Arbogast, K.; Bostrom, O. Head Injury Causation Scenarios for Belted, Rear-Seated Children in Frontal Impacts. *Traffic injury prevention* **12** (**2011**), 62–70.

(39) Forman, J. L.; Lopez-Valdes, F.; Lessley, D. J.; Riley, P.; Sochor, M.; Heltzel, S.; Ash, J.; Perz, R.; Kent, R. W.; Seacrist, T.; Arbogast, K. B.; Tanji, H.; Higuchi, K. Occupant Kinematics and Shoulder Belt Retention in Far-Side Lateral and Oblique Collisions: A Parametric Study. *Stapp Car Crash Journal* **57** (**2013**), 343–385.

(40) Of Highway Safety  Highway Loss Data Institute, I. I. Safety Belts., `http://www.iihs.org/iihs/topics/laws/safetybeltuse`, (accessed: 20.05.2018).

(41) Klinich, K. D.; Beebe, M. S.; Pritz, H. B.; Welty, K. E.; Burton, R. W. *Study of Older Child Restraint/Booster Seat Fit and NASS Injury Analysis.* Tech. rep.; University of Michigan, 1994.

(42) Kahane, C. J. *An Evaluation of Child Passenger Safety: The Effectiveness and Benefits of Safety Seats.* Tech. rep. POT HS 806 890; National Highway Traffic Safety Administration (NHTSA), 1986.

(43) Evans, L. The effectiveness of safety belts in preventing fatalities. *Accident Analysis  Prevention* **18** (**1986**), 229–241.

(44) Huelke, D. F.; Sherman, H. W.; Murphy, M. J.; Kaplan, R. J.; Flora, J. D. Effectiveness of Current and Future Restraint Systems in Fatal and Serious Injury Automobile Crashes. *Automotive Engineering Congress and Exposition* (**1979**), DOI: `https://doi.org/10.4271/790323`.

(45) Huelke, D. F.; Murray-Mackay, G.; Morris, A.; Bradford, M. Car Crashes and Non-Head Impact Cervical Spine Injuries in Infants and Children. *SAE International* (**1992**), DOI: `https://doi.org/10.4271/920562`.

(46) Osvalder, A.; Hansson, I.; Stockman, I.; Carlsson, A.; Bohman, K.; Jakobsson, L. Older Children's Sitting Postures, Behaviour and Comfort Experience during Ride – A Comparison between an Integrated Booster Cushion and a High Back Booster. *Proceedings of International Research Conference on the Biomechanics of Impact (IRCOBI), Gothenburg, Sweden* (**2013**).

(47) Santschi, M.; Echavé, V.; Laflamme, S.; McFadden, N.; Cyr, C. Seat-belt injuries in children involved in motor vehicle crashes. *Canadian Journal of Surgery* **48** (**2005**), 373–376.

(48) Durbin, D. R.; Elliott, M. R.; Winston, F. K. Belt-Positioning Booster Seats and Reduction in Risk of Injury Among Children in Vehicle Crashes. *JAMA* **289** (**2003**), 2835–2840.

(49) Arbogast, K. B.; Chen, I.; Nance, M. L.; Durbin, D. R.; Winston, F. K. Predictors of Pediatric Abdominal Injury Risk. *Stapp Car Crash Journal* **48** (**2004**), 479–494.

(50) Arbogast, K. B.; Jermakian, J. S.; Kallan, M. J.; Durbin, D. R. Effectiveness of Belt Positioning Booster Seats: An Updated Assessment. *Pediatrics* **124** (**2009**), 1281–1286.

(51) Forman, J. L.; Segui-Gomez, M.; Ash, J. H.; Lopez-Valdes, F. J. Child Posture and Shoulder Belt Fit During Extended Night-Time Traveling: An In-Transit Observational Study. *Annals of Advances in Automotive Medicine* **55** (**2011**), DOI: `PMC3256839`.

(52) Andersson, M. Child Safety in Car Crashes: A Modeling Approach for Safety System Improvements., PhD Thesis, Chalmers University of Technology, Gothenburg, Sweden, 2012.

(53) Lundell, B.; Carlsson, G.; Nilsson, P.; Persson, M.; Rygaard, C. Improving rear seat safety: a continuing process. *Proc of 13th International Technical Conference of the Enhanced Safety of Vehicles* (**2017**), 1194–1200.

(54) Bohman, K.; Boström, O.; Osvalder, A.-L.; Eriksson, M. Rear seat frontal impact protection for children seated on booster cushions - an attitude, handling and safety approach. *20th International Technical Conference on the Enhanced Safety of Vehicles (ESV), Lyon, France* (**2007**).

(55) Chipman, M.; Liu, J.; Hu, X. The Effectiveness of Safety Belts in Preventing Fatalities and Major Injuries Among School-Aged Children. *Proceedings of the 39th Annual Meeting of the Association for the Advancement of Automotive Medicine* (**1995**).

(56) Corden, T. Analysis of booster seat and seat belt use: How many Wisconsin childhood deaths and hospitalizations could have been prevented in 1998-2002? *WMJ : official publication of the State Medical Society of Wisconsin* **104** (**2005**), 42–45.

(57) O'Neil, J.; Daniels, D. M.; Talty, J. L.; Bull, M. J. Seat belt misuse among children transported in belt-positioning booster seats. *Accident Analysis  Prevention* **41** (**2009**), 425 –429.

(58) Arbogast, K. B.; Durbin, D. R.; Kallan, M. J.; Menon, R. A.; Lincoln, A. E.; Winston, F. K. The Role of Restraint and Seat Position in Pediatric Facial Fractures. *The Journal of Trauma: Injury, Infection, and Critical Care. 52(4):693-698, APR 2002* **54** (**2002**), 693–698.

(59) Arbogast, K. B.; Durbin, D. R. *Pediatric Injury Biomechanics*, Crandall, J. R., Myers, B. S., Meaney, D. F., Schmidtke, S. Z., Eds.; Springer: New York, 2013; Chapter 2, pp 33–86.

(60) Shanahan, D. F. Shoulder belt-induced flexion–distraction fractures of the cervical spine. *International Journal of Crashworthiness* **18** (**2013**), 559–569.

(61) Chamouard, F.; Tarriere, C.; Baudrit, P. Protection of Children On Board Vehicles. Influence of Pelvis Design and Thigh and Abdomen Stiffness on the Submarining Risk for Dummies Installed on a Booster. *Proceedings of the Fiftheenth International Technical Conference on the Enhanced Safety of Vehicles, Melbourne, Australia* **2** (**1996**).

(62) Lutz, N.; Arbogast, K. B.; Cornejo, R. A.; Winston, F. K.; Durbin, D. R.; Nance, M. L. Suboptimal restraint affects the pattern of abdominal injuries in children involved in motor vehicle crashes. *Journal of Pediatric Surgery* **38** (**2003**), 919 –923.

(63) Randhawa, M. P.; Menzoian, J. O. Seat Belt Aorta. *Annals of Vascular Surgery* **4** (**1990**), 370 –377.

(64) Reed, M. P.; Ebert-Hamilton, S. M.; Klinich, K. D.; Manary, M. A.; Rupp, J. D. *Assessing Child Belt Fit, Volume I: Effects of Vehicle Seat and Belt Geometry on Belt Fit for Children with and without Belt Positioning Booster Seats.* Tech. rep. UMTRI-2008-49-1; University of Michigan Transportation Research Institute, 2008.

(65) Kent, R.; Forman, J.; Parent, D. P.; Kuppa, S. Rear Seat Occupant Protection In Frontal Crashes And Its Feasibility. *INNOVATIONS FOR SAFETY: OPPORTUNITIES AND CHALLENGES, U.S. Department of Transportation National Highway Traffic Safety Administration* (**2007**), 4–16.

(66) Forman, J.; Michaelson, J.; Kent, R.; Kuppa, S.; Boström, O. Occupant Restraint in the Rear Seat: ATD Responses to Standard and Pre-tensioning, Force-Limiting Belt Restraints. *Association for the Ad-*

*vancement of Automotive Medicine. Association for the Advancement of Automotive Medicine. Scientific Conference* **52** (**2008**), 141–54.

(67) Forman, J.; Lopez-Valdes, F.; Lessley, D.; Kindig, M.; Kent, R.; Ridella, S.; Bostrom, O. Rear seat occupant safety: an investigation of a progressive force-limiting, pretensioning 3-point belt system using adult PMHS in frontal sled tests. **53** (**2009**), 49–74.

(68) Lopez-Valdes, F.; Forman, J.; Bostrom, O.; Kent, R. A comparison between a child-size PMHS and the Hybrid III 6 YO in a sled frontal impact. *Annals of Advances in Automotive Medicine* **53** (**2009**), 237—246.

(69) Bohman, K.; Fredriksson, R. Pretensioner loading to rear-seat occupants during static and dynamic testing. *Traffic Injury Prevention* **15** (**2014**), 111–118.

(70) Andersson, M.; Bohman, K.; Osvalder, A.-L. Effect of Booster Seat Design on Children's Choice of Seating Positions During Naturalistic Riding. *Annals of Advances in Automotive Medicine* **54** (**2010**), 171—180.

(71) Stockman, I. Child Passenger Kinematics in Emergency Manoeuvres., Licentiate Thesis, Chalmers University of Technology, Gothenburg, Sweden, 2012.

(72) Administration, N. H.T. S. Car Seats and Booster Seats., `https://www.nhtsa.gov/equipment/car-seats-and-booster-seats#find-compare-seats`, (accessed: 20.05.2018).

(73) Maltese, M. R.; Tylko, S.; Belwadi, A.; Locey, C.; Arbogast, K. B. Comparative Performance of Forward-Facing Child Restraint Systems on the C/FMVSS 213 Bench and Vehicle Seats. *Traffic Injury Prevention* **15** (**2014**), PMID: 25307374, S103–S110.

(74) Lorente, O. J.; Alba, J. J.; Lopez-Valdes, F. J. A comparison of the performance of child restraint systems between a variant of the ECE R44 bench and a vehicle seat. *IRCOBI Conference* (**2014**).

(75) Tylko, S.; Dalmotas, D. Protection of Rear Seat Occupants in Frontal Crashes. (**2018**), 2–8.

(76) Klinich, K. D.; Reed, M. P. *Pediatric Injury Biomechanics*, Crandall, J. R., Myers, B. S., Meaney, D. F., Schmidtke, S. Z., Eds.; Springer: New York, 2013; Chapter 1, pp 1–32.

(77) Beillas, P.; Soni, A.; Chevalier, M.; Johannsen, H.; Müller, G.; Holtz, J. Q6 dummy thoracic response and diagonal belt interactions: observations based on dummy testing and human and dummy simulations. *International Research Council on the Biomechanics of Injury Conference 2014 Berlin, Germany* (**2014**).

(78) Yang, K.; Hu, J.; White, N. A.; King, A.; Chou, C.; Prasad, P. Development of Numerical Models for Injury Biomechanics Research: A Review of 50 Years of Publications in the Stapp Car Crash Conference. *Stapp Car Crash Journal* **50** (**2006**), 429–490.

(79) Iraeus, J.; Lindquist, M. Pulse shape analysis and data reduction of real-life frontal crashes with modern passenger cars. *International Journal of Crashworthiness* **20** (**2015**), 535–546.

(80) Giordano, C.; Kleiven, S. Development of a 3 Year Old Child FE Head Model, Continuously Scalable from 1.5 to 6 Year Old. *International Research Council on the Biomechanics of Injury Conference* (**2016**).

(81) Iwamoto, M.; Nakahira, Y.; Kimpara, H. Development and Validation of the Total HUman Model for Safety (THUMS) Toward Further Understanding of Occupant Injury Mechanisms in Precrash and During Crash. *Traffic Injury Prevention* **16** (**2015**), DOI: `https://doi.org/10.1080/15389588.2015.1015000`.

(82) Dong, L.; Li, G.; Mao, H.; Marek, S.; Yang, K. H. Development and Validation of a 10-Year-Old Child Ligamentous Cervical Spine Finite Element Model. *Annals of Biomedical Engineering* **41** (**2013**), 2538–2552.

(83) Östh, J.; Brolin, K.; Bråse, D. A Human Body Model With Active Muscles for Simulation of Pretensioned Restraints in Autonomous Braking Interventions. *Traffic Injury Prevention* **16** (**2014**), DOI: `https://doi.org/10.1080/15389588.2014.931949`.

(84) Beillas, P.; Giordano, C.; Alvarez, V.; Li, X.; Ying, X.; Chevalier, M.-C.; Kirscht, S.; Kleiven., S. Development and performance of the PIPER scalable child human body models *14th International Conference Protection of Children in Cars Munich, Germany* (**2016**).

(85) Beillas, P.; Lafon, Y.; Smith, F. W. The effects of posture and subject-to-subject variations on the position, shape and volume of abdominal and thoracic organs. *Stapp car crash journal* **53** (**2009**), 127–154.

(86) Cheng, H.; Obergefell, L.; Rizer, A. Generator of Body Data (GEBOD) , Manual., version Report No. AL/CF-TR-1994-0051; Human Effectiveness Directorate, Crew Survivability and Logistics Division, Write-Patterson Air Force ase Ohio, 71 pp.

(87) Byoung-Keon, D. P.; Reed, M. P. UMTRI Child Body Shape., `http://childshape.org`, (accessed: 20.05.2018).

(88) Doxygen PIPER Software Framework and Application: User guide., version Version 1.0.1; PIPER Project, 329 pp.

(89) Beillas, P.; Ruyet, A. L.; Chevalier, M.-C. Side impact applications of the PIPER scalable child human body model. *15th International IRCOBI Protection of Children in Cars Munich, Germany* (**2017**).

(90) Beillas, P.; Giordano, C.; Alvarez, V.; Collot, J.; Kischt, S.; Kleiven, S. Ongoing efforts on scalable child models, associated tools and procedures in the PIPER project. *13th International Conference Protection of Children in Cars. Munich. Germany* **December** (**2015**), 1–17.

(91) Yoganandan, N.; Pintar, F. A.; Kumaresan, S.; Gennarelli, T. A.; Sun, E.; Kuppa, S.; Maltese, M.; Eppinger, R. H. Pediatric and small female neck injury scale factors and tolerance based on human spine biomechanical characteristics. *Proceedings of the International Research Council on the Biomechanics of Injury conference, Montpellier, France* **28** (**2000**), 345–359.

(92) Jolivet, E.; Lafon, Y.; Petit, P.; Beillas, P. Comparison of Kriging and Moving Least Square Methods to Change the Geometry of Human Body Models. *Stapp Car Crash Journal* **59** (**2015**), 337–357.

(93) Wu, S. R.; Gu, L., *Introduction to the Explicit Finite Element Method for Nonlinear Transient Dynamics.* John Wiley Sons: 2012.

(94) Boman, M. On A Posteriori Error Estimation in the Maximum Norm., PhD Thesis, Chalmers University of Technology, Gothenburg, Sweden, 2000.

(95) Cook, R. D.; Malkus, D. D.; Plesha, M. E. *Concepts and Applications of Finite Element Analysis*; John Wiley and Sons: New York; Chapter 13.

(96) Of Technology, C. U. Open HBM: ViVA - Virtual Vehicle-safety Assessment: OpenSource Human Body Models addressing gender diversity., `https://www.chalmers.se/en/projects/Pages/OpenHBM.aspx`, (accessed: 20.06.2018).

(97) Marzougui, D.; Samaha, R. R.; Cui, C.; Kan, C.-D. S.; Opiela, K. S. Extended Validation of the Finite Element Model for the 2010 Toyota Yaris Passenger Sedan. (**2012**).